Check for updates

NIST Technical Note
NIST TN 2348B

New Precast Concrete Moment Connections under a Column Removal Scenario

Malcolm Ammons
Jonathan Weigand
Travis Thonstad

This publication is available free of charge from:
https://doi.org/10.6028/NIST.TN.2348B

NATIONAL INSTITUTE OF STANDARDS AND TECHNOLOGY
U.S. DEPARTMENT OF COMMERCE

NIST Technical Note
NIST TN 2348B

New Precast Concrete Moment Connections under a Column Removal Scenario

Malcolm Ammons
Jonathan Weigand
Materials and Structural Systems Division
Engineering Laboratory

Travis Thonstad
Department of Civil and Environmental Engineering
University of Washington

This publication is available free of charge from:
https://doi.org/10.6028/NIST.TN.2348B

September 2025

U.S. Department of Commerce
Howard Lutnick, Secretary

National Institute of Standards and Technology
Craig Burkhardt, Acting Under Secretary of Commerce for Standards and Technology and Acting NIST Director

NIST TN 2348B
September 2025

Certain equipment, instruments, software, or materials, commercial or non-commercial, are identified in this paper in order to specify the experimental procedure adequately. Such identification does not imply recommendation or endorsement of any product or service by NIST, nor does it imply that the materials or equipment identified are necessarily the best available for the purpose.

NIST Technical Series Policies
Copyright, Use, and Licensing Statements
NIST Technical Series Publication Identifier Syntax

Publication History
Approved by the NIST Editorial Review Board on 2025-09-15

How to Cite this NIST Technical Series Publication
Ammons M, Weigand J, Thonstad T (2025) New Precast Concrete Moment Connections under a Column Removal Scenario. (National Institute of Standards and Technology, Gaithersburg, MD), NIST Technical Note (TN) NIST TN 2348B. https://doi.org/10.6028/NIST.TN.2348B

Author ORCID iDs
Malcolm Ammons: 0000-0003-2033-9936
Jonathan Weigand: 0000-0002-6938-6197
Travis Thonstad: 0000-0002-1575-3617

Abstract

This technical note presents an experimental investigation of the performance of five novel precast concrete moment-resisting connections subjected to a column-removal scenario. The objectives of the investigation were 1) to characterize the behavior and failure modes of the connection assemblies and 2) assess their viability for use in precast concrete construction to achieve robust performance against disproportionate collapse. The tested assemblies were derived at a five-eighth scale from a 10-story prototype building and consisted of two half-span spandrel beams connected to a central column. The assemblies were designed specifically for moments induced from the loss of an exterior column in the prototype building. A capacity design approach was taken to concentrate inelastic action in designated components at the beam-to-column interface. Each assembly was subjected to monotonically increasing vertical displacement applied to the unsupported column until connection failure. The assemblies were extensively instrumented to measure the vertical force applied to the assembly, displacement at different locations along the beams and column, in-plane rotations of the precast concrete components, and strains in the reinforcing bars and steel connection components.

All the assemblies failed as was intended by design, with rotational deformations concentrating in designated ductile components until their eventual failure. A computational methodology was used in conjunction with the experimental results to evaluate the structural robustness of the assemblies against sudden column loss. All the assemblies were shown capable of withstanding loads greater than the applicable gravity loading that they would need to sustain to prevent collapse under sudden column loss. Although the threaded rod connection assembly's connections were the easiest to make in a laboratory setting, all the connection concepts were proven viable for use in precast concrete construction, with each concept having unique advantages and disadvantages.

Keywords

Connections; disproportionate collapse; experimental; moment-resisting connections; precast concrete; progressive collapse; robustness.

Table of Contents

1. Introduction 1
1.1. Prototype Precast Concrete Moment Frame Building 1
1.2. Connection Concepts 6
1.3. Test Setup and Loading 7
1.4. Design of Test Specimens 9
1.5. Report Outline 12
2. Fabrication and Erection of Test Assemblies 13
2.1. Design Drawings 13
2.2. Fabrication of Test Specimens 13
2.2.1. Threaded Rod 15
2.2.2. Bolted 17
2.2.3. Bar Coupler 19
2.2.4. Grouted Bar 21
2.2.5. Modified Link Plate 22
2.3. Instrumentation 24
2.4. Laboratory Constructability 27
3. Mechanical Properties 37
3.1. Concrete 37
3.2. Steel Connection Components 38
3.3. Grout 41
4. Experimental Results 43
4.1. Preamble 43
4.1.1. Moment-Rotation Behavior 43
4.1.2. Damage Progression and Failure Mode 43
4.1.3. Displacement Profile and Rotation 44
4.2. Threaded Rod 44
4.2.1. Moment-Rotation Behavior 44
4.2.2. Damage Progression and Failure Mode 46
4.2.3. Displacement Profile and Rotation 47
4.2.4. Strain Measurements 49
4.3. Bolted 52
4.3.1. Moment-Rotation Behavior 52
4.3.2. Damage Progression and Failure Mode 54
4.3.3. Displacement Profile and Rotation 54

4.3.4. Strain measurements 56
4.4. Bar Coupler 56
4.4.1. Moment-Rotation Behavior 56
4.4.2. Damage Progression and Failure Mode 58
4.4.3. Displacement Profile and Rotation 60
4.4.4. Strain Measurements 61
4.5. Grouted Bar 64
4.5.1. Moment-Rotation Behavior 64
4.5.2. Damage Progression and Failure Mode 65
4.5.3. Displacement Profile and Rotation 66
4.5.4. Strain Measurements 68
4.6. Modified Link Plate 69
4.6.1. Moment-Rotation Behavior 69
4.6.2. Damage Progression and Failure Mode 70
4.6.3. Displacement Profile and Rotation 71
4.6.4. Strain Measurements 73
4.7. Summary and Discussion 76
5. Structural Robustness 79
5.1. Background 79
5.2. Results, Comparisons, and Limitations 80
6. Summary and Conclusions 83
6.1. Recommendations 84
References 86
Appendix A. Design Drawings 89
Appendix B. Locations of Strain Gauges 111

List of Tables

Table 1-1. Summary of design forces for third floor spandrel beams (from Thonstad et al., 2025) 11
Table 1-2. Summary of design forces for scaled spandrel beams 11
Table 2-1. Measurement uncertainty. 26
Table 3-1. Compressive strength of concrete. 38
Table 3-2. Modulus of elasticity of concrete. 38
Table 3-3. Splitting tensile strength of concrete. 38
Table 3-4. Average material properties of steel connection components. 41
Table 3-5. Average compressive strength of grout. 42

Table 4-1. Measured vertical column displacement at the end of each loading increment (threaded rod). 46

Table 4-2. Measured vertical column displacement at the end of each loading increment (bolted). 53

Table 4-3. Measured vertical column displacement at the end of each loading increment (bar coupler). 58

Table 4-4. Measured vertical column displacement at the end of each loading increment (grouted bar). 65

Table 4-5. Measured vertical column displacement at the end of each loading increment (modified link plate)....70

Table 4-6. Summary of experimental results. 76

Table 5-1. Robustness indexes of the tested assemblies 82

List of Figures

Fig. 1-1. Plan layout for SDC D building. 3

Fig. 1-2. Elevation of SDC building (from Main et al. 2015). 4

Fig. 1-3. Connection details (from Kim et al., 2009). All dimensions are shown in inches. 1.00 in = 25.4 mm....5

Fig. 1-4. Connection concepts: (a) prototype (b) modified link plate (c) threaded rod (d) grouted bar (e) bar coupler (f) bolted. 7

Fig. 1-5. Precast concrete moment frame assembly extracted from prototype precast SDC D building (adapted from Main et. al. 2015). 8

Fig. 1-6. Schematic of experimental setup. 9

Fig. 1-7. Extracted portion of exterior precast concrete moment frame (note: spandrel beams of the tested assemblies extend to half the scaled span on either side of the column): (a) amplified gravity loads and assumed plastic mechanism (a) shear diagram for the spandrel beams (c) moment diagram for the spandrel beams. 10

Fig. 1-8. Typical dimensions of scaled precast concrete moment connection assembly. All dimensions are in inch with mm equivalents in parenthetical brackets. 12

Fig. 2-1. An assembly (a) beam and (b) column before concrete was cast. 14

Fig. 2-2. An assembly beam and column after concrete was cast. 14

Fig. 2-3. Bar couplers embedded in the threaded rod connection assembly column. 15

Fig. 2-4. Steel angles and corrugated duct in a threaded rod connection assembly beam. 16

Fig. 2-5. Built-up steel box sections with longitudinal reinforcement welded to their tops and bottoms. 16

Fig. 2-6. HSS with plates welded to their ends and longitudinal reinforcement welded to the tops and bottoms of the HSS. 18

Fig. 2-7. Coupling nuts and plate washers embedded in the bolted connection assembly column. 19

Fig. 2-8. No. 7 link bars (couplers) used in the bar coupler connection assembly. 20

Fig. 2-9. Back of the column with foam inserts (left) to create the column blockouts (right). 20

Fig. 2-10. Continuity bars with debonding sleeves and foam blockouts to create voids in the beams to recess the collars. 21

Fig. 2-11. Right beam of the grouted bar connection assembly with hand holes and corrugated duct. 22

Fig. 2-12. Link plates protruding from the ends of the left and right beams. 23

Fig. 2-13. Link plate and three anchorage bars welded to the same face of steel channel. 23

Fig. 2-14. Dog-bone shaped link plates used in the modified link plate connection assembly. 24

Fig. 2-15. A schematic of the instrumentation layout. Dimensions are specified in inches with mm equivalents in parentheses. 25

Fig. 2-16. Instrumentation: (a) string potentiometer; (b) linear variable inductance transducer; (c) load cell; (d) inclinometer; (e) linear variable differential transformer. 26

Fig. 2-17. Load cells and spherical washers used for the (a) threaded rod and (b) bolted connection assemblies. 27

Fig. 2-18. Threadbars recessed in the left beam before they are threaded into the couplers in the column. 28

Fig. 2-19. Hex nut threaded on the end of a threadbar. 29

Fig. 2-20. Close-up view of the (a) anchor bolt and (b) threadbar threads. 29

Fig. 2-21. Left beam being shifted to the right after the anchor bolts were threaded into the coupling nuts embedded in the column. 30

Fig. 2-22. Before (left) and after (right) a portion of the endplate at the bottom of the right beam was cut and removed. 31

Fig. 2-23. Hex nut threaded on the end of an anchor bolt. 31

Fig. 2-24. Reinforcing bar coupler used to make the bar coupler connections. 32

Fig. 2-25. The collars protruding from the beams (left) and the upper two connections (right). 32

Fig. 2-26. Grout pump (left) and locations of grout injection ports (right) used for the bar coupler connection assembly. 32

Fig. 2-27. Continuity bars spanning the hand holes near the midlength of the right beam. 33

Fig. 2-28. Continuity bar with debonding sleeve and continuity bar centered on the column width. ...34

Fig. 2-29. Gap between the steel link plates and embedded column channels before insertion of filler plates. 35

Fig. 2-30. Steel plates to fill the gap between the link plates and embedded column channels 35

Fig. 2-31. Top (left) and bottom (right) link plates after welding 36

Fig. 3-1. Stress versus engineering strain curves based on two tension tests of threadbars. 39

Fig. 3-2. Stress versus engineering strain curves based on two tension tests of anchor bolts. 40

Fig. 3-3 Stress versus engineering strain curves based on two tension tests of continuity bars. 41

Fig. 4-1. Applied connection moment versus beam chord rotation for the threaded rod connection assembly. 45

Fig. 4-2. Failure mode of the threaded rod connection assembly. 47

Fig. 4-3. Vertical displacement profiles of the threaded rod connection assembly. 48

Fig. 4-4. Measured in-plane rotations of the precast concrete beams and columns for the threaded rod connection assembly. 49

Fig. 4-5. Strain in flexural reinforcing bars at the bottom of the right beam (threaded rod connection assembly). 50

Fig. 4-6. Strain in the threadbar in the top of the right beam (threaded rod connection assembly). 51

Fig. 4-7. Strain in the threadbar in the bottom of the left beam (threaded rod connection assembly). 52

Fig. 4-8. Applied connection moment versus beam chord rotation for the bolted connection assembly. 53

Fig. 4-9. Failure mode of the bolted connection assembly. 54

Fig. 4-10. Vertical displacement profiles of the bolted connection assembly. 55

Fig. 4-11. Measured in-plane rotations of the precast concrete beams and columns for the bolted connection assembly. 56

Fig. 4-12. Applied connection moment versus beam chord rotation for the bar coupler connection assembly. 57

Fig. 4-13. Failure mode of the bar coupler connection assembly. 59

Fig. 4-14. Vertical displacement profiles of the bar coupler connection assembly. 60

Fig. 4-15. Measured in-plane rotations of the precast concrete beams and columns for the bar coupler connection assembly. 61

Fig. 4-16. Labeling scheme for bar couplers. 62

Fig. 4-17. Strains in the bar couplers. 63

Fig. 4-18. Applied connection moment versus beam chord rotation for the grouted bar connection assembly. 65

Fig. 4-19. Failure mode of the grouted bar connection assembly. 66

Fig. 4-20. Vertical displacement profiles of the grouted bar connection assembly. 67

Fig. 4-21. Measured in-plane rotations of the precast concrete beams and columns for the grouted bar connection assembly. 68

Fig. 4-22. Strain in flexural reinforcing bars at the bottom of the left beam (grouted bar connection assembly). 69

Fig. 4-23. Applied connection moment versus beam chord rotation for the modified link plate connection assembly. 70

Fig. 4-24. Failure mode of the modified link plate connection assembly. 71

Fig. 4-25. Vertical displacement profiles of the modified link plate connection assembly. 72

Fig. 4-26. Measured in-plane rotations of the precast concrete beams and columns for the modified link plate connection assembly. 72

Fig. 4-27. Strains in the link plates. 74

Fig. 4-28. Strains in the anchorage bars. 75

Fig. 4-29. Force versus displacement responses for all five connection assemblies. 76

Fig. 5-1 Force versus displacement responses considering static loading and sudden column loss. 81

Fig. B-1. Locations of strain gauges on the beam steel reinforcement for the threaded rod connection assembly. 111

Fig. B-2. Locations of strain gauges on the beam steel reinforcement for the bolted connection assembly. 111

Fig. B-3. Locations of strain gauges on the beam steel reinforcement for the bar coupler, grouted bar, and modified link plate connection assemblies. 112

Fig. B-4. Locations of strain gauges on the threadbars for the threaded rod connection assembly. ...112

Fig. B-5. Locations of strain gauges on the No. 7 link bars (couplers) for the bar coupler connection assembly. 112

Fig. B-6. Locations of strain gauges on steel components for the modified link plate connection assembly. 113

Acknowledgments

Financial and technical support for this project was provided by the Precast/Prestressed Concrete Institute (PCI). The test specimens were fabricated by Tindall Corp. A committee of experts provided valuable input on the design of the connections. The committee consisted of the following precast concrete experts: Greg Force (Tindall Corp.), Jared Brewe (former Vice President of Technical Services at PCI), Roger Becker (retired PCI), Romany Gergious (Tindall Corp.), Isaac Perkins (Tindall Corp.), Michael Willis (Tindall Corp.), Andrew Osborn (Wiss, Janey, Elstner Associates, Inc.), Craig Barrett (LEAP Associates International, Inc.), Ned Cleland (Blue Ridge Design Inc.), Harry Gleich (Metromont Corp.), S. K. Ghosh (S. K. Ghosh and Associates Inc.), Sam Kakish (Enterprise Properties, Inc.), Walter Korkosz (The Consulting Engineers Group Inc.), Alex Mihaylov (Vector Structures), Clay Naito (Lehigh University), Spencer Quiel (Lehigh University), Perry Schram (Pennoni Associates, Inc.), Kim Seeber (Seaboard Services of Virginia Inc.), and Aaron Vnuk (Precast Services, Inc.).

1. Introduction

The National Institute of Standards and Technology (NIST) has completed a multi-year research program focused on mitigating disproportionate collapse in structural systems typical of United States (U.S.) building construction. Disproportionate collapse is a phenomenon characterized by local damage or failure of a relatively small part of a structure leading to collapse of the entire structure or a large part of it (ASCE 2023). In the first phase of this research (termed NIST Phase I), five ten-story archetype buildings were designed for seismic loads with each building having a different conventionally designed lateral load resisting system: steel braced frames, reinforced concrete shear walls, steel moment frames, reinforced concrete moment frames, or precast concrete moment frames. Within NIST Phase I, full-scale testing of beam-column assemblies representing single-story two-span portions of a steel moment frame (Sadek et al., 2010), reinforced concrete moment frame (Lew et al., 2011), and precast concrete moment frame (Main et al., 2015) were performed to characterize their robustness under an exterior column removal scenario. Additional background information on the design of the precast concrete moment frame building is provided in Sec. 1.1.

In both precast concrete moment frame assemblies tested by Main et al. (2015), failure initiated prior to achieving the nominal flexural capacity of the beam sections, revealing potential vulnerabilities in the collapse resistance of precast beam-to-column moment connections subjected to column removal. The premature failures of the connections were attributed to the combined influences of eccentricities in the tensile force transfer path and reduced ductility of the reinforcement caused by welding. Motivated by the suboptimal performance of these assemblies, NIST initiated a second phase of research (termed NIST Phase II), in which alternative precast concrete connection concepts were developed in coordination with an industry review committee of Precast/Prestressed Concrete Institute (PCI) members.

Unlike for the NIST Phase I specimens, the connection assemblies in NIST Phase II were designed specifically for moments arising from a middle column removal scenario in the exterior moment frame of a ten-story prototype precast concrete moment frame building. Five novel precast concrete beam-column moment connection concepts were selected for experimental study at a five-eighths scale, as described in Sec. 1.2. The development of these connection concepts, and the comprehensive design of the five associated scaled connection assemblies utilizing the new connection concepts, are described in Thonstad et al. (2025).

This report summarizes the results of experimental testing of these five five-eighths scale precast beam-column connection assemblies subjected to a middle column removal scenario to characterize their robustness against disproportionate collapse.

1.1. Prototype Precast Concrete Moment Frame Building

For consistency with NIST Phase I, the NIST Phase II research program utilized the prior studies' prototype precast concrete frame buildings that were designed by S.K. Ghosh and Associates in 2009 (Kim et al., 2009) in accordance with the 2006 International Building Code (IBC 2006),

ACI 318-05 *Building Code Requirements for Structural Concrete and Commentary* (ACI 2005) published by the American Concrete Institute (ACI), ASCE 7-05 *Minimum Design Loads for Buildings and Other Structures* (ASCE 2005) published by the American Society of Civil Engineers (ASCE), and AISC 360-05 *Specification for Structural Steel Buildings* (AISC 2005) published by the American Institute of Steel Construction (AISC). Two precast concrete office buildings were designed for different Seismic Design Categories (SDCs) as part of the NIST Phase I research. For both buildings, exterior moment frames with deep spandrel beams were used as the lateral force resisting system in both orthogonal directions. One building was designed assuming a moderate seismic hazard level (SDC C) with the exterior moment frames detailed as Ordinary Moment Frames (OMFs). The second building was designed assuming a higher seismic hazard level (SDC D) with the exterior moment frames detailed as Special Moment Frames (SMFs). Only the prototype building designed by Kim et al. (2009) for SDC D is summarized here because only this configuration was considered in the NIST Phase II testing program.

The SDC D prototype building was a 10-story office building with precast concrete moment-resisting frames constituting the lateral force-resisting system in each orthogonal direction. The building was designed for a location in Seattle, WA with Site Class D. The Occupancy Category of the building was determined to be II based on ASCE 7-05 Table 1-1. Figure 1-1 shows a plan view of the building, which had plan exterior north-south and east-west dimensions of 150 ft × 150 ft (45.7 m × 45.7 m), with five equal-span bays in each direction. The exterior framing consisted of columns and spandrel beams that were designed to provide the entire lateral resistance. These same columns and spandrel beams formed the exterior architectural finish of the building. The interior framing consisted of gravity columns and simply supported inverted-T beams. The floor system consisted of double-T members spanning the north-south directions and resting on east-west-spanning inverted-T beams. To accommodate the camber in the double-T members, the thickness of concrete topping varied from 2.50 in (6.35 cm) at midspan of the floor to 3.50 in (8.89 cm) over the centerlines of the inverted-T beams.

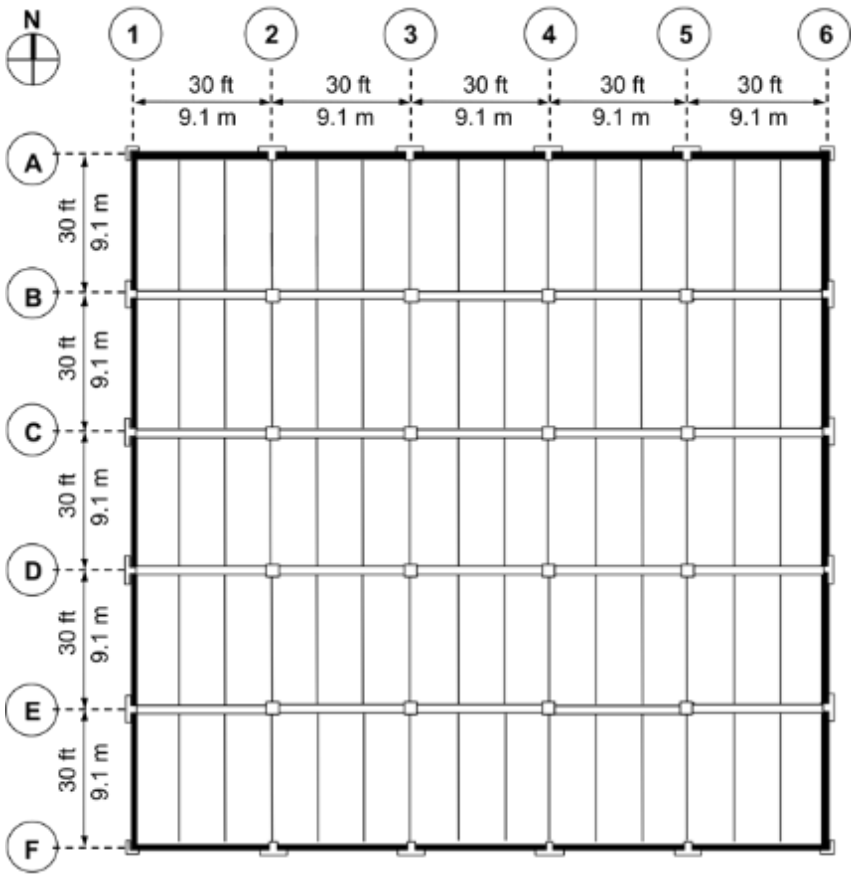

Fig. 1-1. Plan layout for SDC D building.

Figure 1-2 shows an elevation view of the building. The height of the first story (from ground to the first-floor level, which is at the mid-height of the first-floor's spandrel beams) was 15.0 ft (4.57 m). The heights of the other stories were 13.0 ft (3.96 m).

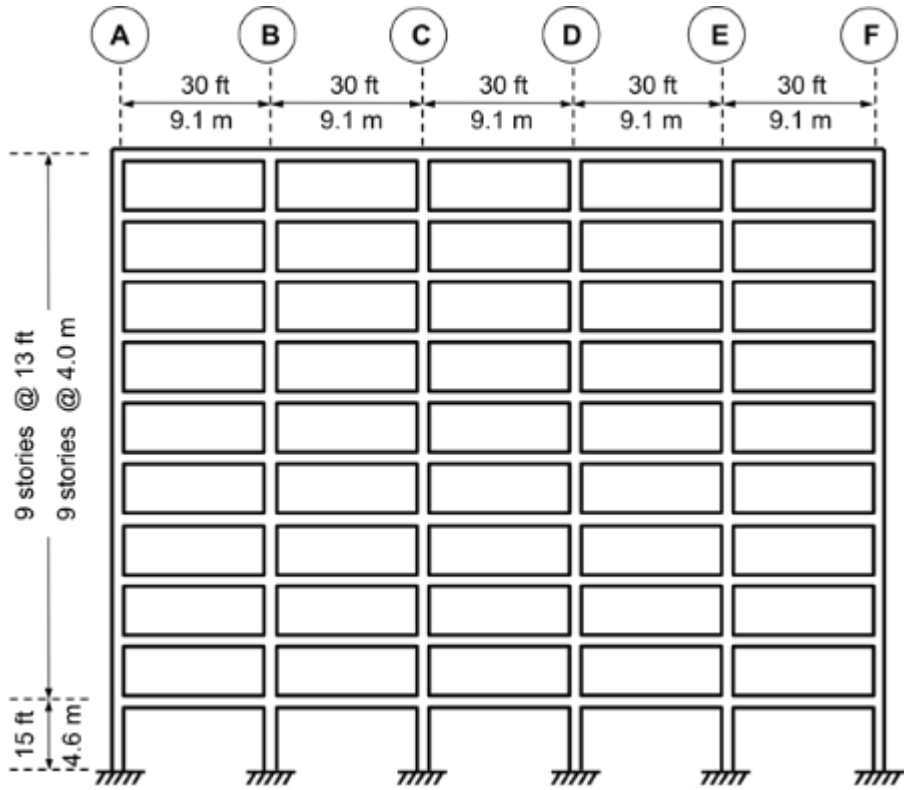

Fig. 1-2. Elevation of SDC building (from Main et al. 2015).

A superimposed dead load of 10 lbf/ft^2 (48.8 kg/m^2) was considered in addition to the self-weight of the structure. Typical floors were designed for a live load of 100 lbf/ft^2 (488 kg/m^2), which was reduced in accordance with ASCE 7-05 Section 4.8. The roof was designed for a live load of 25 lbf/ft^2 (122 kg/m^2). Both the precast concrete structural members and the concrete topping were designed using normal-weight concrete with a specific weight of 150 lbf/ft^3 (2403 kg/m^3). A minimum compressive strength of 6000 psi (41.4 MPa) was specified for the precast structural members, and a minimum compressive strength of 4000 psi (27.6 MPa) was specified for the concrete topping. A minimum yield strength of f_y = 60 ksi (414 MPa) was specified for the deformed bar reinforcement.

The connections between the spandrel beams and the columns were designed as *strong connections* in accordance with ACI 318-05 Section 21.6.2; i.e., the design intent was to promote flexural yielding in the precast beams (away from the connection regions). The spandrel beams of the OMFs (for the SDC C prototype building) and SMFs (for the SDC D prototype building) were differentiated primarily by their depths and longitudinal reinforcement; the beams of the OMFs were deeper and had fewer longitudinal reinforcing bars than those of the SMFs. In both designs, the same type of welded link plate connection was used between the beams and the column. Figure 1-3 shows the details of the welded link plate connections for the SDC D prototype building. The spandrel beams are placed inside pockets in the exterior columns. Moment connections are made by first welding steel link plates (PL 8×12×1 = PL 200×300×25) to steel angles (L8×6×1 = L200×150×25) embedded in the top and bottom of the beams and then to steel column plates (PL 22×20×1 = PL 560×510×25) embedded in the columns using headed studs.

Anchorage bars in the spandrel beams are welded to the interior faces of the angles. Noncontact Class B splices between the anchorage bars and the beam flexural reinforcement maintain continuity of the beam reinforcement through the connection, as required by ACI 318-05 Section 21.6.2. The beam moment is transferred to the column by the coupling forces (axial tension and axial compression) generated in the top and bottom link plates. Torsional restraint of the spandrel beams is provided by torsion rods installed through sleeves in the beams and columns.

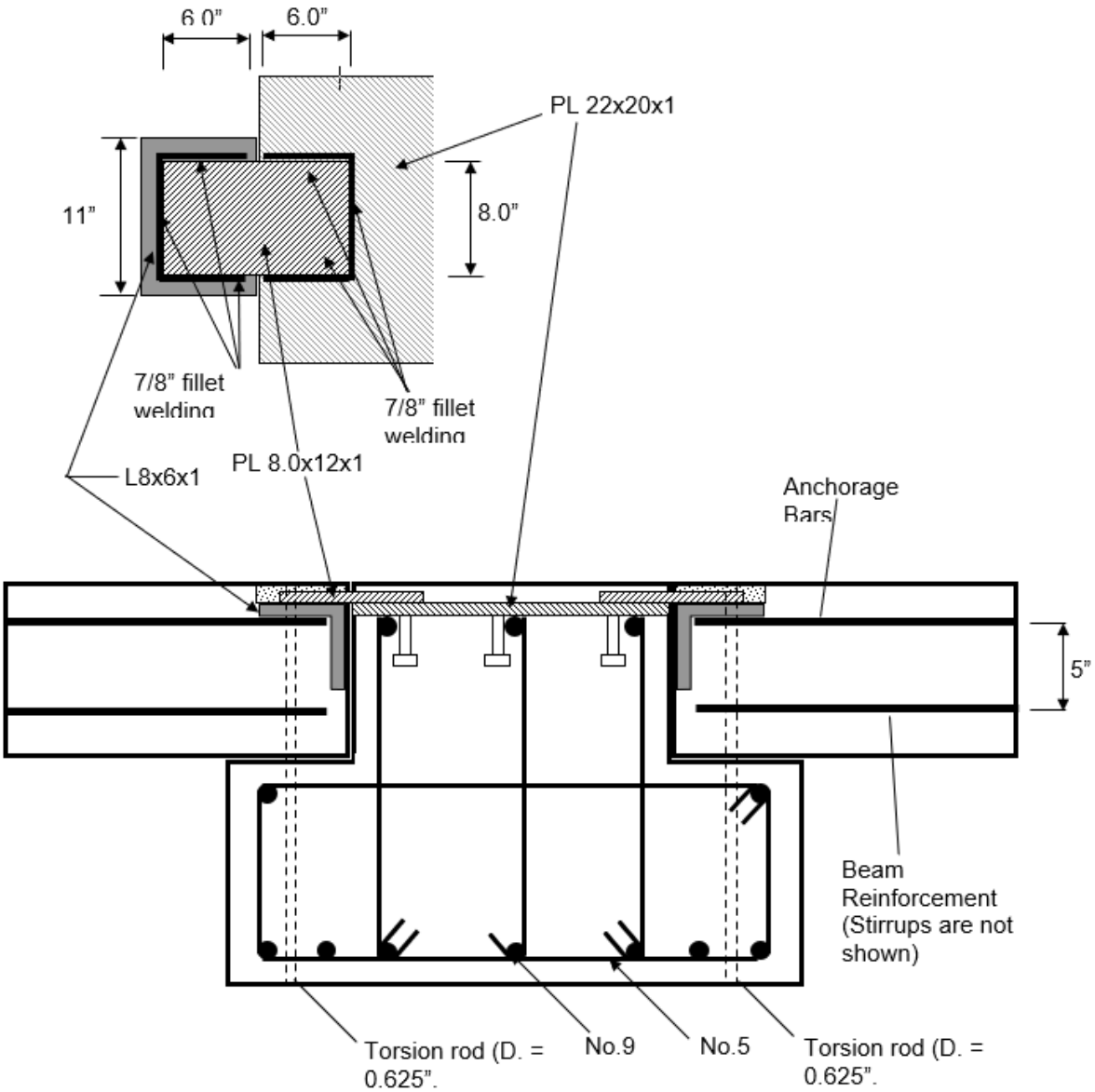

Fig. 1-3. Connection details (from Kim et al., 2009). All dimensions are shown in inches. 1.00 in = 25.4 mm.

1.2. Connection Concepts

Motivated by the performance of the precast concrete assemblies tested during NIST Phase I, which was marginally adequate to resist disproportionate collapse, new alternative connection concepts were developed by NIST in coordination with an industry review committee of PCI members. These alternative connection concepts were intended to provide improved robustness over the connection examined in NIST Phase I by addressing the vulnerabilities in the welded link plates identified during testing. To improve the robustness of the spandrel beam-to-column connections under column removal scenarios, three strategic modifications to the prototype design were targeted:

1. Reduce the eccentricity in the tensile force transfer mechanism,
2. Protect the welded bars by designing the link plates as fusing elements, and
3. Replace the welded link plate with a non-welded field connection.

Five connection concepts, shown in Fig. 1-4b to Fig. 1-4f, were conceived and selected for further experimental study. These connection concepts are summarized as follows:

- A ***modified link plate*** connection concept, shown in Fig. 1-4b, that represents the minimum modifications to the prototype connection tested in NIST Phase I necessary to improve its robustness under a column removal.

- A ***threaded rod*** connection concept, shown in Fig. 1-4c, that is somewhat like the connection tested by Quiel et al. (2015) and previously developed Precast Seismic Structural Systems (PRESSS) connection details (French et al., 1989a; French et al., 1989b; Palmieri et al., 1996) but with the threaded rod passing through the center of the spandrel beam rather than through corbels. This concept eliminates field welding but requires coupling threaded rods on-site to create continuity in the tension load path through the column.

- A ***grouted bar*** connection concept, shown in Fig. 1-4d, that is similar in connecting strategy to the UMn-TCY (University of Minnesota tension/compression yielding) detail tested by Palmieri et al. (1996) as part of the PRESSS program. Continuity bars are passed from one spandrel beam into the adjacent spandrel beam through ducts in the column. The ducts running through the beams and columns are grouted to complete the connection. This concept eliminates field welding but requires field grouting.

- A ***bar coupler*** connection concept, shown in Fig. 1-4e, that uses mechanical couplers to enforce continuity of beam anchorage reinforcement through the column. This connection eliminates field welding, but requires pockets in the column, containing the mechanical couplers, that must be field grouted.

- A ***bolted*** connection concept, shown in Fig. 1-4f, that is based on the connection concept featured in Figure B.7.2 of the PCI Design Handbook 8th Ed. (PCI 2017). This connection uses ductile anchor bolts or rods to connect the beams to couplers embedded in the column.

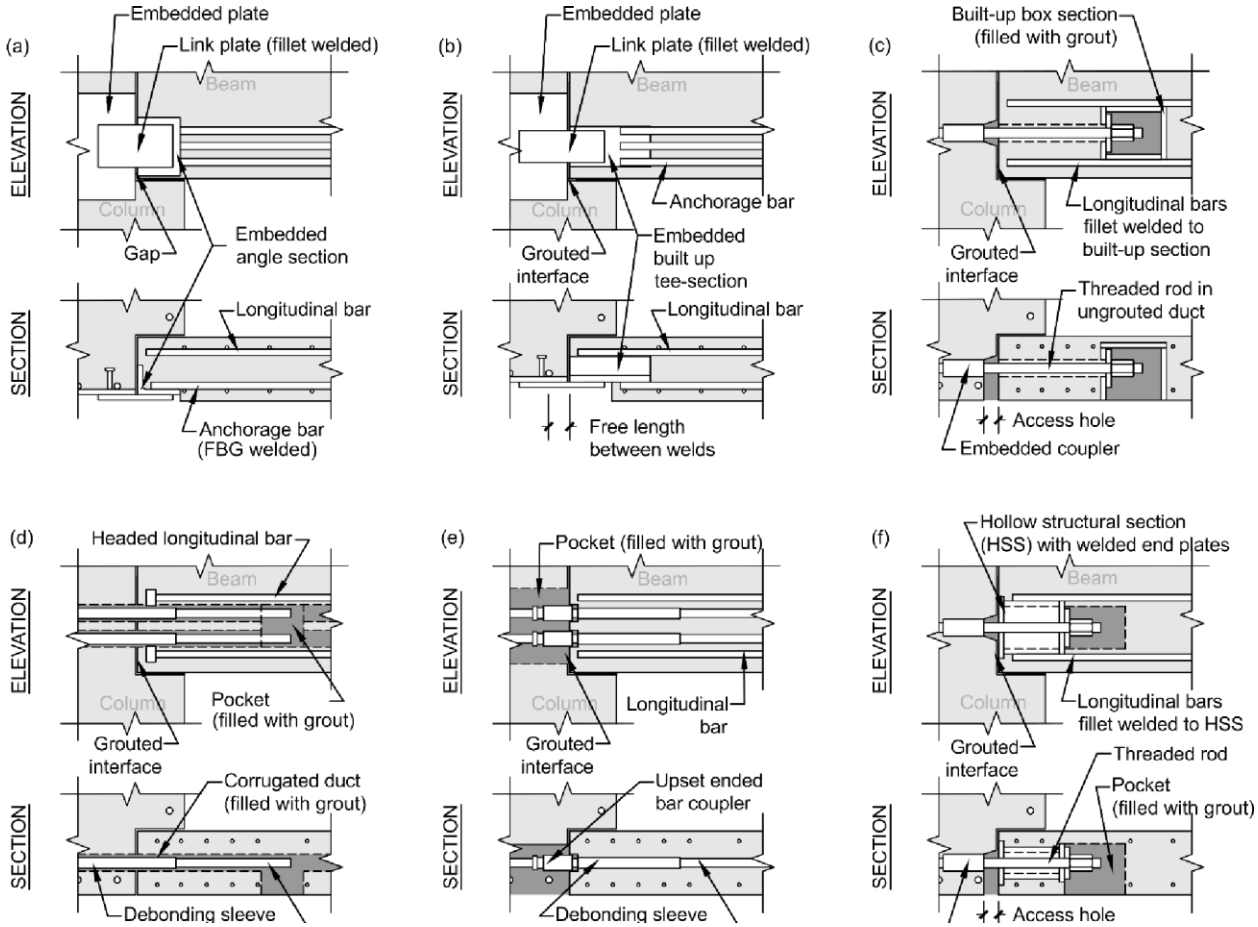

Fig. 1-4. Connection concepts: (a) prototype (b) modified link plate (c) threaded rod (d) grouted bar (e) bar coupler (f) bolted.

1.3. Test Setup and Loading

The NIST Phase II experimental program, conducted at five-eighths scale, was used to evaluate and compare the robustness of the five selected alternative connection concepts. The experimental program also provided data for validation of computational models that can be used in assessing the robustness of precast concrete moment frame buildings that incorporate the alternative connection types.

The precast concrete moment connection assemblies considered in this study were extracted from the prototype perimeter moment frames in the north-south directions at the third-story level, as is indicated in Fig. 1-5. Each assembly consisted of a central column connected to two spandrel beams. The spandrel beams extend to mid-span of the prototype bay width in each direction, corresponding to the assumed inflection points of the spandrel beams under a central column removal scenario.

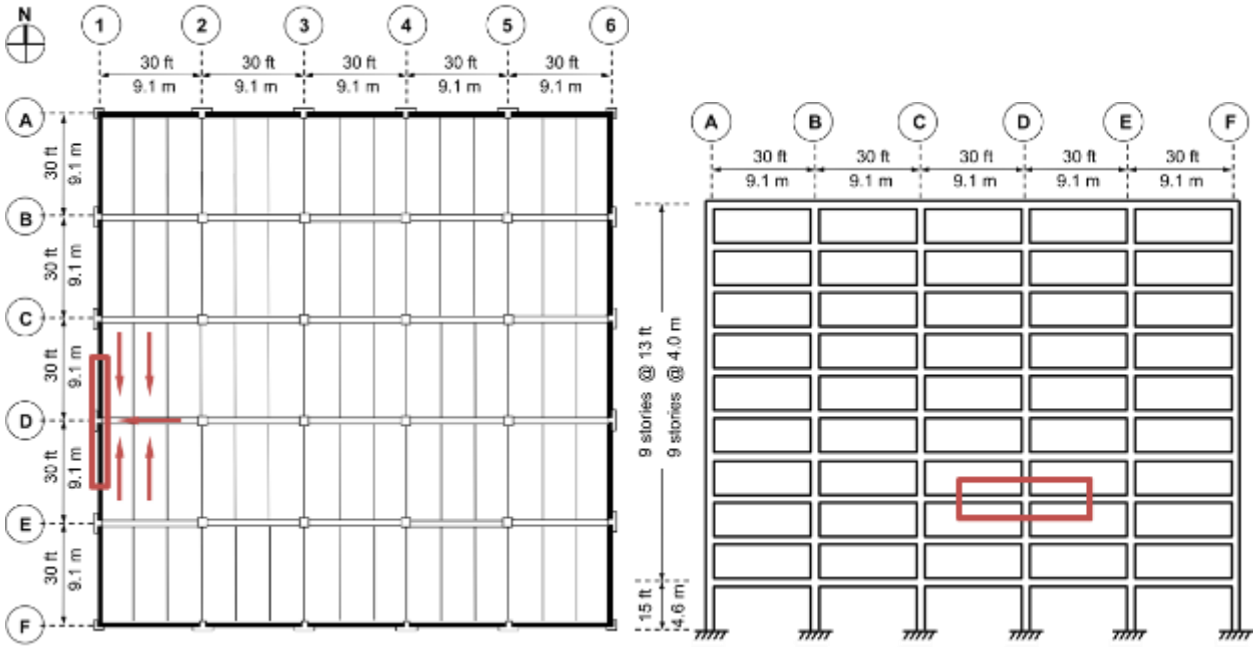

Fig. 1-5. Precast concrete moment frame assembly extracted from prototype precast SDC D building (adapted from Main et. al. 2015).

The experimental setup, schematically shown in Fig. 1-6, constrains the center column to move vertically in the plane of the frame while permitting in-plane rotation. Vertical loads are applied by a hydraulic actuator aligned with the centerline of the spandrel beams, with horizontal movements of the actuator prevented by lateral bracing. The ends of the half-bay spandrel beams are supported at their mid-depths by large-diameter steel pins that span steel cradles. The cradles sit on a low-friction surface that permits the cradles to move laterally in the plane of the frame. In this configuration, the connections and the beams will be subjected to flexural and shear forces while torsional and axial forces will be minimized. In a column loss scenario in the prototype building, the beams and columns in the moment frame would be subjected to a combination of axial, flexural, and torsional forces, and the performance of the frame would depend on the complex interaction of the resulting stresses. However, the flexural resistance of the beam-to-column connections will play a dominant role in preventing collapse, and providing alternative connection details with enhanced flexural performance will represent a major step forward in developing precast concrete building systems with improved robustness against disproportionate collapse.

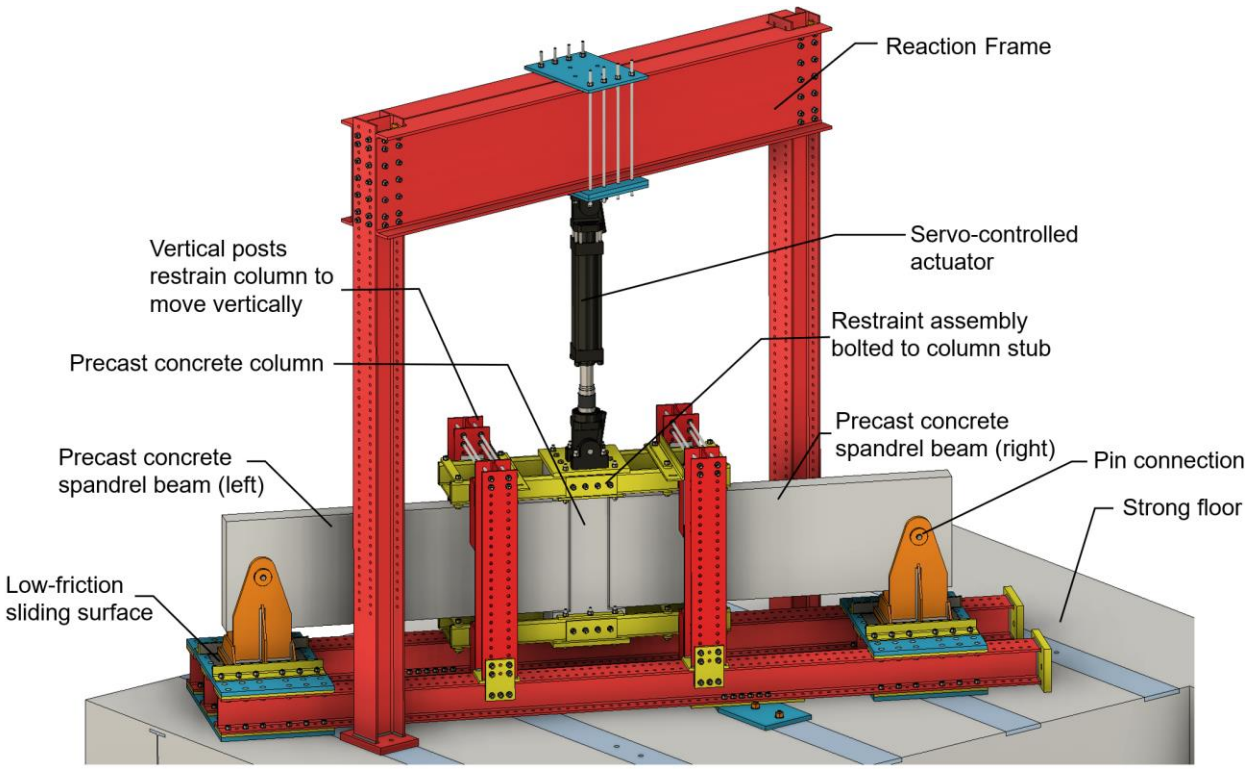

Fig. 1-6. Schematic of experimental setup.

1.4. Design of Test Specimens

To estimate the forces applied to the beam-to-column connections under a notional column removal, the loads acting on an exterior column (Column D1, see Fig. 1-5) were calculated for the third floor under the ASCE 7 load combination for extraordinary events, $P = 1.2\,D + 0.5\,L + A_k$, where D is dead load, L is live load, and A_k is the load or load effect resulting from the extraordinary event (ASCE 2022). When calculating P, note that A_k equals 0 because the load effect resulting from the extraordinary event (i.e., column loss) is physically considered in the testing by pushing down the unsupported column. Omitting A_k also is consistent with the provisions of the *ASCE/SEI Standard for Mitigation of Disproportionate Collapse Potential in Buildings and Other Structures* (ASCE/SEI 76-23), Section C5.3.8.5, for evaluation of the potential for disproportionate collapse using the Alternative Load Path Analysis method.

In this analysis, the following three contributors to the flexural forces at the beam-to-column connections were considered:

1. The gravity loads collected by the inverted-tee members directly applied to the joint above the removed column,
2. The self-weight of the spandrel beams applied as a distributed load along the length of the beam, and
3. The self-weight of the column.

The magnitudes of these quantities are calculated in detail in Thonstad et al. (2025). The concrete was specified as normal-weight concrete, with a unit weight of 150 lbf/ft^3 (2403 kg/m^3) The unit weight of reinforced concrete components was taken as 155 lbf/ft^3 (2483 kg/m^3) to account for an average of 1.5 % steel per unit volume.

Figure 1-7a, from Thonstad et al. (2025), shows the idealized plastic beam mechanism that was analyzed under the dynamically amplified gravity loads to estimate the forces at the beam-to-column connection under a sudden exterior column loss in the prototype structure. It is assumed in this analysis that plastic hinges form in the beam at the beam-ends (i.e., at the beam-to-column connections) per the design intent. The reduced span length L_r = 28.17 ft (8.585 m) used in calculating the assembly's shear and moment diagrams, was determined by subtracting the distance between the column pockets of 22.0 in = 1.83 ft (559 mm = 0.559 m) from the nominal span between column centerlines of 30.0 ft (9.10 m). Were these calculations being done by a practitioner as part of designing a building, it is anticipated that (after designing the connections for these loads) a non-linear static analysis of the building would be conducted with the as-designed connections to assess whether the connections were sufficient to arrest disproportionate collapse. Within the scope of the NIST Phase II research, the experimental testing is used in lieu of this analysis, since the nonlinear behavior of the connections that would be needed to validate the finite element analysis is unknown.

The shear and moment diagrams of the extracted precast concrete moment frame under the amplified loads are shown in Fig. 1-7b and Fig. 1-7c, respectively.

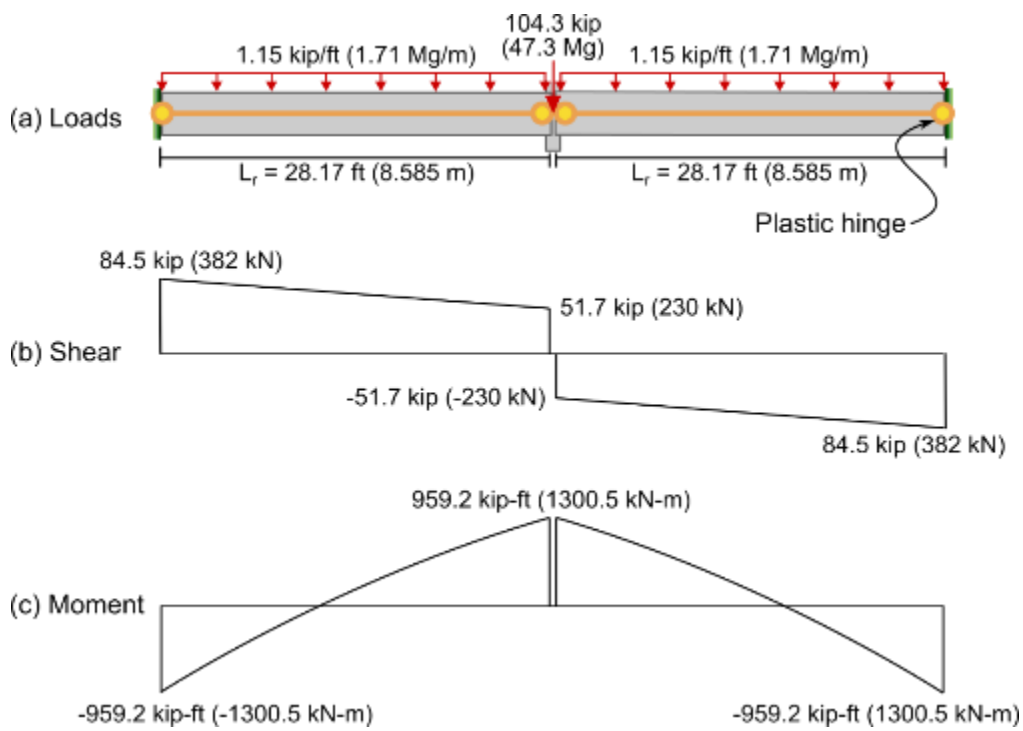

Fig. 1-7. Extracted portion of exterior precast concrete moment frame (note: spandrel beams of the tested assemblies extend to half the scaled span on either side of the column): (a) amplified gravity loads and assumed plastic mechanism (a) shear diagram for the spandrel beams (c) moment diagram for the spandrel beams.

Table 1-1, taken from Thonstad et al. (2025) and shown below for convenience, shows the shear and moment demands at the beam-to-column connections under the column heading "Column loss scenario" based on the assumed plastic mechanism shown in Fig. 1-7. Additionally, the design loads from Kim et al. (2009) based on the factored dead, live, and seismic forces are presented for comparison under the heading "Seismic and other loads".

Table 1-1. Summary of design forces for third floor spandrel beams (from Thonstad et al., 2025)

Load	Location	Seismic and other loads	Column loss scenario
Positive Moment, M_u^+	Support	702.0 kip-ft (951.8 kN-m)	-959.2 kip-ft (-1300.5 kN-m)
	Midspan	355.0 kip-ft (481.3 kN-m)	959.2 kip-ft (1300.5 kN-m)
Negative Moment, M_u^-	Support	-716.2 kip-ft (-971.0 kN-m)	-959.2 kip-ft (-1300.5 kN-m)
Shear, V	Support	124.6 kip (554.2 kN)[a]	84.5 kip (375.9 kN)

[a]Capacity design based on gravity loads on ledger beams and the reduced plastic capacity of the beam section, M_{pr} = 1016 kip-ft (1378 kN-m) (ACI 318-05 Section 21.3.4.1).

Table 1-1 shows that, after the consideration of the dynamic increase factor, the estimated moment demands on the precast concrete beam-to-column connections under an exterior column loss were larger [959.2 kip-ft / 716.2 kip-ft = 1.34 (1300.5 kN-m / 971.0 kN-m = 1.34)] than those than those arising from the combination of the factored dead, live, and earthquake loads by roughly 34 % for the prototype structure developed in NIST Phase I.

For the design of the NIST Phase II precast concrete beam-to-column connection test assemblies, both the beam dimensions and the estimated moment demand under a column loss scenario were scaled to five-eighths of those from the prototype structure to achieve geometric similitude. Thonstad et al. (2025) describes the procedures used in scaling the test assemblies in comprehensive detail. The dimensions of the scaled assembly are shown in Fig. 1-8, and the design moments for the scaled assemblies under notional removal of the central column are provided in Thonstad et al. (2025) and shown below in Table 1-2 for convenience.

Table 1-2. Summary of design forces for scaled spandrel beams

Load	Location	Prototype Magnitude	Scale Factor	Scaled Magnitude
Positive Moment, M_u^+	Support	959.2 kip-ft (1300.5 kN-m)	0.2441	234.1 kip-ft (317.4 kN-m)
Negative Moment, M_u^-	Support	-959.2 kip-ft (-1300.5 kN-m)	0.2441	-234.1 kip-ft (-317.4 kN-m)
Shear, V	Beam	84.5 kip (375.9 kN)	0.3906	33.0 kip (146.8 kN)

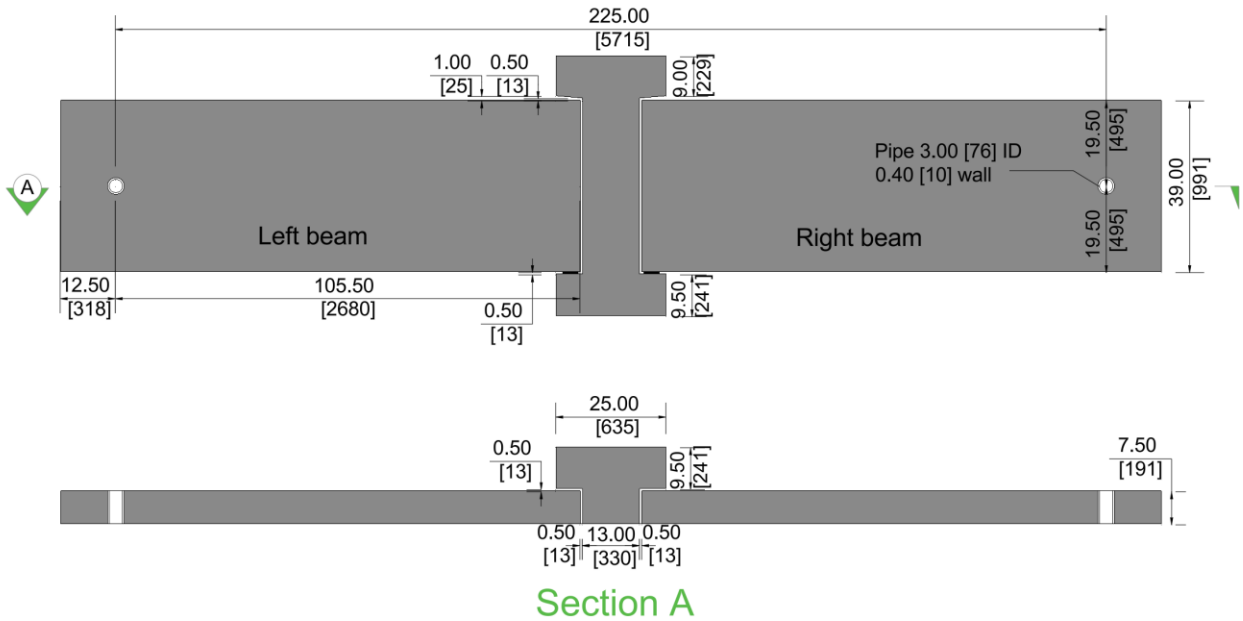

Fig. 1-8. Typical dimensions of scaled precast concrete moment connection assembly. All dimensions are in inch with mm equivalents in parenthetical brackets.

1.5. Report Outline

The remainder of this report is divided into the following sections:

- Section 1, this section, provides background information on the overarching long-term project from which the testing program presented in this report was derived.
- Section 2 describes the fabrication and erection of the precast concrete moment connection assemblies in the laboratory.
- Section 3 covers material properties.
- Section 4 describes the experimental results of each connection test, including the vertical load versus deflection response and the moment versus rotation behavior.
- Section 5 evaluates the structural robustness of each precast concrete moment connection concept against collapse under a middle column removal scenario.
- Section 6 provides a summary, conclusions, and recommendations.

2. Fabrication and Erection of Test Assemblies

2.1. Design Drawings

Thonstad et al. (2025) describes the development of the five connection concepts discussed in this report and provides detailed calculations and assumptions made during their design. The design drawings are included in Thonstad et al. (2025) but are also included in Appendix A of this report for convenience.

2.2. Fabrication of Test Specimens

The following section briefly describes and shows photographs of important components used for the fabrication of the test assemblies featuring the five connection concepts detailed in this report. Because the beams and columns were cast horizontally, the photographs presented in this section typically provide a top-down perspective. Photographs of the reinforcing steel in the column formwork before concrete was cast show the back of the column, which corresponds to the exterior face of the prototype building shown in Fig. 1-5 and is opposite to the front of the column, which is visible in Fig. 1-6.

All the precast concrete beams and columns were fabricated in a high-bay precast concrete production facility at Tindall Corporation in Petersburg, VA. The forms for the beams were made of steel and had wooden side rails. The forms for the columns were made of wood. The reinforcing steel for the columns was tied together using steel wire and then lowered into the forms. Similarly, the reinforcing steel and connection components for the beams were lowered into the forms. Figure 2-1 shows the reinforcing steel and formwork for an assembly beam and column prior to casting. Figure 2-2 shows an assembly beam and column after casting. The leadwires for strain gauges adhered to the reinforcing steel in the beams were wrapped in polyethylene to protect them from potential moisture exposure as the beams cured. The polyethylene and strain gauge wires are visible in Fig. 2-1 and Fig. 2-2.

(a) (b)

Fig. 2-1. An assembly (a) beam and (b) column before concrete was cast.

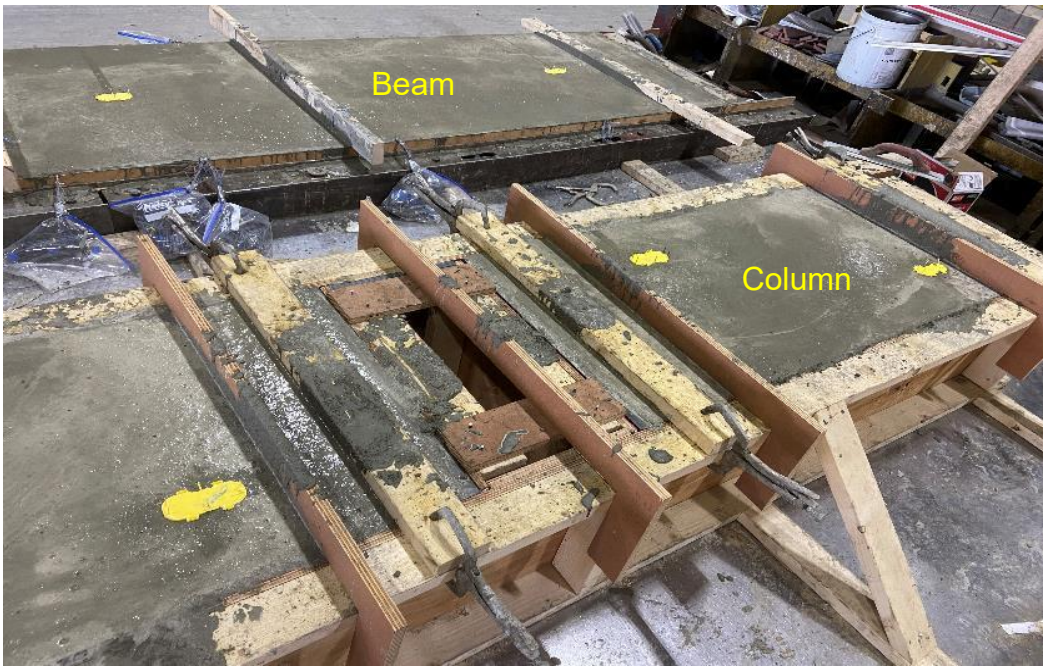

Fig. 2-2. An assembly beam and column after concrete was cast.

2.2.1. Threaded Rod

For the threaded rod connection assembly, threadbars passed through corrugated ducts in the beams and were coupled in the column with cylindrical bar couplers to make a moment-resisting connection. The couplers were embedded near the top and bottom of the column and were connected with 6.75 in (171 mm) long threadbars and tightened against a 0.50 in (13 mm) thick plate washer made from ASTM A36 (ASTM 2019) steel. Figure 2-3 shows the cylindrical bar couplers that were embedded in the column, and Fig. 2-4 shows the corrugated ducts through which the threadbars passed. Figure 2-4 also shows steel angles that were embedded in the beams at their corners to help prevent potential spalling and the subsequent loss of strength in the beam concrete as large bearing stresses developed with increasing connection rotation. The threadbars were anchored by hex nuts against built-up steel box sections that were embedded in the beams. As shown in Fig. 2-5, beam longitudinal reinforcement was welded to the tops and bottoms of the built-up sections. Axial forces in the threadbars were transferred to the beams through bearing of the built-up box sections against the beam concrete and through the steel reinforcement welded to the built-up sections.

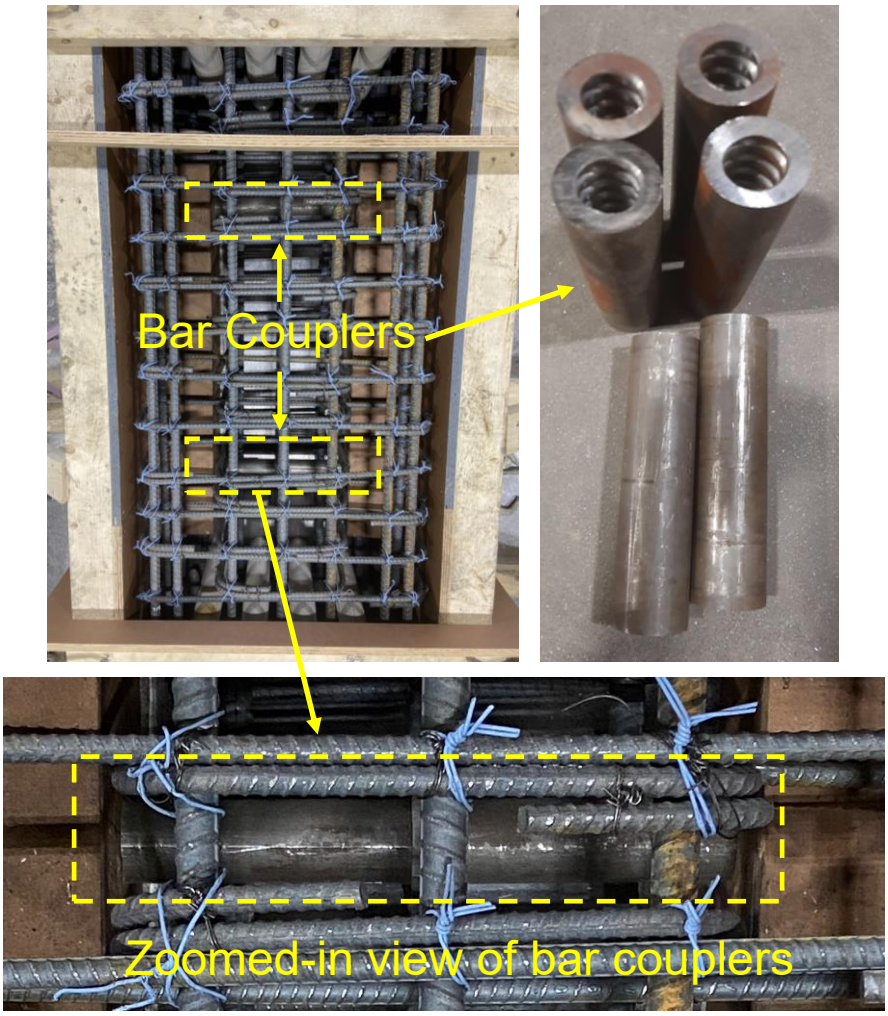

Fig. 2-3. Bar couplers embedded in the threaded rod connection assembly column.

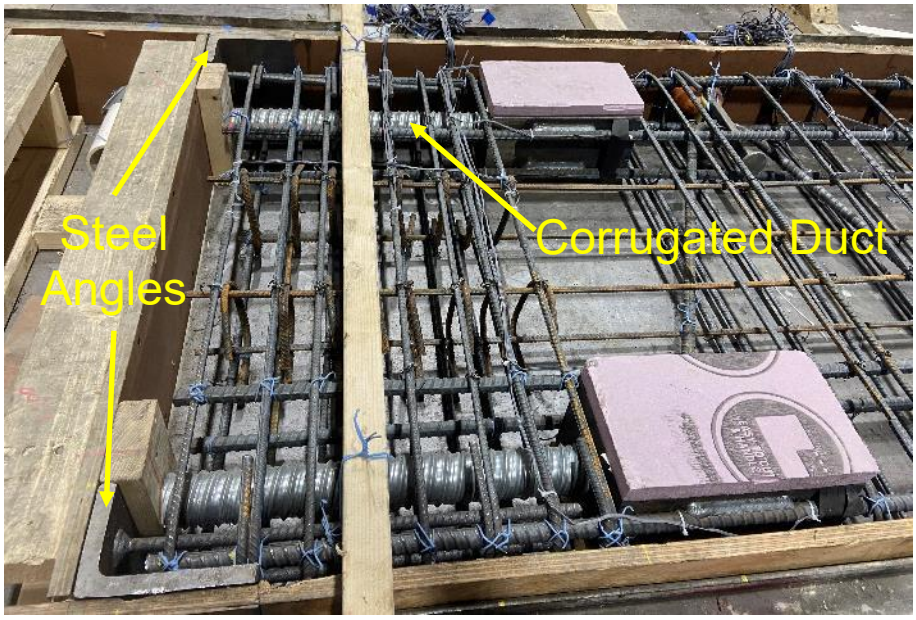

Fig. 2-4. Steel angles and corrugated duct in a threaded rod connection assembly beam.

Fig. 2-5. Built-up steel box sections with longitudinal reinforcement welded to their tops and bottoms.

2.2.2. Bolted

The bolted connection concept is similar to the threaded rod connection concept, with the main difference being the length of bar and the associated grade of steel that was used to connect the beams to the column. The bolted connection's anchor bolts were 17 in (432 mm) long and used a Grade 55 steel (i.e., steel with a minimum specified yield strength of 55 ksi), whereas the threaded rod connection's threadbars were 31 in (787 mm) long and used a Grade 150 steel (i.e., steel with a minimum specified tensile strength of 150 ksi). Because the lengths of the anchor bolts were shorter than those of the threadbars, a lower-strength ductile steel was necessary for the bolted connection to achieve the target rotational capacity of 0.04 radians (2.29°), which as described in the connection design report (Thonstad et al., 2025), was the target rotational capacity for all five connection assemblies.

The anchor bolts used for the bolted connection passed through steel hollow structural sections (HSS) embedded in the beams (Fig. 2-6). Steel plates were welded to the ends of the HSS, and each anchor bolt was anchored against an HSS by a hex nut on one end, while the other end terminated in coupling nuts embedded in the column. The coupling nuts, which were embedded near the top and bottom of the column, were held together by a 5.50 in (140 mm) long anchor bolt and tightened against a 1.00 in (25 mm) thick plate washer made from ASTM A36 steel, as shown in Fig. 2-7. Similar to the threaded rod connection, beam longitudinal reinforcement was welded to the top and bottom of the HSS to allow axial forces in the anchor bolts to be transferred to the beams (Fig. 2-6).

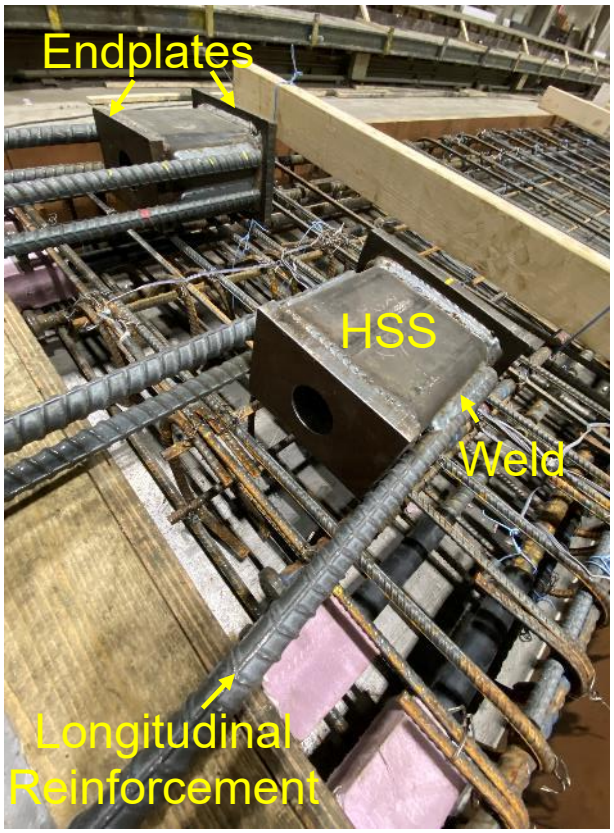

Fig. 2-6. HSS with plates welded to their ends and longitudinal reinforcement welded to the tops and bottoms of the HSS.

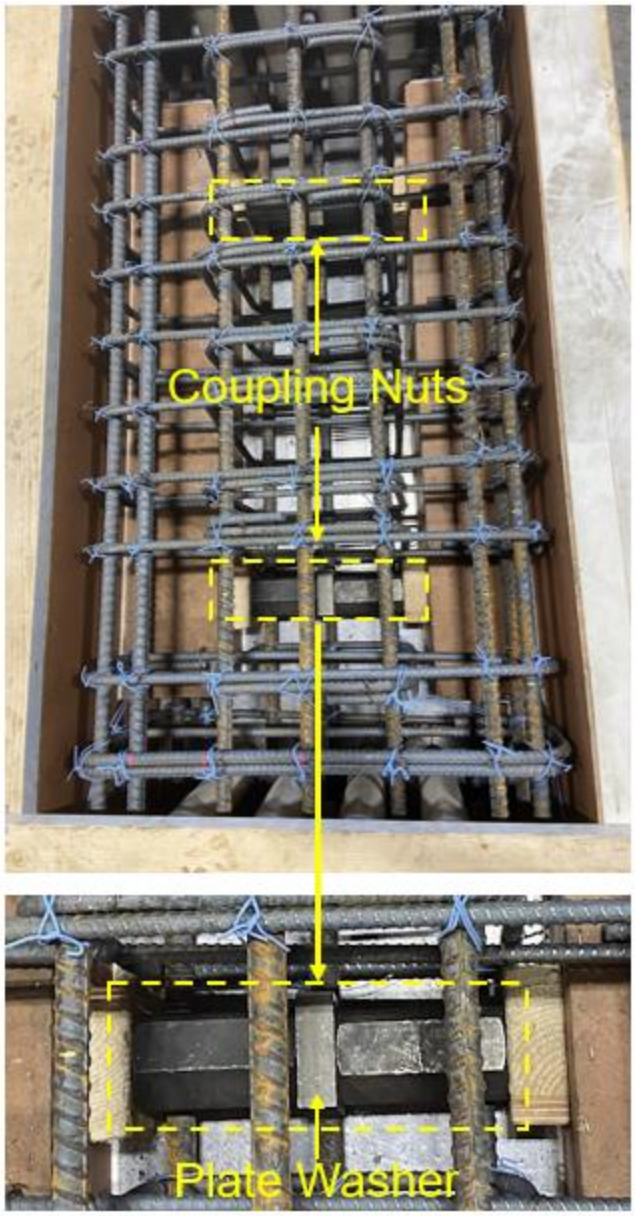

Fig. 2-7. Coupling nuts and plate washers embedded in the bolted connection assembly column.

2.2.3. Bar Coupler

For the bar coupler connection assembly, loose No. 7 link bars (couplers) with upset ends were used to connect the beams to the column. As shown in Fig. 2-8, the couplers consisted of two parts: 1) a deformed No. 7 steel reinforcing bar with both ends upset and 2) cylindrical steel collars with external threads that rotate independently from the reinforcing bar and are located at opposite ends of the reinforcing bar. As shown in Fig. 2-9, the column was fabricated with two blockouts near its top and bottom, which provided space to connect the couplers to the four 60 in (1524 mm) long No. 7 continuity bars protruding from each beam. The ends of the continuity bars that were protruding from the beams were also upset and had collars with

internal threads, which allowed them to thread into the collars with external threads to establish a moment-resisting connection. Each continuity bar had 7 in (178 mm) of its length debonded from the beam concrete using a debonding sleeve made from flexible polyvinyl chloride (Fig. 2-10). During production of the beams, the collars of the continuity bars were housed in foam, which created voids in the beam to recess the collars.

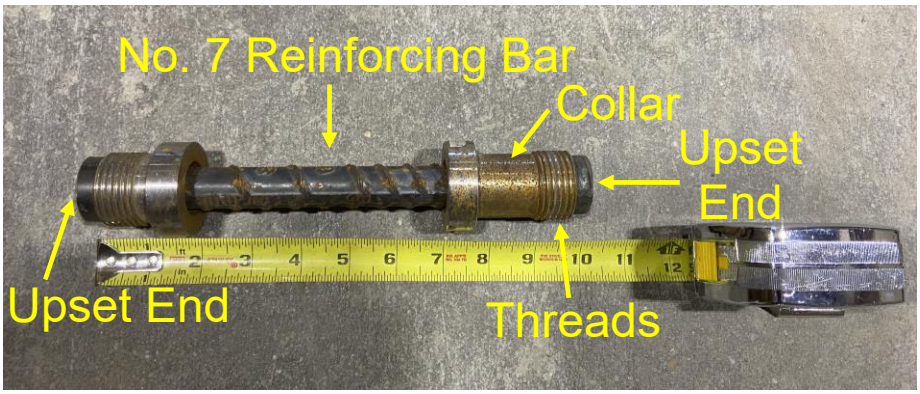

Fig. 2-8. No. 7 link bars (couplers) used in the bar coupler connection assembly.

Fig. 2-9. Back of the column with foam inserts (left) to create the column blockouts (right).

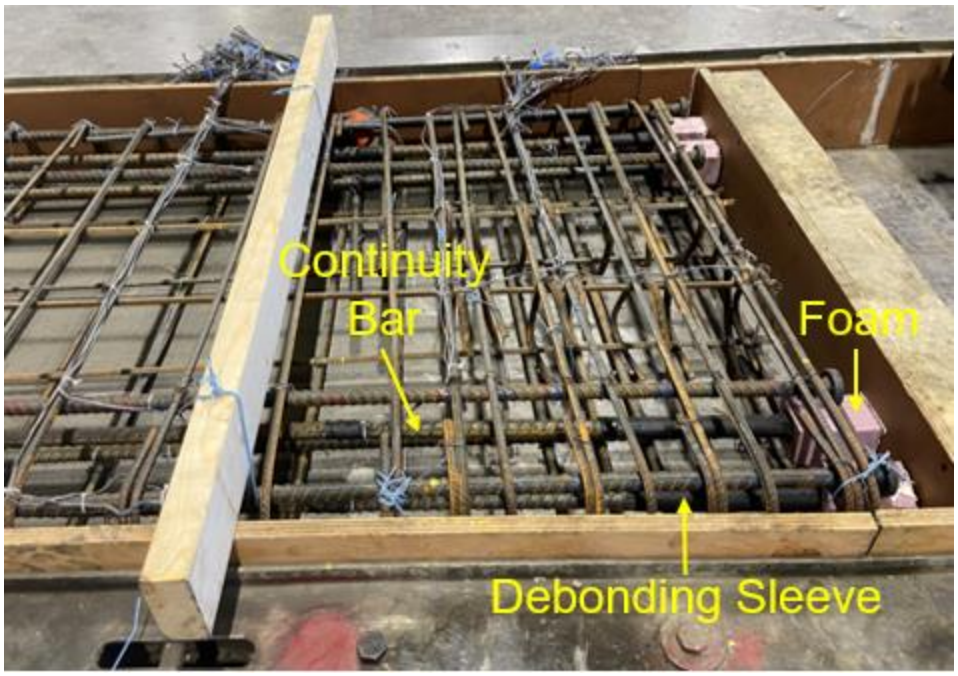

Fig. 2-10. Continuity bars with debonding sleeves and foam blockouts to create voids in the beams to recess the collars.

2.2.4. Grouted Bar

The moment connections for the grouted bar assembly were made by passing 56 in (1422 mm) long No. 7 continuity reinforcing bars from the right beam, through the column, and into the left beam via corrugated ducts. Handholes in both beams (four handholes in the right beam and two in the left beam) were used to pass the bars from the right beam into the left one. Figure 2-11 shows the right beam with annotations highlighting the corrugated duct and built-up wooden boxes used to create the hand holes. Once the grouted bars were centered on the width of the column during erection, the handholes, ducts in the beams and column, and interfaces between the beams and column, were grouted. Axial forces in the continuity bars were transferred to the beams through bond.

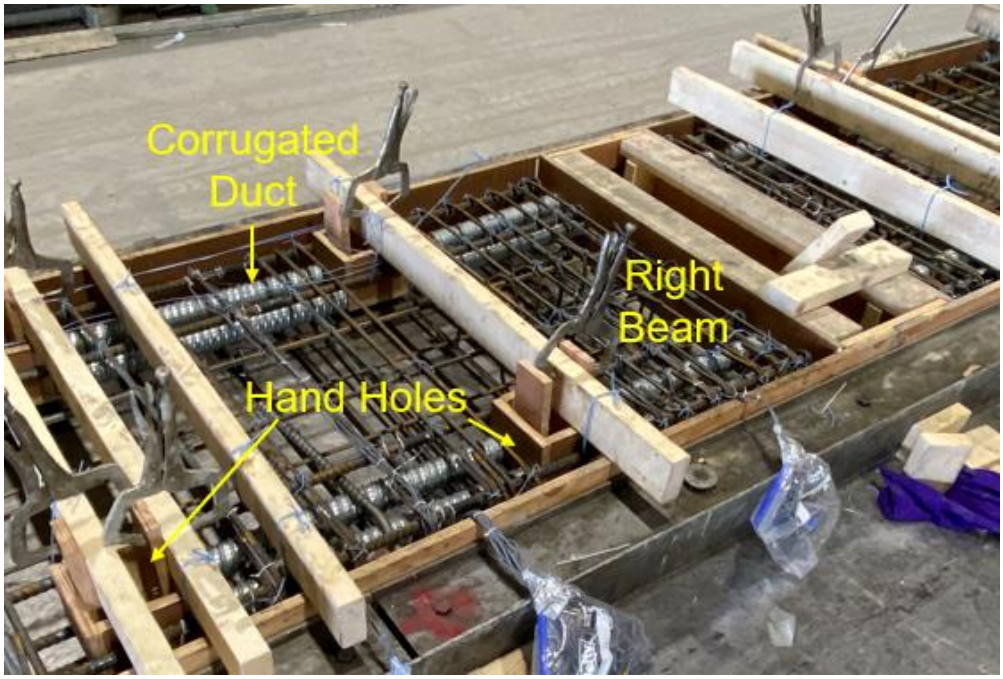

Fig. 2-11. Right beam of the grouted bar connection assembly with hand holes and corrugated duct.

2.2.5. Modified Link Plate

For the modified link plate connection, a moment connection was made in the laboratory by welding steel link plates protruding from one end of the beams (Fig. 2-12) to steel channels embedded near the top and bottom of the column. Before the beam concrete was cast, the link plates and three No. 7 anchorage bars were welded to steel channels embedded in the beams. The link plates and anchorage bars were welded to the same face of the steel channels to limit the eccentricity of the tensile force transfer between the beams and column (Fig. 2-13). The link plates were dog-bone-shaped, with ends that were wider than the middle section of the plates (Fig. 2-14). The dog-bone shape was chosen over conventional rectangular plates to encourage inelastic deformations to concentrate away from the welds and into the reduced-width section of the link plates. However, due to a fabrication error, welding occurred along the reduced-width section of the link plates. The excess axial restraint provided by these unintended welds concentrated axial deformations along only a small length of the reduced-width section at one end of the link plates (rather than along the full length of the reduced-width section, as intended), which hindered the ductility of the link plates and led to this connection not achieving the rotation for which it was designed.

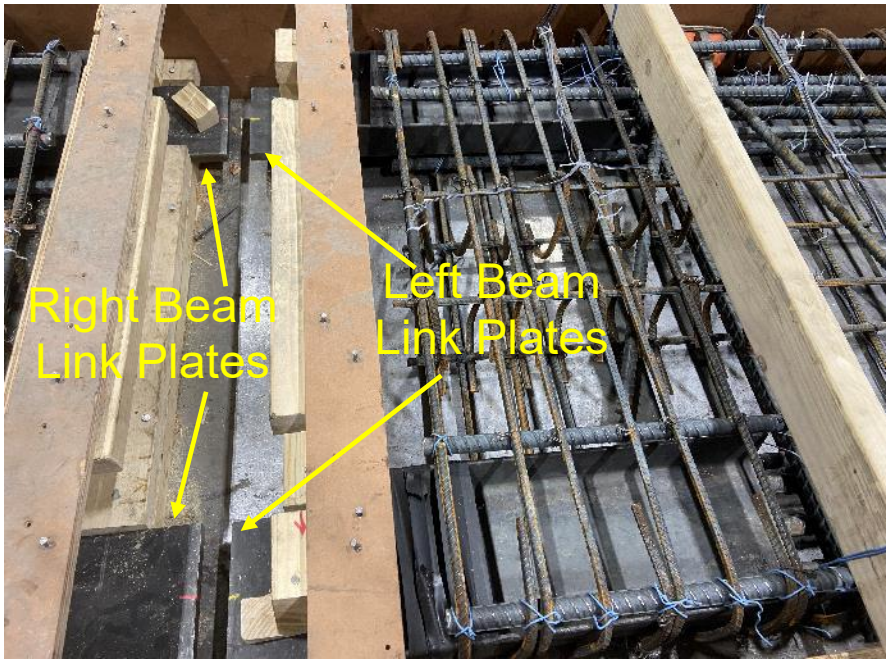

Fig. 2-12. Link plates protruding from the ends of the left and right beams.

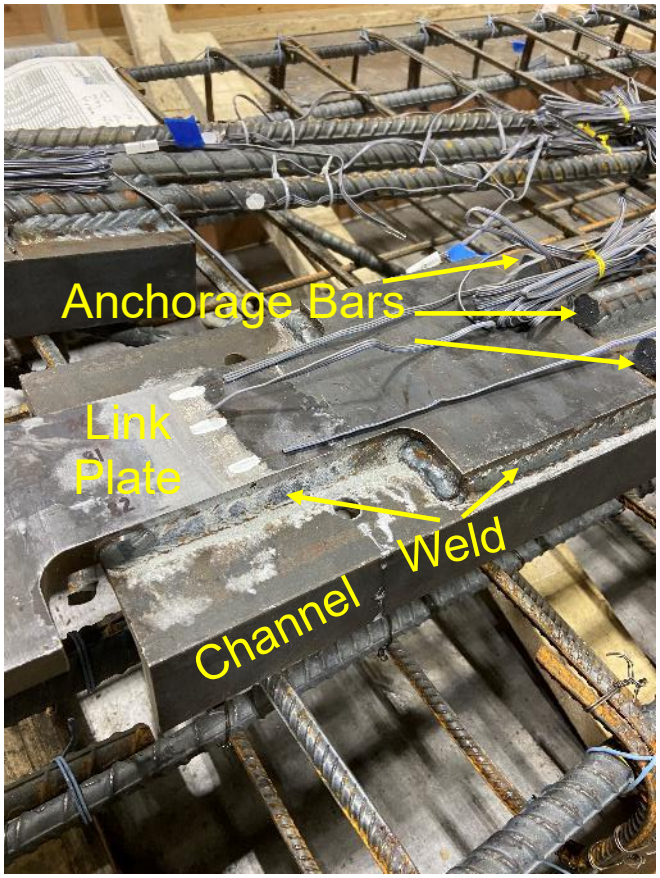

Fig. 2-13. Link plate and three anchorage bars welded to the same face of steel channel.

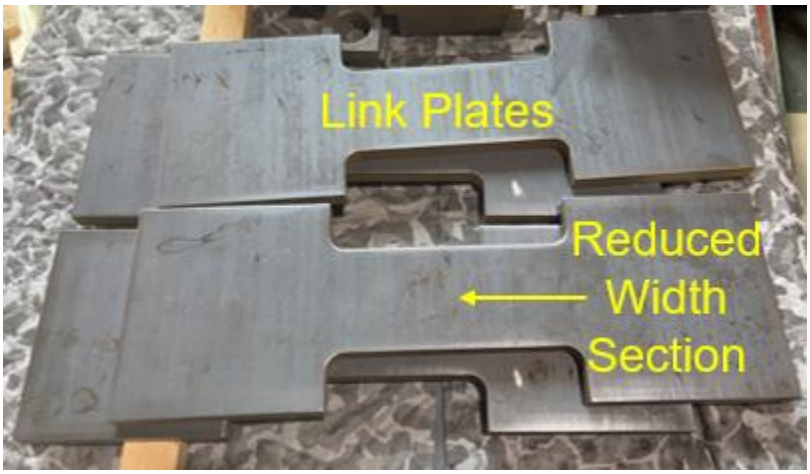

Fig. 2-14. Dog-bone shaped link plates used in the modified link plate connection assembly.

2.3. Instrumentation

A schematic of the instrumentation layout used for all five tests, including the location of each instrument, is shown in Fig. 2-15. Figure 2-16 shows photographs of each instrument type. The compressive force applied to the assemblies by the hydraulic actuator was measured using four through-hole (donut) load cells (LC01 – LC04), which were sandwiched between the steel plate embedded at the top of each respective concrete column and the steel plate bolted to the actuator [Fig. 2-16(c)]. Each load cell was preloaded in compression to approximately 15 kip (66.7 kN) to ensure it remained in compression for the duration of the test. The vertical displacement of the assembly was measured using 10 string potentiometers (D01 – D10) mounted to aluminum beams suspended above the assembly and oriented parallel to the length of the precast concrete beams [Fig. 2-16(a)]. Five inclinometers [Fig. 2-16(d)] were mounted to the front surface of the assembly, two on each beam and one centered on the column width (R01 – R05). The inclinometers measured the in-plane rotation of each precast component. Four linear variable inductance transducers [Fig. 2-16(b)] were mounted to each beam near its connection to the column, two on the top face and two on the bottom face of each beam (T01 – T08), to measure the axial elongation and contraction of the beams. Linear variable differential transformers [Fig. 2-16(e)] were used to measure the horizontal displacement of the steel cradles located at the pin-connected end of the beams (L11 and L12).

The uncertainty in measurements presented in this report was calculated in accordance with Taylor and Kuyatt (1994). Table 2-1 shows the estimated total expanded uncertainty of the measured forces, rotations, displacements, and strains, which was calculated using a coverage factor *k* of 2. The total expanded uncertainty was calculated by multiplying the combined standard uncertainty by the coverage factor *k*. A coverage factor of 2 was chosen to define an interval in which the measured value lies with a level of confidence of 95 %. The combined standard uncertainty, which is the estimated standard deviation of the measured value and accounts for both Type A and Type B uncertainties, was calculated using the root-sum-of-

squares method. The uncertainties in Table 2-1 apply to all the measurements presented in the subsequent experimental results section of this report (see Sec. 4).

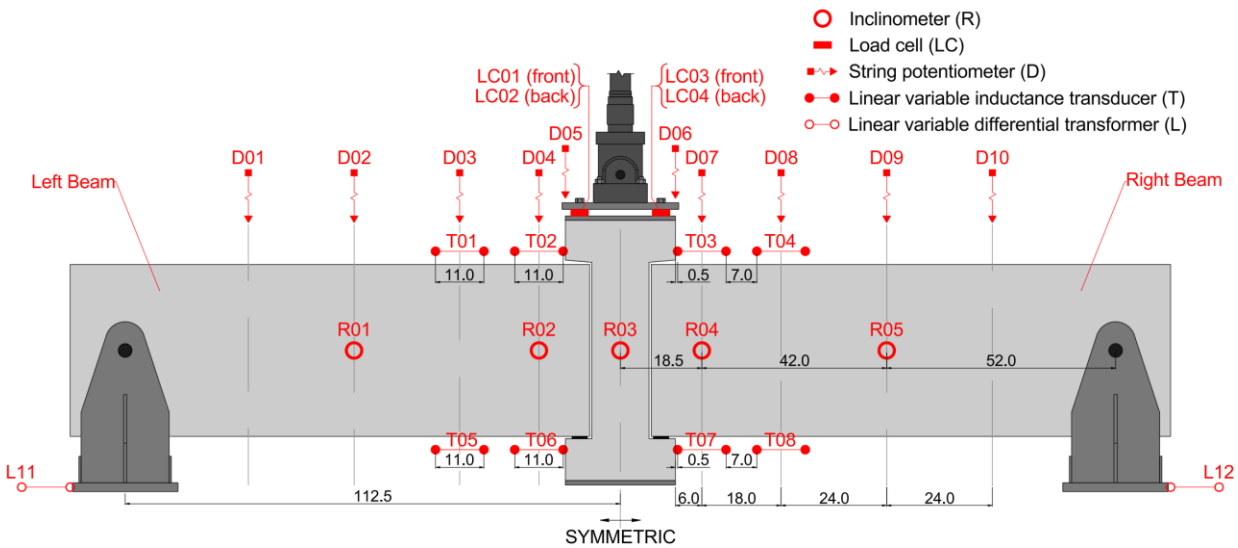

Fig. 2-15. A schematic of the instrumentation layout. Dimensions are specified in inches with mm equivalents in parentheses.

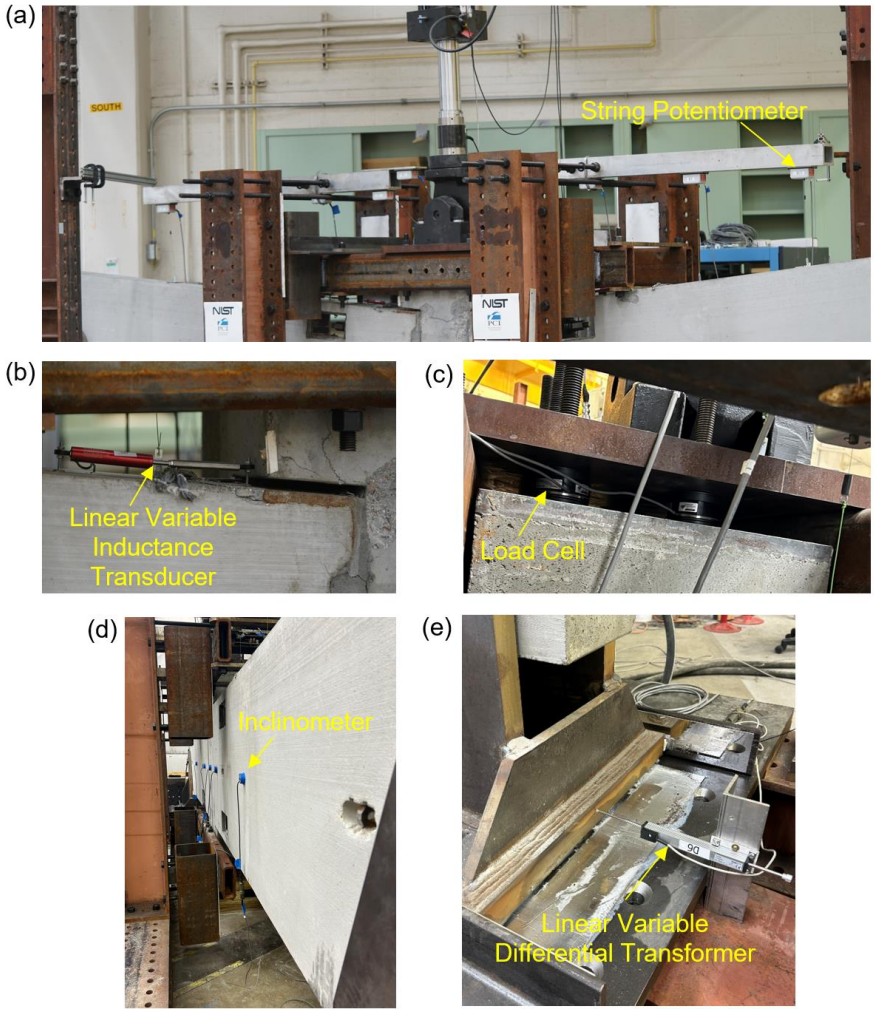

Fig. 2-16. Instrumentation: (a) string potentiometer; (b) linear variable inductance transducer; (c) load cell; (d) inclinometer; (e) linear variable differential transformer.

Table 2-1. Measurement uncertainty.

Measurand	Measurement device	Measuring range	Estimated expanded uncertainty
Distance	Tape measure	300 in (7620 mm)	0.06 in (1.5 mm)
Strain	Resistance-based strain gauge	~10 %	1 %
Vertical displacement	String potentiometer	20 in (508 mm)	0.08 in (2.0 mm)
Horizontal displacement	Linear variable differential transformer	4 in (102 mm)	0.02 in (0.51 mm)
Horizontal displacement	Linear variable inductance transducer	2 in (51 mm)	0.01 in (0.25 mm)
Rotation	Inclinometer	± 10 ° (± 0.175 rad)	0.05 ° (0.00087 rad)
Compressive force	Load cell	190 kip (845 kN)	1.5 kip (6.7 kN)
Moment	Derived quantity	1670 kip-ft (2264 kN-m)	14.1 kip-ft (19.2 kN-m)

Additional through-hole load cells were used for the threaded rod and bolted connection assemblies to measure the axial force in the respective threadbars and anchor bolts. Spherical washers were used between the nuts and load cells to compensate for any lack of

perpendicularity in the bearing surfaces. Figure 2-17 shows the load cells and spherical washers.

Fig. 2-17. Load cells and spherical washers used for the (a) threaded rod and (b) bolted connection assemblies.

In addition to the instrumentation shown in Fig. 2-16, electrical resistance foil-type strain gauges were adhered to the surfaces of the reinforcing steel embedded in the beams and to the surfaces of selected steel components. The strain gauges were applied to reinforcing steel embedded in the beams while at Tindall Corp. and prior to casting the concrete. For the modified link plate assembly, strain gauges were adhered to the steel link plates and anchorage bars embedded in the beams before the concrete was cast, and strain gauges were adhered to the embedded column channels in the laboratory after the concrete had cured. For the threaded rod assembly, strain gauges were adhered to the surface of the top and bottom sides of the threadbars, 4.50 in (114 mm) from their ends which were embedded in the column. For the bar coupler assembly, strain gauges were adhered to the surface of the top and bottom sides of the upset-ended No. 7 link bars at their mid-length. Schematics showing the locations of the strain gauges for all five assemblies are provided in Appendix B.

2.4. Laboratory Constructability

The following section presents a comparison of the constructability of all five connections, highlighting the advantages and disadvantages that were found during their assembly. Although the dimensions of the tested assemblies were scaled to five-eighths of those of the prototype building from which they were derived, product and erection tolerances do not scale, and thus care should be taken when interpreting observations about constructability in the laboratory.

The threaded rod connections were made by first fully recessing the threadbars into the beams until one end of the threadbars contacted the back plate of the built-up box sections that were embedded in the beams (Fig. 2-18). Once the beam ends were resting on the bearing pads in the side column pockets, the threadbars were connected by hand with the cylindrical bar couplers embedded in the column with occasional use of a strap wrench. The connections were

completed by threading a hex nut on the end of each threadbar, as shown in Fig. 2-19, and then dry packing the interface between the beams and column with a cementitious non-shrink grout.

The threaded rod connections were easy to make, largely due to the coarse threads of the threadbars (two threads per 1.0 in (25 mm) of length) which made them easy to thread into the cylindrical bar couplers that were embedded in the column. The 31 in (787 mm) length of the threadbars, coupled with their nominal diameter of 1.0 in (25 mm), made them flexible and easy to maneuver, which facilitated aligning them to mate with the cylindrical bar couplers. No field welding was required to make the connections.

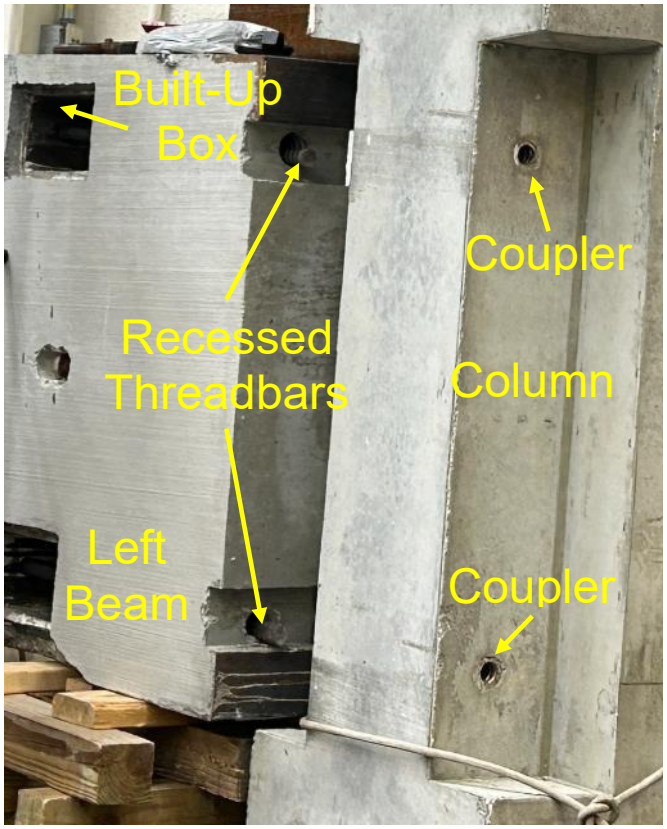

Fig. 2-18. Threadbars recessed in the left beam before they are threaded into the couplers in the column.

Fig. 2-19. Hex nut threaded on the end of a threadbar.

The anchor bolts used for the bolted connections had finer threads (six threads per 1.0 in (25 mm) of length) compared to those of the threadbars, which made them susceptible to damage during fit-up and difficult to thread smoothly and fully into the coupling nuts embedded in the column. For comparison, Fig. 2-20 shows a close-up view of the anchor bolt and threaded rod threads. The shorter length of the anchor bolts, 17.0 in (432 mm), coupled with their larger diameter, 1.50 in (38 mm), made them difficult to maneuver to make the connections. A tap and die were used to clean the threads of the nuts and anchor bolts, respectively, to ensure that the pair could be threaded during assembly. A pipe wrench was needed to thread the anchor bolts into the coupling nuts, as the coupling nuts may have slightly shifted during casting, resulting in the bottom anchor bolts being inclined from horizontal and skewed out of the plane of the connection. Similar to the threaded rod connection assembly, no field welding was required to make the connections.

(a) (b)

Fig. 2-20. Close-up view of the (a) anchor bolt and (b) threadbar threads.

Due to the shifts of the coupling nuts during casting, a different approach than was used for the threaded rod connections was used to make the bolted connections. To connect the left beam to the column, the anchor bolts were first threaded into the coupling nuts embedded in the column using a pipe wrench. Next, the beam was laterally shifted until its end was resting on the bearing pad inside the column pocket, with care taken to ensure that the anchor bolt threads were not damaged as the anchor bolts passed through the HSS embedded in the beam. Figure 2-21 shows this approach. A similar approach was used to make the right beam connections, except that a section of the endplate welded to the HSS embedded near the bottom of the right beam had to be cut away to accommodate the out-of-plane skewness of the anchor bolt (Fig. 2-22). With a section of the endplate removed, the beam could be moved

laterally into the column pocket without interference from the anchor bolts. The connections were completed by threading a hex nut on the end of each anchor bolt, as shown in Fig. 2-23, and then dry packing the interface between the beams and column with cementitious nonshrink grout.

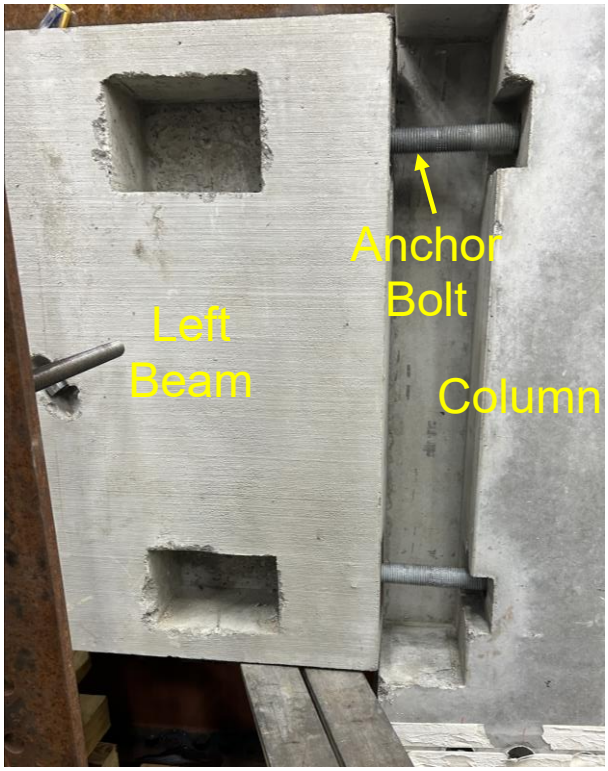

Fig. 2-21. Left beam being shifted to the right after the anchor bolts were threaded into the coupling nuts embedded in the column.

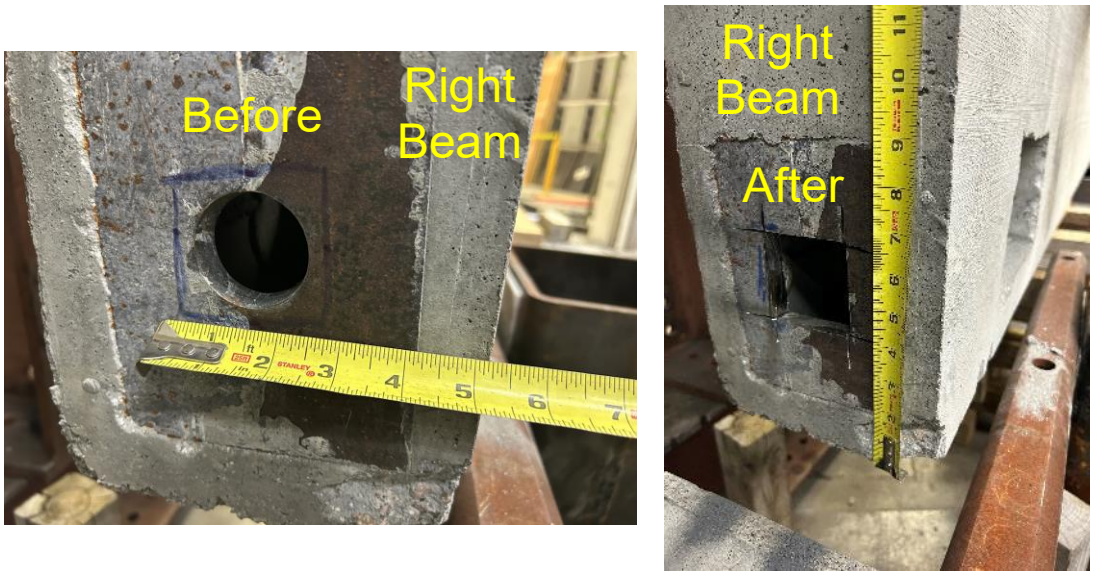

Fig. 2-22. Before (left) and after (right) a portion of the endplate at the bottom of the right beam was cut and removed.

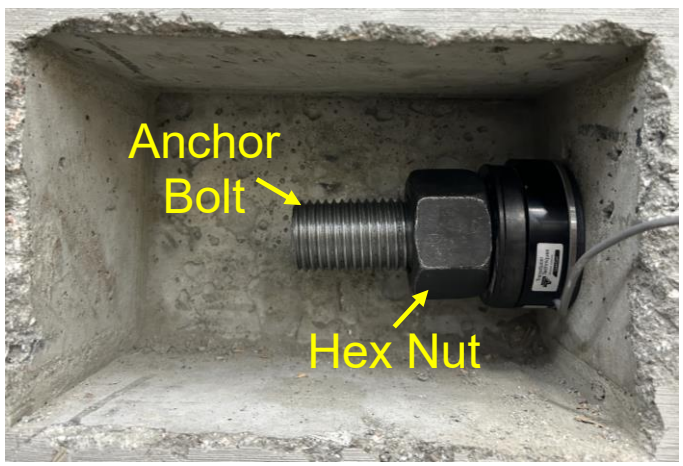

Fig. 2-23. Hex nut threaded on the end of an anchor bolt.

The bar coupler connection used No. 7 reinforcing bar couplers that were 10 in (254 mm) in length and made from ASTM A706 Grade 80 (ASTM 2016) steel. As shown in Fig. 2-24, the couplers consisted of two parts: 1) a steel reinforcing bar with both ends upset and 2) a cylindrical steel collar with external threads that rotates independently from the reinforcing bar, one at each end of the reinforcing bar. Once the beam ends were resting on the bearing pads inside the column pockets, the reinforcing bar couplers were inserted into the blockouts at the front of the column and threaded with the collars containing internal threads, which were protruding from one end of each beam (Fig. 2-25). The connections were hand-tightened to a snug fit condition per the manufacturer's specifications. After the connections were made, the top and bottom column blockouts housing the connections and the gaps between the beam-to-column interfaces were filled with a flowable grout using a hand-operated grout pump (Fig. 2-26).

Fig. 2-24. Reinforcing bar coupler used to make the bar coupler connections.

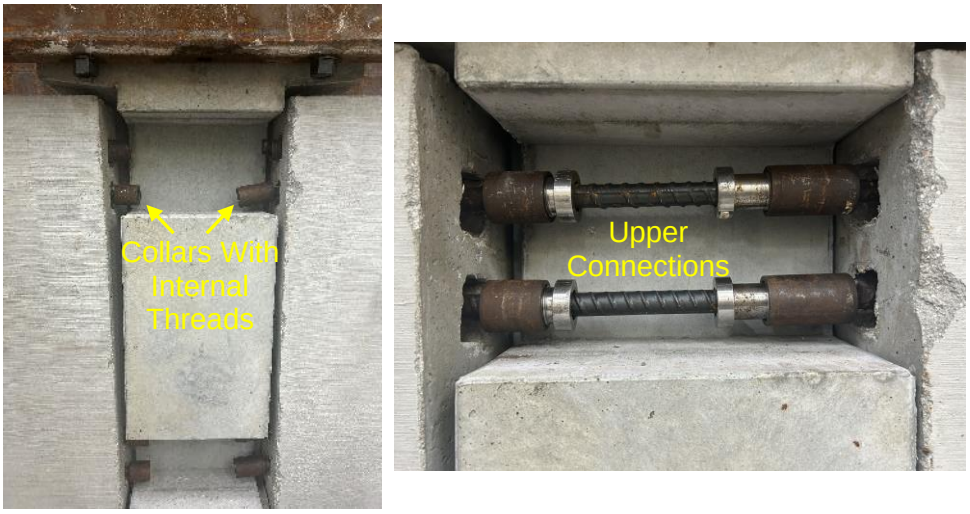

Fig. 2-25. The collars protruding from the beams (left) and the upper two connections (right).

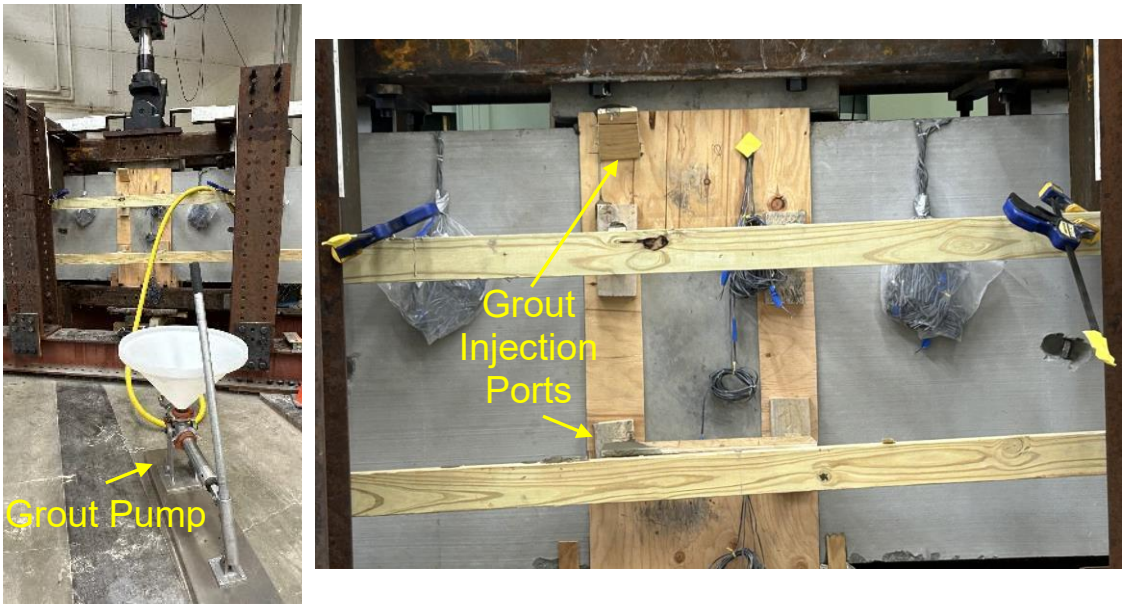

Fig. 2-26. Grout pump (left) and locations of grout injection ports (right) used for the bar coupler connection assembly.

The bar coupler connections were simple to make and did not require the use of field welding. However, the grouting operation was more complex than for the threaded rod and bolted connections, since the bar coupler connection required pumping of a flowable grout instead of hand-tamping of drypack grout. Additionally, the grouting operation required supplementary formwork, which would inevitably increase costs related to material and labor were this connection to be put into practice. Tight fabrication and assembly tolerances were required for this design, since the connection components needed to bridge the gap between the beams, and the rigidity of the reinforcing bar couplers with their threaded ends did not allow for much deviation from level to ensure that the connections could thread properly.

The grouted bar connection required the most complex grouting operation of the five tested connections. Prior to grouting, the four No. 7 ASTM A706 Grade 80 continuity bars used for the connection were wrapped at their midlength with a 21.0 in (533 mm) long debonding sleeve made from flexible polyvinyl chloride. The bars were then slid into their respective corrugated ducts in the right beam until the bars spanned the hand holes located near the midlength of the beam (Fig. 2-27). Once the beam ends were resting on the bearing pads inside the column pockets, the bars were slid by hand from the right beam, through the column, and into the left beam until they were centered on the width of the column (Fig. 2-28). The bars were placed on top of wooden shims in the ducts to ensure that they were centered on the diameters of the ducts. Formwork was then attached to the assembly so that the six hand holes, beam and column ducts, and beam-to-column joints could be filled with a flowable grout.

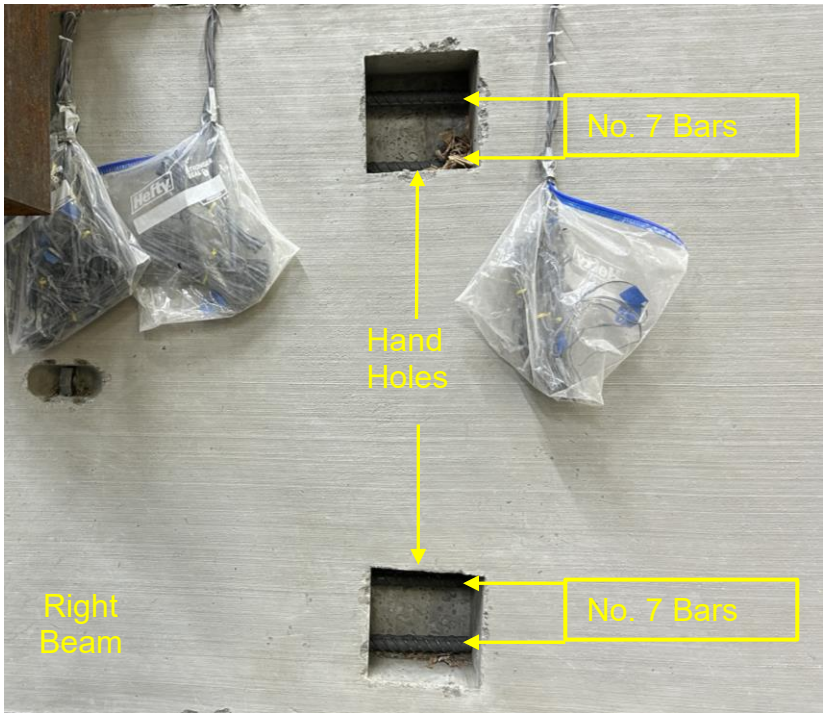

Fig. 2-27. Continuity bars spanning the hand holes near the midlength of the right beam.

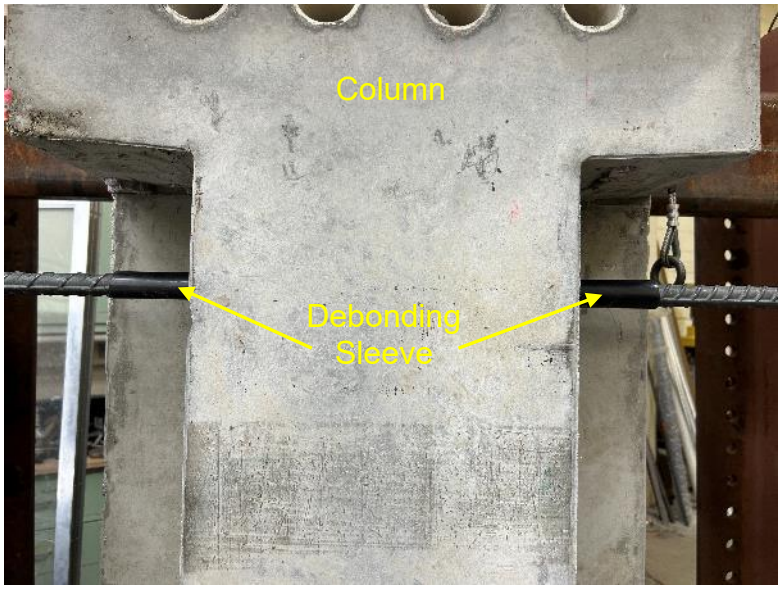

Fig. 2-28. Continuity bar with debonding sleeve and continuity bar centered on the column width.

The complexity of the grouting operation for the grouted bar connection arose because the grout needed to travel both horizontally and vertically to fill the voids. A multi-purpose electric pump was used instead of a hand pump to achieve a greater grout flow rate, which helped ensure that the grout remained workable through the duration of the grouting operation.

The modified link plate connection was the only connection that required welding in the laboratory. Once the beam ends were resting on the bearing pads inside the column pockets, the link plates were fillet welded to the steel channels embedded in the column. Because the link plates extended from the beam ends at an angle (i.e., the front and back faces of the link plates were not parallel to the front and back faces of the beams), the link plates did not contact the embedded column channels on all three edges where the welds needed to be laid (Fig. 2-29). As needed, steel filler/backing plates were inserted between the link plates and column channels to fill the gap between them, and then welded to the column channels to ensure proper transfer of tensile force through the link plates during the pushdown test. Of the four link plates, only the bottom left link plate did not require a plate to fill the gap behind it (Fig. 2-30). The filler plates had thicknesses of either 0.38 in (10 mm) or 0.25 in (6.4 mm). The size and thicknesses of the plates complied with the structural welding code (AWS 2020).

The steel filler plates were initially held in place by magnets before being tack welded and then fillet welded to the embedded column channels. An up-close view of the link plates after welding is shown in Fig. 2-31. After welding was completed, the interface between the beams and column was dry-packed with a nonshrink cementitious grout.

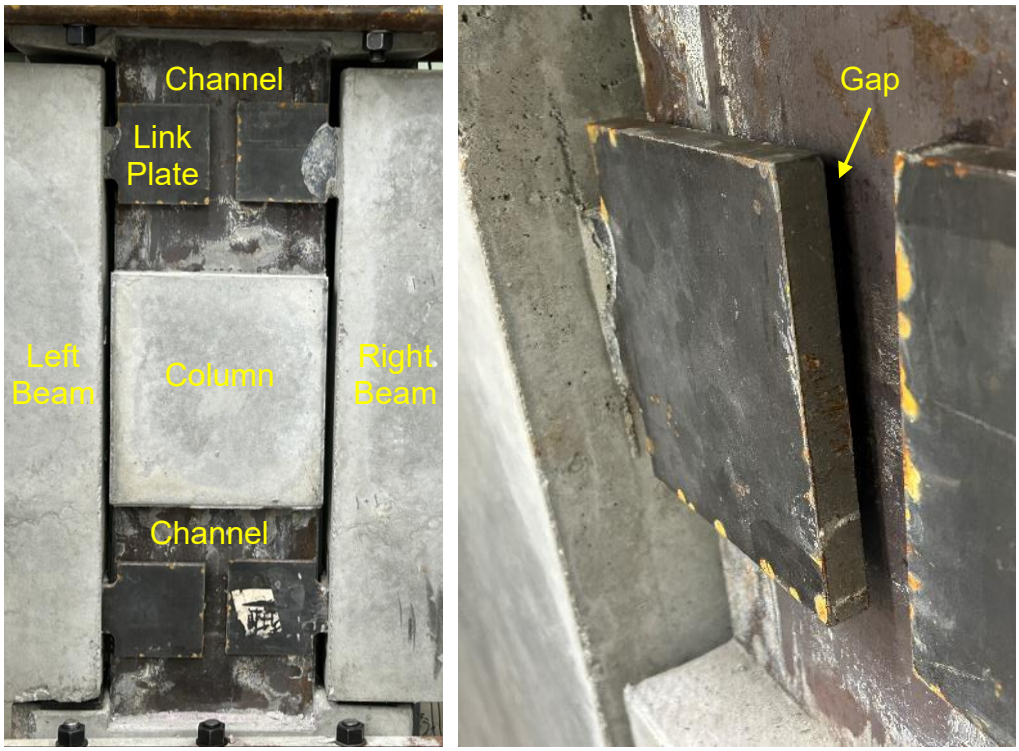

Fig. 2-29. Gap between the steel link plates and embedded column channels before insertion of filler plates.

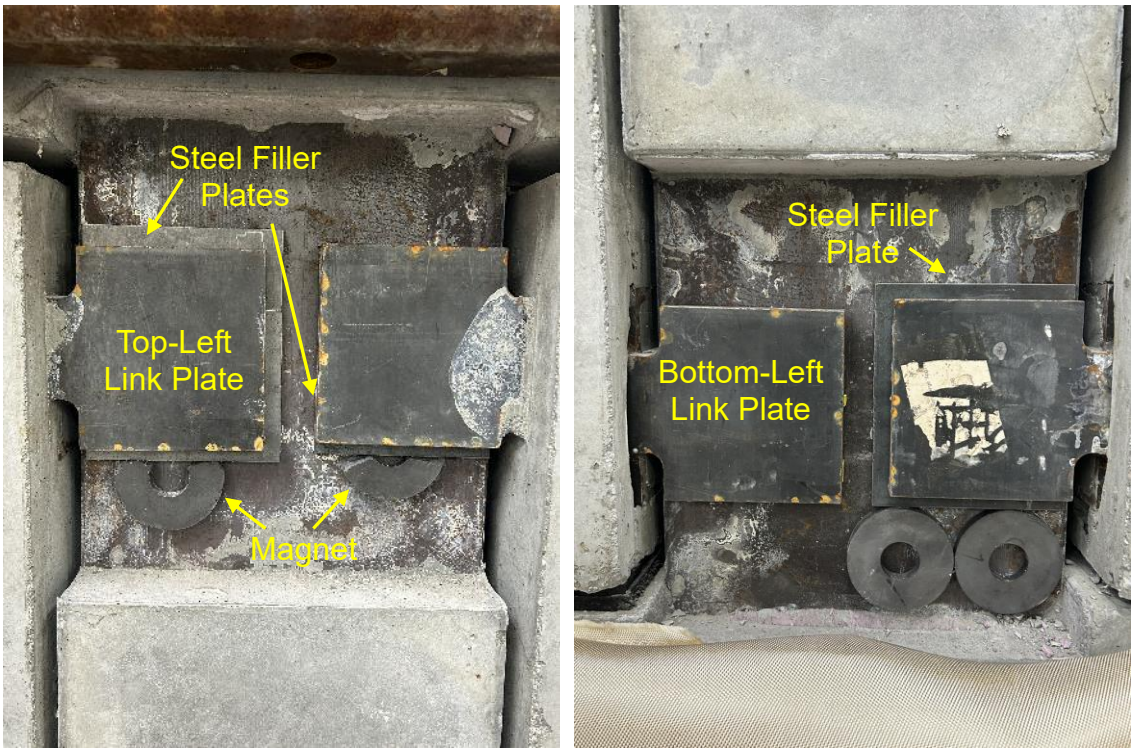

Fig. 2-30. Steel plates to fill the gap between the link plates and embedded column channels

Fig. 2-31. Top (left) and bottom (right) link plates after welding

3. Mechanical Properties

3.1. Concrete

The material properties of the assembly concrete were measured through testing of standard 4 in × 8 in (0.102 m × 0.203 m) cylinders obtained from the concrete used to cast the beams and columns. All the beams and columns were cast consecutively on the same day and came from the same concrete batch and mixture design. A total of 64 cylinders were obtained from the concrete batch, which allowed for uniaxial compressive strength, modulus of elasticity, and splitting tensile strength tests to be conducted. Testing was conducted in compliance with ASTM C39/C39M-21 (ASTM 2021b), ASTM C469/C469M-22 (ASTM 2022), and ASTM C496/C496M-17 (ASTM 2017) to obtain uniaxial compressive strength, modulus of elasticity, and splitting tensile strength of the concrete cylinders, respectively. Compressive strength testing was conducted at 28 days after the cast. A suite of all three tests was conducted on the same day as each connection assembly test.

A nominal concrete compressive strength of 6000 psi (41.4 MPa) was specified for the design of the precast beams and columns, with an expected concrete compressive strength of 1.5 × 6000 psi = 9000 psi (62.1 MPa). The 28-day compressive strength of the concrete, tested in accordance with ASTM C39-21 and based on six breaks of 4 in × 8 in (0.102 m × 0.203 m) cylinders, was 8050 psi ± 200 psi (55 MPa ± 1.4 MPa), where 8050 psi (55 MPa) is the mean value, μ of the six break strengths and 200 psi (1.4 MPa) is the expanded uncertainty, U. The expanded uncertainty is calculated using Eq. (3.1):

$$U = \frac{ku_c}{\sqrt{n}} \tag{3.1}$$

where k is the coverage factor calculated using the two-tailed Student's t distribution to define an interval in which the true mean lies with a level of confidence of 95 %, u_c is the sample standard deviation, and n is the number of independent measurements. All the material strength values in this section (Sec. 3) are presented in the form $\mu \pm U$.

Table 3-1 provides the measured compressive strength of the concrete from each connection assembly based on at least six cylinder breaks conducted on the same day as each connection test. The coefficient of variation shown in subsequent tables is calculated by multiplying the sample standard deviation, u_c by 1.96 (z-score that is used to create an interval on which the true population mean lies with a confidence of 95 %) and then dividing that value by the mean, μ.

Table 3-1. Compressive strength of concrete.

Connection (Days After Cast)	Compressive Strength, psi (MPa)	Coefficient of Variation, %
Threaded rod (404)	9380 ± 190 (65 ± 1.3)	3.8
Bolted (497)	9140 ± 350 (63 ± 2.4)	7.2
Bar Coupler (568)	9400 ± 240 (65 ± 1.7)	4.8
Grouted Bar (658)	9510 ± 190 (66 ± 1.3)	3.7
Modified Link Plate (910)[a]	9050 ± 660 (62 ± 4.6)	11.5

[a]Based on five cylinder breaks

Table 3-2 provides the measured compressive modulus of elasticity of the concrete from each connection assembly based on three tests conducted on the same day as each connection test.

Table 3-2. Modulus of elasticity of concrete.

Connection (Days After Cast)	Compressive Modulus of Elasticity, ksi (GPa)	Coefficient of Variation, %
Threaded rod (404)	5250 ± 660 (36.2 ± 4.6)	9.9
Bolted (497)	5170 ± 410 (35.6 ± 2.8)	6.3
Bar Coupler (568)	5405 ± 80 (37.3 ± 0.6)	1.2
Grouted Bar (658)	4910 ± 690 (33.9 ± 4.8)	11.1
Modified Link Plate (910)	5080 ± 200 (35 ± 1.4)	3.1

Table 3-3 provides the measured splitting tensile strength of the concrete from each connection assembly based on three tests conducted on the same day as each connection test.

Table 3-3. Splitting tensile strength of concrete.

Connection (Days After Cast)	Splitting Tensile Strength, psi (MPa)	Coefficient of Variation, %
Threaded rod (404)	920 ± 160 (6.3 ± 1.1)	13.7
Bolted (497)	910 ± 280 (6.3 ± 1.9)	24.3
Bar Coupler (568)	890 ± 390 (6.1 ± 2.7)	34.6
Grouted Bar (658)	880 ± 400 (6.1 ± 2.8)	35.9
Modified Link Plate (910)	609 ± 202 (4.2 ± 1.4)	26.2

3.2. Steel Connection Components

Tensile tests of the steel connection components used for the threaded rod connection, bolted connection, and grouted bar connection assemblies were conducted. All these tensile tests were performed using a servohydraulic load frame equipped with hydraulic wedge grips. The bars were tested in force control at a rate of 25.0 kip/min (111 kN/min) up to approximately half the minimum specified yield strength of the respective bars. Loading was then continued in displacement control at a rate of 0.25 in/min (6.4 mm/min) until bar rupture. An extensometer

with an 8 in (0.203 m) gauge length was attached near the mid-length of each bar to measure strain. Yield strength was calculated using the 0.2% offset method, and stress was calculated by dividing the force measured by the in-line load cell of the load frame by the cross-sectional area specified in the corresponding ASTM standard.

The 1.00 in (25 mm) diameter (nominal) Type II high-strength threadbar used for the threaded rod connection was produced by Dywidag Systems International in accordance with ASTM A722/A722M-18 (ASTM 2018), and had a minimum specified yield strength and tensile strength of 120 ksi (827 MPa) and 150 ksi (1034 MPa), respectively. Two 31 in (787 mm) long threadbars were tested, which corresponded to the length of the bars used in the experimental assembly tests. For these tests, the extensometer was removed at 5% strain to avoid damaging it in the event of sudden fracture. For stress calculations, the cross-sectional area was taken as 0.85 in^2 (548 mm^2), per ASTM A722/A722M-18. Figure 3-1 shows the stress versus engineering strain curves from the tests of two threadbars.

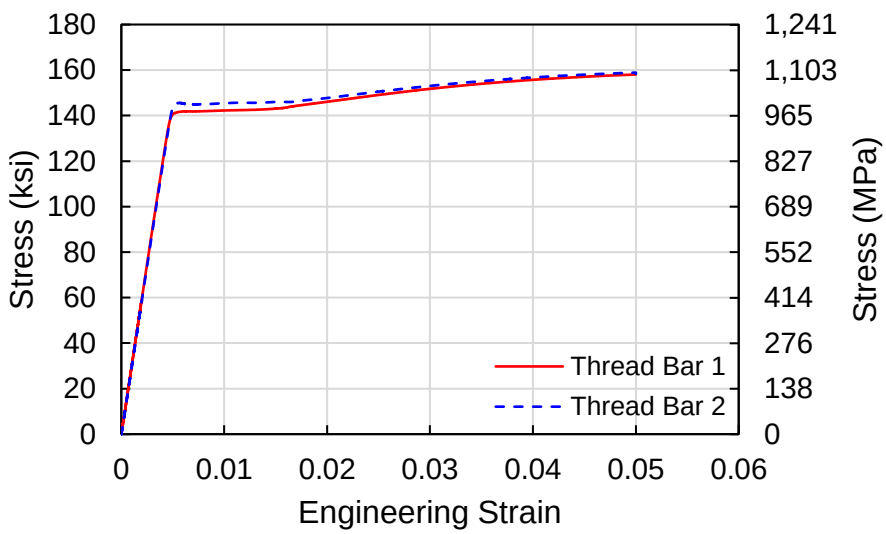

Fig. 3-1. Stress versus engineering strain curves based on two tension tests of threadbars.

The bolted connection used Grade 55 1.50 in (38 mm) diameter (nominal) fully threaded anchor bolt produced in accordance with ASTM F1554-20 (ASTM 2020b). The anchor bolts had a minimum specified yield strength of 55 ksi (379 MPa) and a specified tensile strength between 75 ksi (517 MPa) and 95 ksi (655 MPa). Two 17 in (432 mm) long anchor bolts were tested, which corresponded to the length of the bolts used in the experimental assembly tests. For stress calculations, the cross-sectional area was taken as 1.405 in^2 (906 mm^2), per ASTM F1554-20 (ASTM 2020b). Figure 3-2 shows the stress versus engineering strain curves from the tests of two anchor bolts.

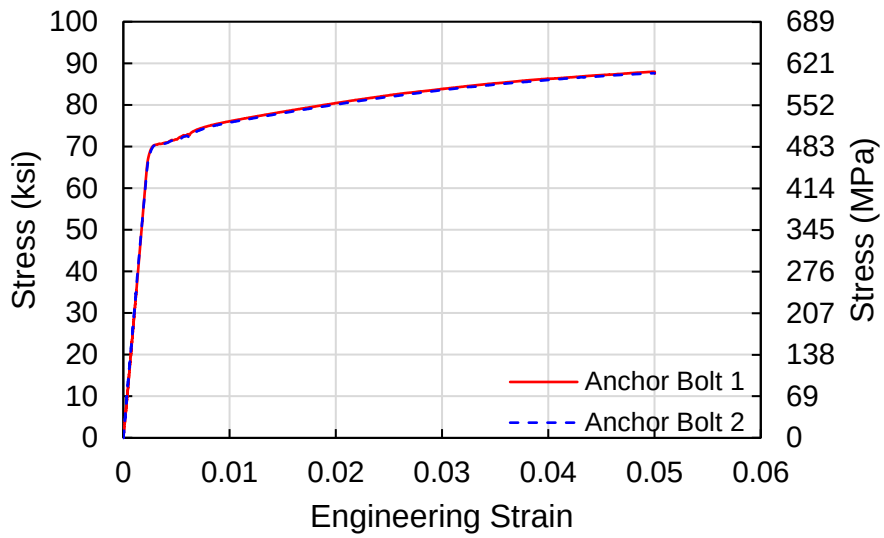

Fig. 3-2. Stress versus engineering strain curves based on two tension tests of anchor bolts.

The No. 7 ASTM A706 Grade 80 bars used for the grouted bar connection were produced in accordance with ASTM A706/A706M-16 (ASTM 2016) and had a nominal diameter of 0.875 in (22.2 mm) and a nominal cross-sectional area of 0.60 in^2 (387 mm^2). The minimum and maximum specified yield strength of the bars was 80 ksi (550 MPa) and 98 ksi (675 MPa), respectively. The minimum specified tensile strength was 100 ksi (690 MPa), with the requirement that the tensile strength be not less than 1.25 multiplied by the measured yield strength. Two 48 in (1219 mm) long bars were tested, which is slightly shorter than the 56 in (1420 mm) bars that were used in the experimental assembly tests. For stress calculations, the cross-sectional area was taken as 0.60 in^2 (387 mm^2), per ASTM A706/A706M-16 (ASTM 2016). Figure 3-3 shows the stress versus engineering strain curves from the tests of two No. 7 continuity bars.

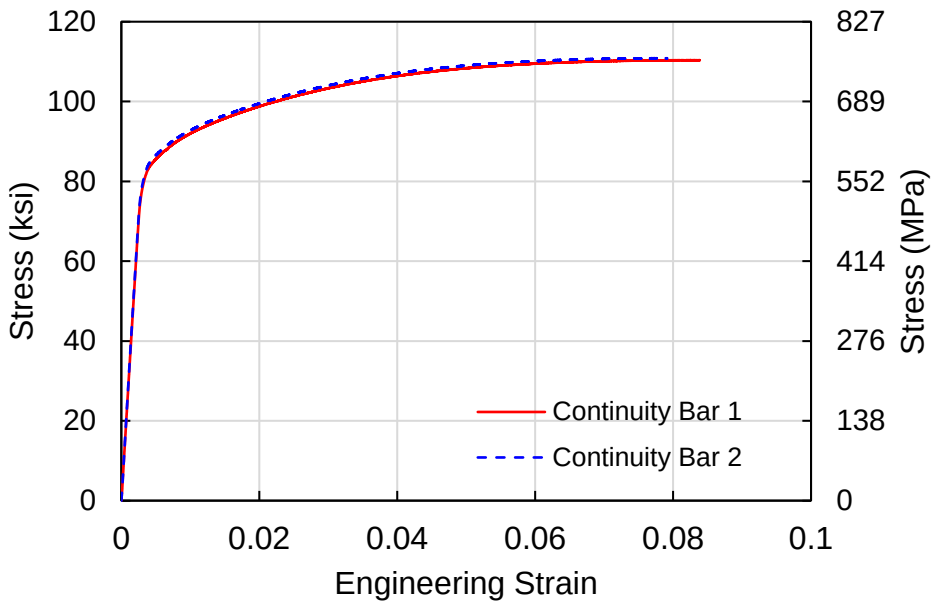

Fig. 3-3 Stress versus engineering strain curves based on two tension tests of continuity bars.

Table 3-4 shows average values of the measured material properties of the steel connection components used in the threaded rod, bolted, and grouted bar connection assemblies.

Table 3-4. Average material properties of steel connection components.

Component	Elastic Modulus, ksi (GPa)	Yield Strength, ksi (MPa)	Ultimate Strength, ksi (MPa)
Dywidag threadbar	29656 ± 1982 (204 ± 13.7)	143 ± 19.7 (986 ± 136)	160 ± 2.4 (1103 ± 16.5)
Anchor bolt	29278 ± 1054 (202 ± 7.3)	71.3 ± 1.3 (492 ± 8.96)	89.8 ± 1.9 (619 ± 13.1)
No. 7 continuity bar	28704 ± 1048 (198 ± 7.2)	86.0 ± 6.4 (593 ± 44.1)	111 ± 3.1 (765 ± 21.4)

3.3. Grout

A dry-pack non-shrink cementitious grout was used to fill the joints between the assembly beams and columns for the threaded rod, bolted, and modified link plate connections. The grout was placed into the joints by hand and then consolidated using sharp and repeated blows from a steel tamping rod. Two batches of grout were used to pack the beam-to-column interface for each connection assembly: one batch for the interface to the left of the column and one for the interface to the right of the column. A minimum of three grout cubes were cast from each batch and tested under uniaxial compression in compliance with ASTM C109-21 (ASTM 2021a) and ASTM C1107/C1107-20 (ASTM 2020a).

A non-shrink cementitious grout mixed to a fluid consistency was used for the grouted bar and bar coupler connection assemblies. The grout was placed using a hand-operated pump for the bar coupler assembly and an electric pump for the grouted bar assembly. Two batches of grout were used for each connection: one for the lower half of the connection and one for the upper half of the connection. A minimum of three grout cubes were cast from each batch and tested

under uniaxial compression in compliance with ASTM C109-21 (ASTM 2021a) and ASTM C1107/C1107-20 (ASTM 2020a).

Table 3-5 shows average values of the measured grout properties for each connection assembly.

Table 3-5. Average compressive strength of grout.

Connection	Left Interface, psi (MPa)	Right Interface, psi (MPa)
Bolted	9540 ± 1490 (65.8 ± 10.3)	10190 ± 1980 (70.3 ± 13.7)
Threaded Rod	10430 ± 1290 (71.9 ± 8.9)	9780 ± 610 (67.4 ± 4.2)
Modified Link Plate	3520 ± 336 (24.3 ± 2.3)	10680 ± 322 (73.6 ± 2.2)
	Lower Interface, psi (MPa)	Upper Interface, psi (MPa)
Grouted Bar	9265 ± 733 (63.9 ± 5.1)	9509 ± 3691 (65.6 ± 25.4)
Bar Coupler	8084 ± 3128 (55.7 ± 21.6)	6679 ± 462 (46.1 ± 3.2)

4. Experimental Results

4.1. Preamble

This section provides important background information for the subsequent discussion of the experimental results of all five connection tests.

4.1.1. Moment-Rotation Behavior

The behavior of each assembly is characterized using the applied connection moment versus beam chord rotation plotted up to connection failure. The applied connection moment was derived using the vertical force applied to the column in conjunction with shear and moment mechanics, which assumed plastic hinge formation at the beam ends, 105.5 in (2680 mm) from the center of the pin connections. The moment due to the weight of the assembly was not considered in the applied moment calculation because it accounts for less than 5 % of the maximum applied connection moment. Beam chord rotation was calculated using the vertical displacement of the column, which was taken as the average of displacement measurements from the two string potentiometers attached to the top of the column on its left and right sides (string potentiometers D05 and D06 in Fig. 2-15). Beam chord rotation was then calculated using the following equation:

$$\theta = tan^{-1}\left(\frac{\delta}{L_1}\right) \tag{4.1}$$

where θ is the beam chord rotation, δ is the average of vertical displacement measurements D05 and D06, and L_1 is the horizontal distance from the centerline of the column to the centerline of the pin connection [112.5 in (2858 mm)]. All the connection assemblies were designed to achieve a rotational capacity of at least 2.29 degrees, or equivalently, 0.04 radians. This rotational capacity of 2.29 degrees is hereafter referred to as the “target” rotational capacity.

4.1.2. Damage Progression and Failure Mode

As was mentioned in Sec. 1.3, the unsupported column was displaced downward in 0.25 in (6.4 mm) increments at a rate of 0.20 in/min (5.1 mm/min). Loading was paused following the completion of each increment to allow for photographs to be taken and cracks and damage to be highlighted with a permanent marker. Cracks and damage that occurred before load was applied to the assembly by the actuator were highlighted with a red marker, whereas cracks and damage that occurred after load was applied to the assembly were highlighted with a black marker. In subsequent discussions of cracking and damage to the assemblies, the front and back faces of the beams and columns are referenced. The front of the assembly is shown in Fig. 1-6 (Sec. 1.3), which corresponds to the interior building face of the prototype building from which the assemblies were derived.

Because of deformations associated with the test setup (i.e., test setup compliance – deformations associated with the portal frame, actuator load cell, donut load cells, erection

tolerances, etc.), the displacement of the actuator piston rod was comparable but not equal to the displacement of the column. The damage progression of the connections is discussed in terms of the vertical displacement increment in which the damage occurred but note that the displacement increments are based on the displacement of the actuator piston rod and not the measured column displacement. To account for the small discrepancy between actuator piston rod displacement and column displacement, a table that includes the measured vertical column displacement and corresponding beam chord rotation is shown in each section that discusses the moment versus rotation behavior of the connection assemblies. The beam chord rotation shown in these tables was calculated by Eq. (4.1).

4.1.3. Displacement Profile and Rotation

In the context of this report, a displacement profile provides measurements of displacement at discrete points along the length of a structural assembly. Such a profile was useful for characterizing the displacement response of the tested connection assemblies as load was applied. The vertical displacement profiles shown in subsequent sections of this report are based on measurements from the 10 symmetrically placed string potentiometers shown in Fig. 2-15. The column centerline corresponds to a spanwise distance of 0 in (0 mm), with positive distances indicating measurements taken to the right of the centerline and negative distances indicating measurements taken to the left of the centerline.

As was mentioned in Sec. 2.3, five inclinometers were attached to the front surface of the precast concrete assemblies, two on each beam and one centered on the column width (see Fig. 2-15). The plots of rotation versus column vertical displacement shown in subsequent sections of this report provide measured in-plane rotations of the beams and column as a function of the measured vertical displacement of the column. Clockwise rotations are shown as positive, and counterclockwise rotations are shown as negative. In addition to the measurements of rotation provided by the inclinometers, these plots also show beam chord rotation, which is calculated using Eq. (4.1). The beam chord rotation appears twice in each plot, once for positive values of rotation and once for negative values, to provide a basis by which to compare the inclinometer measurements to determine the occurrence of rigid-body rotation.

4.2. Threaded Rod

4.2.1. Moment-Rotation Behavior

Fig. 4-1 shows the applied connection moment versus beam chord rotation up to connection failure for the threaded rod connection assembly. The initial response was linear with a slope of 474 kip-ft (643 kN-m) per degree of beam chord rotation. The moment-rotation response remained linear up to a moment of approximately 302 kip-ft (409 kN-m) and a beam chord rotation of 0.73 degrees. The required moment strength stipulated by the design was 234 kip-ft (317 kN-m), and this value was achieved well within the linear response region and after flexural cracks in the beams had initiated. After the transition to a nonlinear response, the

applied connection moment gradually increased until the connection assembly achieved an ultimate moment of 340 kip-ft (461 kN-m) at a beam chord rotation of 3.87 degrees. The threaded rod connection assembly achieved the target rotational capacity before reaching its ultimate moment strength. After the ultimate moment strength was achieved, the applied connection moment began to gradually decrease before tensile rupture of the bottom-right threadbar occurred at a moment of 222 kip-ft (301 kN-m) and a beam chord rotation of 4.44 degrees. The measured vertical column displacement and corresponding beam chord rotations are presented in Table 4-1.

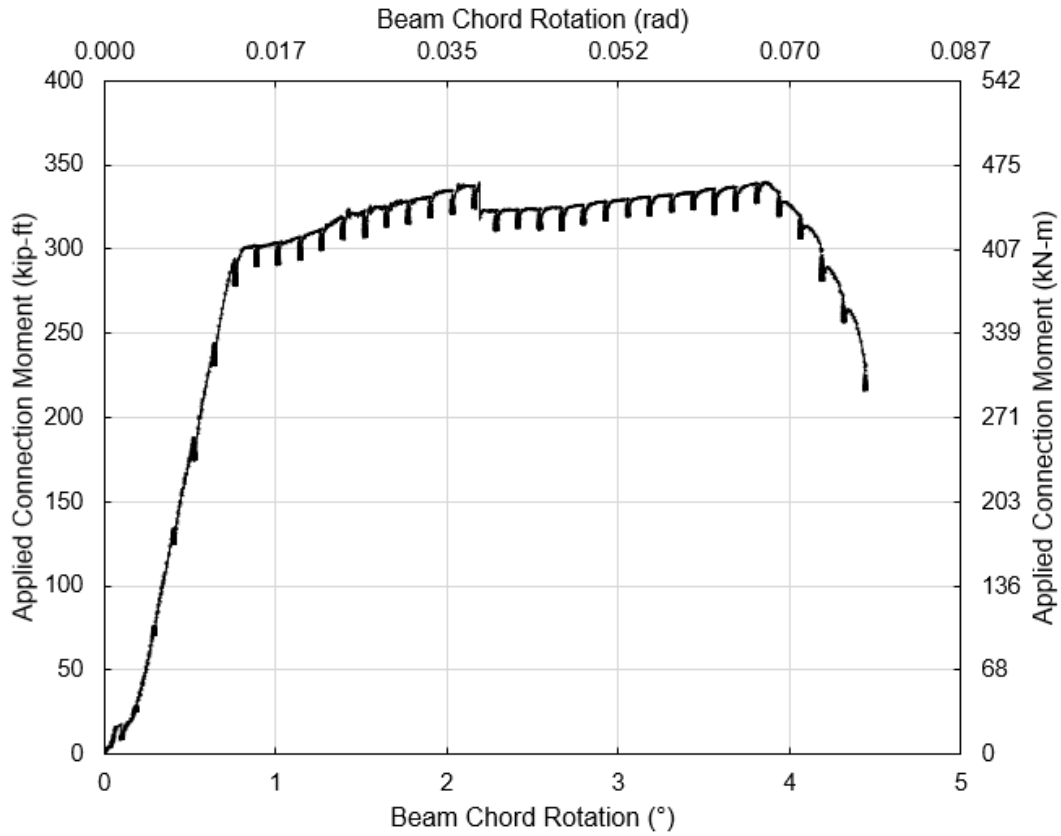

Fig. 4-1. Applied connection moment versus beam chord rotation for the threaded rod connection assembly.

Table 4-1. Measured vertical column displacement at the end of each loading increment (threaded rod).

Increment of Vertical Column Displacement, in (mm)	Measured Vertical Column Displacement, in (mm)	Corresponding Beam Chord Rotation, °	Increment of Vertical Column Displacement, in (mm)	Measured Vertical Column Displacement, in (mm)	Corresponding Beam Chord Rotation, °
0.00 (0)	0.00 (0)	0.00	4.75 (121)	4.49 (114)	2.29
0.25 (6.4)	0.20 (5)	0.10	5.00 (127)	4.73 (120)	2.41
0.50 (13)	0.36 (9)	0.18	5.25 (133)	4.99 (127)	2.54
0.75 (19)	0.57 (15)	0.29	5.50 (140)	5.21 (132)	2.65
1.00 (25)	0.80 (20)	0.41	5.75 (146)	5.50 (140)	2.80
1.25 (32)	1.03 (26)	0.52	6.00 (152)	5.75 (146)	2.93
1.5 (38)	1.26 (32)	0.64	6.25 (159)	6.01 (153)	3.06
1.75 (44)	1.50 (38)	0.76	6.50 (165)	6.26 (159)	3.18
2.00 (51)	1.75 (44)	0.89	6.75 (171)	6.51 (165)	3.31
2.25 (57)	1.99 (51)	1.02	7.00 (178)	6.76 (172)	3.44
2.50 (64)	2.24 (57)	1.14	7.25 (184)	6.98 (177)	3.55
2.75 (70)	2.49 (63)	1.27	7.50 (191)	7.25 (184)	3.69
3.00 (76)	2.74 (70)	1.39	7.75 (197)	7.47 (190)	3.80
3.25 (83)	2.99 (76)	1.52	8.00 (203)	7.74 (197)	3.94
3.50 (89)	3.21 (81)	1.63	8.25 (210)	7.94 (202)	4.04
3.75 (95)	3.48 (88)	1.77	8.50 (216)	8.24 (209)	4.19
4.00 (102)	3.71 (94)	1.89	8.75 (222)	8.49 (216)	4.32
4.25 (108)	3.96 (100)	2.01	9.00 (229)	8.70 (221)	4.42
4.50 (114)	4.23 (107)	2.15			

4.2.2. Damage Progression and Failure Mode

Flexural cracking initiated at the bottom of the front and back faces of the beams during the vertical column displacement increment from 1.00 in to 1.25 in (25 mm to 32 mm). The flexural cracks extended upward toward the tops of the beams as loading progressed. The assembly response transitioned to nonlinear during the vertical column displacement increment from 1.50 in to 1.75 in (38 mm to 44 mm). During the vertical column displacement increment from 2.25 in to 2.50 in (57 mm to 64 mm), the right end of the top of the left beam began to bind, leading to minor spalling in the column at the top left pocket. During the next increment, spalling occurred at the top of the right column pocket. Gaps between the grout interface and the bottom of the beams at their ends widened symmetrically until the vertical column displacement increment from 4.50 in to 4.75 in (114 mm to 121 mm). During that increment, the gap at the bottom right was approximately 0.13 in (3 mm) larger than the gap at the bottom left and the bottom-right gap continued to increase at a higher rate. A reduction in moment occurred at a vertical column displacement of 4.30 in (109 mm). The reduction in moment was potentially caused by slippage of one of the threadbars, which was suspected due

to an audible metallic-sounding noise emitted from one of the threadbars during the test. As shown in Fig. 4-2, deformations were concentrated at the bottom-right connection until tensile rupture of the bottom-right threadbar occurred near the beam end at a vertical column displacement of 8.74 in (222 mm), which corresponded to a beam chord rotation of 4.44 degrees.

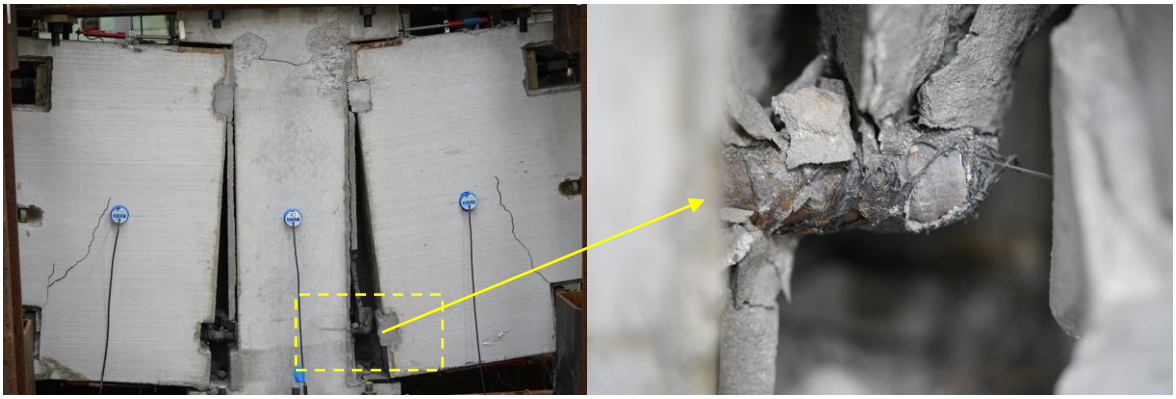

Fig. 4-2. Failure mode of the threaded rod connection assembly.

4.2.3. Displacement Profile and Rotation

Fig. 4-3 shows vertical displacement profiles of the threaded rod connection assembly corresponding to different points in the loading. Beginning at the first displacement profile and moving sequentially to the last profile from smallest to largest vertical displacements, the profiles correspond to approximately midway through the linear region of assembly response (θ = 0.36°), the transition point from linear to nonlinear response (θ = 0.73°), the point at which there was a sudden decrease in vertical force or moment (θ = 2.19°), the ultimate moment resistance attained (θ = 3.87°), and the instant just before tensile rupture of the bottom-right threadbar (θ = 4.44°). The displacement profiles were fairly symmetric in the linear response region; however, with increasing vertical column displacement the column rotated increasingly clockwise within the plane of the connection, leading to a concentration of axial deformation at the bottom-right connection that eventually led to fracture of the bottom-right threadbar.

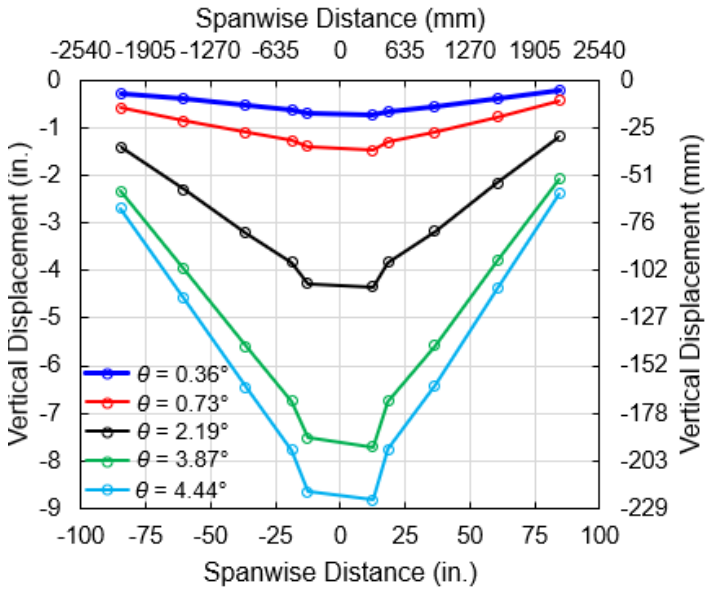

Fig. 4-3. Vertical displacement profiles of the threaded rod connection assembly.

Fig. 4-4 shows the in-plane rotation of the precast concrete components, excluding the rotation of the column (R03), which was not captured due to a malfunction of the inclinometer. The curves indicating rotation measurements from inclinometers on the left beam (R01 and R02) and right beam (R04 and R05) are nearly the same as the curves for the beam chord rotation. This finding indicates that the beams underwent predominantly rigid-body rotations and that deformations were localized at the beam-to-column connections. The measured rotation near midspan of the right beam (R05) deviated most from the beam chord rotation, exceeding the beam chord rotation by 0.30 degrees, which is indicative of close agreement.

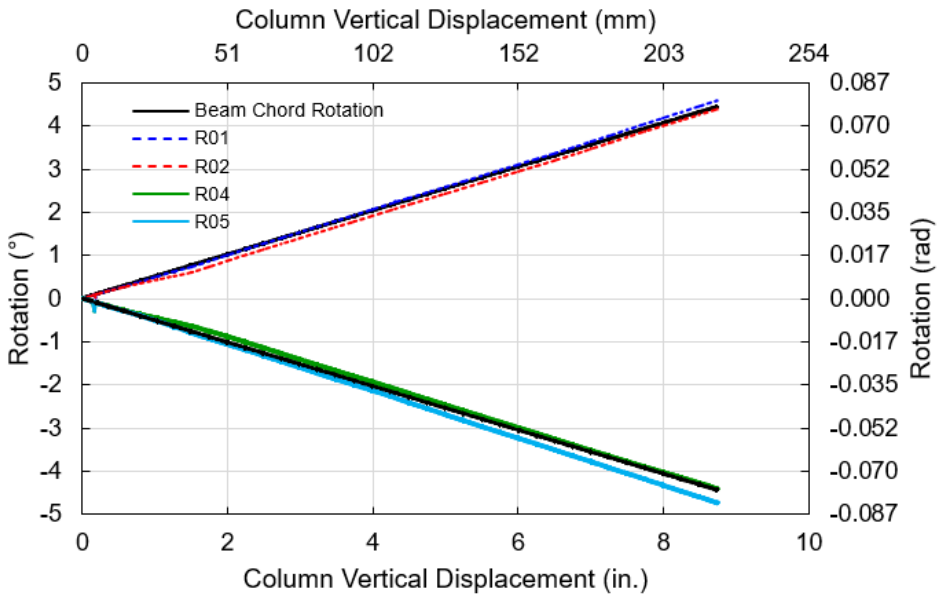

Fig. 4-4. Measured in-plane rotations of the precast concrete beams and columns for the threaded rod connection assembly.

4.2.4. Strain Measurements

Strain gauges on the stirrups of the threaded rod connection assembly beams recorded small strains, well below measurements that would indicate yield. Figure 4-5 shows measured strains of the flexural reinforcing steel in the bottom of the right beam as a function of column vertical displacement. The steel yielded at a column vertical displacement of 2.30 in (58 mm) and a beam chord rotation of 1.17 degrees. This initiation of yielding occurred near where the moment versus rotation response transitioned from linear to nonlinear. A strain of 0.0026 was considered as indicative of yield in any reinforcing bar, assuming that the ASTM A706 Grade 60 (414 MPa) steel had a yield strength of 74 ksi (510 MPa) and an elastic modulus of 29,000 ksi (200 GPa).

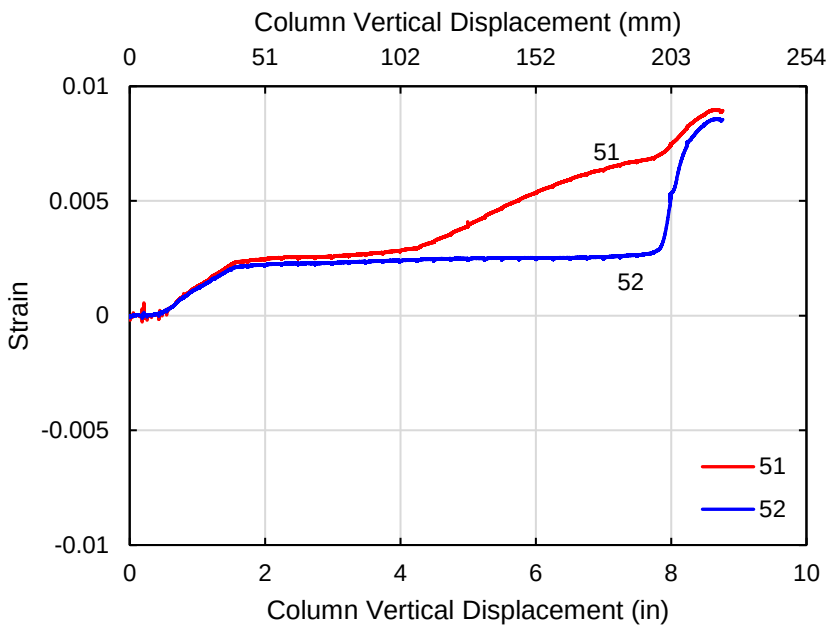

Fig. 4-5. Strain in flexural reinforcing bars at the bottom of the right beam (threaded rod connection assembly).

Fig. 4-6 and Fig. 4-7 show strain measurements from strain gauges on the threadbars. The strain gauges were placed in pairs on the top and bottom sides of the bar at the same cross section location (see Appendix B for gauge locations). Figure 4-6 shows that the top threadbar in the right beam was subjected to flexure, as indicated by the magnitude of the tensile strain at the bottom side of the bar being nearly equal to the magnitude of the compressive strain at the top side of the bar. The bottom strain gauge on the top threadbar in the left beam showed tensile strains, but the top strain gauge malfunctioned. It is inferred that the top threadbar in the left beam also underwent flexure because of symmetry in the assembly displacement profile. According to strain gauge measurements and force data from the through-hole compression load cells at the ends of the bars, both top threadbars remained elastic. A threadbar was considered to have yielded at a strain of 0.0048, which was calculated by dividing the average yield strength by the average elastic modulus obtained from monotonic tension tests of two threadbars (Sec 3.2).

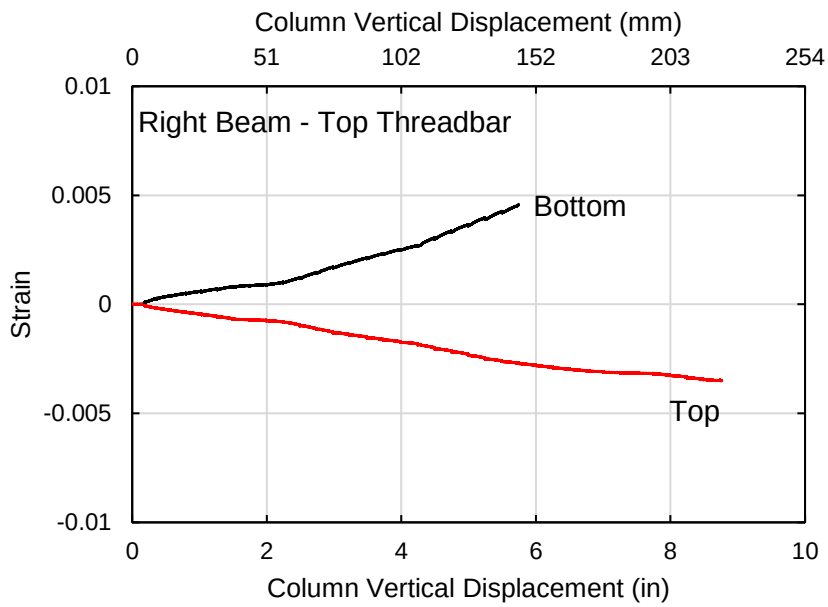

Fig. 4-6. Strain in the threadbar in the top of the right beam (threaded rod connection assembly).

The bottom threadbar in the left beam (i.e., the bottom threadbar that did not rupture) had tensile strains at the top and bottom of the bar (Fig. 4-7). The readings from the top and bottom strain gauges were nearly equal until the top strain gauge malfunctioned at approximately 2.00 in (51 mm) of vertical column displacement. The bottom strain gauge peaked at a strain of 0.07 and functioned for the duration of the test. The equal tensile strains at the top and bottom of the bar indicate that the bar was initially subjected to pure axial loading. Whether the bar remained under a pure state of axial force is unknown because the top strain gauge malfunctioned.

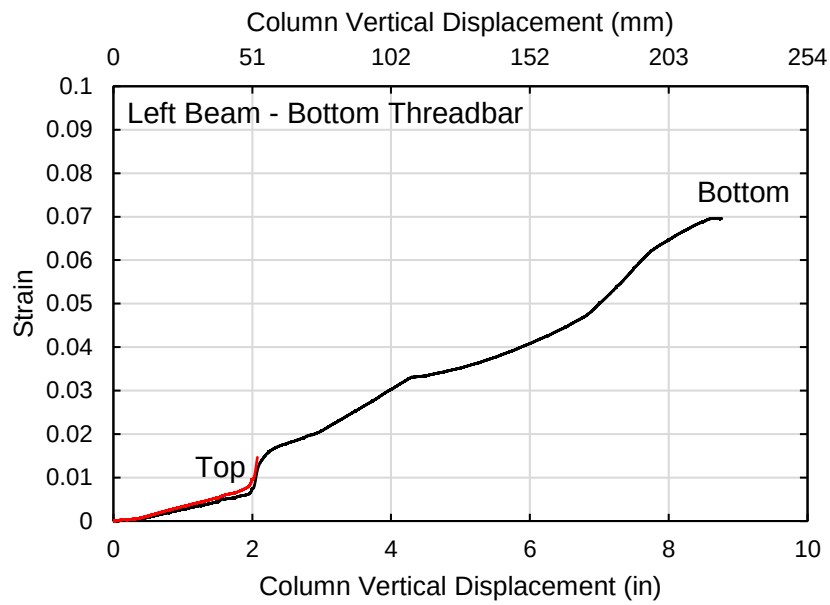

Fig. 4-7. Strain in the threadbar in the bottom of the left beam (threaded rod connection assembly).

4.3. Bolted

4.3.1. Moment-Rotation Behavior

Fig. 4-8 shows the applied connection moment versus beam chord rotation up to connection failure for the bolted connection assembly. The initial response was linear with a slope of 713 kip-ft (967 kN-m) per degree of beam chord rotation. The moment-rotation response remained linear up to a moment of approximately 251 kip-ft (340 kN-m) and a beam chord rotation of 0.53 degrees. After the transition to a nonlinear response, the applied connection moment gradually increased until the connection assembly achieved an ultimate moment of 419 kip-ft (568 kN-m) at a beam chord rotation of 2.43 degrees. The bolted connection assembly achieved the target rotational capacity before reaching its ultimate moment strength. Subsequently, the applied connection moment began to decrease before tensile rupture of the bottom-left anchor bolt occurred at a moment of 308 kip-ft (418 kN-m) and a beam chord rotation of 2.78 degrees. The measured vertical column displacement and corresponding beam chord rotations are presented in Table 4-2.

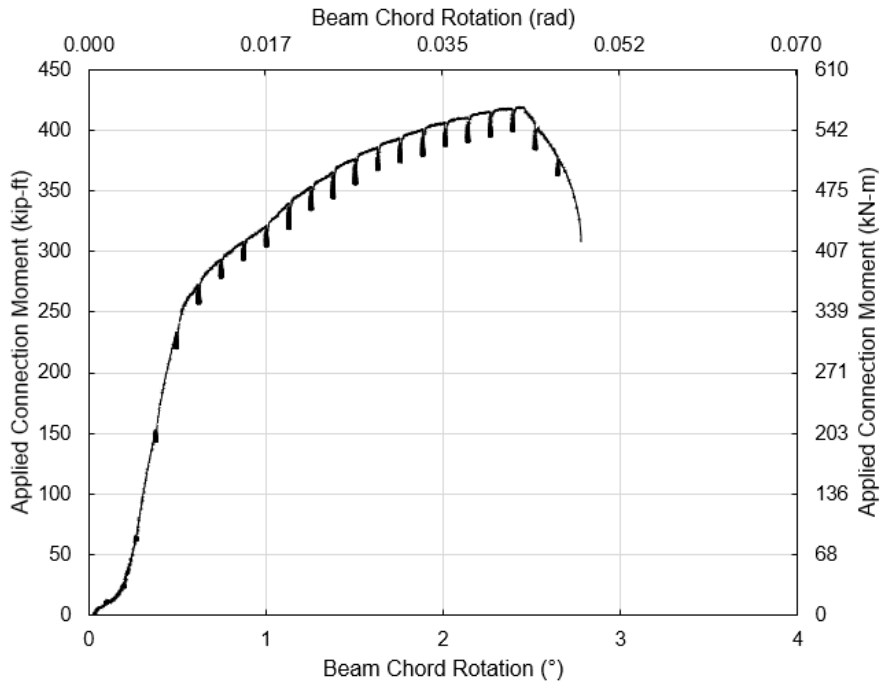

Fig. 4-8. Applied connection moment versus beam chord rotation for the bolted connection assembly.

Table 4-2. Measured vertical column displacement at the end of each loading increment (bolted).

Increment of Vertical Column Displacement, in (mm)	Measured Vertical Column Displacement, in (mm)	Corresponding Beam Chord Rotation, °	Increment of Vertical Column Displacement, in (mm)	Measured Vertical Column Displacement, in (mm)	Corresponding Beam Chord Rotation, °
0.00 (0)	0.00 (0)	0.00	3.00 (76)	2.71 (69)	1.38
0.25 (6.4)	0.20 (5)	0.10	3.25 (83)	2.95 (75)	1.50
0.50 (13)	0.39 (10)	0.20	3.50 (89)	3.20 (81)	1.63
0.75 (19)	0.53 (13)	0.27	3.75 (95)	3.45 (88)	1.76
1.00 (25)	0.74 (19)	0.38	4.00 (102)	3.70 (94)	1.88
1.25 (32)	0.97 (25)	0.50	4.25 (108)	3.95 (100)	2.01
1.5 (38)	1.22 (31)	0.62	4.50 (114)	4.20 (107)	2.14
1.75 (44)	1.46 (37)	0.75	4.75 (121)	4.45 (113)	2.27
2.00 (51)	1.72 (44)	0.87	5.00 (127)	4.70 (119)	2.39
2.25 (57)	1.97 (50)	1.00	5.25 (133)	4.95 (126)	2.52
2.50 (64)	2.22 (56)	1.13	5.50 (140)	5.20 (132)	2.65
2.75 (70)	2.47 (63)	1.26			

4.3.2. Damage Progression and Failure Mode

Flexural cracking in the beams of the bolted connection assembly initiated during the vertical column displacement increment from 0.75 in to 1.00 in (19 mm to 25 mm). This initial cracking consisted of one flexural crack near midspan of the right spandrel beam on its front face, with the crack initiating at the bottom of the beam and extending about halfway up its depth. Flexural cracking was not observed in the left beam after the same increment of vertical column displacement, since the beam was resting on the bottom anchor bolt resulting in deformation initially being concentrated in that anchor bolt as the column displaced downward.

The moment versus rotation response transitioned to nonlinear during the vertical column displacement increment from 1.25 in to 1.50 in (32 mm to 38 mm). During this same increment, numerous flexural cracks formed near midspan of both beams on their front and back faces. During the vertical column displacement increment from 2.25 in to 2.50 in (57 mm to 64 mm), the top corners of both beams began to bear firmly on the grout, generating compressive forces in the column that led to cracking and spalling on its left and right sides. Audible sounds of crushing and spalling of the column at its top end near the top corners of the beams occurred during the vertical column displacement increment from 2.50 in to 2.75 in (57 mm to 70 mm). As loading continued, the gap between the bottom corner of the left beam and the grout grew at a rate that outpaced the growth of the gap on the right side of the assembly, eventually leading to tensile rupture of the bottom-left anchor bolt near the inner face of the hand hole at a vertical column displacement of 5.46 in (139 mm), which corresponded to 2.78 degrees of beam chord rotation. Figure 4-9 shows the failure mode of the bolted connection assembly.

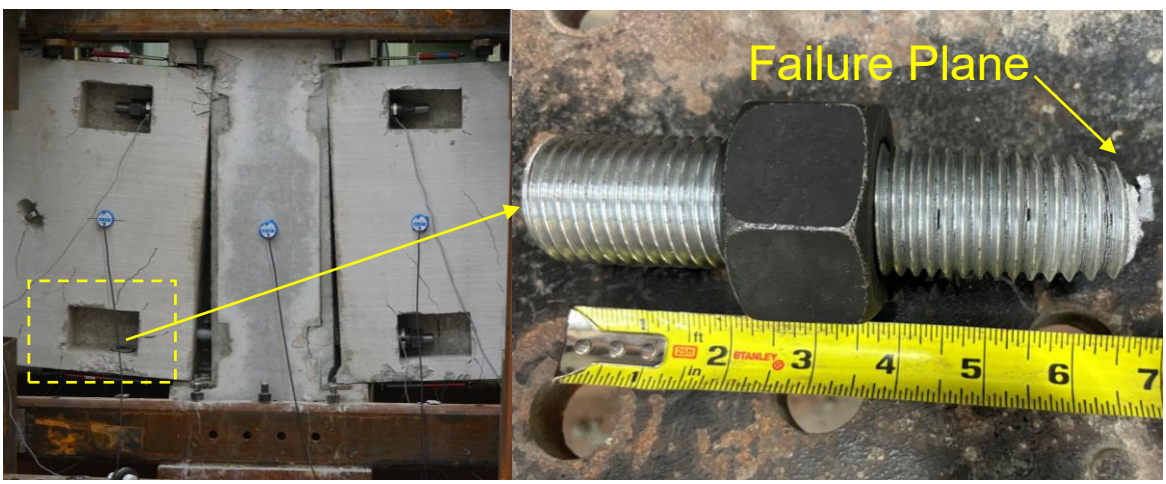

Fig. 4-9. Failure mode of the bolted connection assembly.

4.3.3. Displacement Profile and Rotation

Fig. 4-10 shows vertical displacement profiles of the bolted connection assembly corresponding to different points in the loading. In order of increasing displacement, the profiles correspond to approximately midway through the linear region of assembly response (θ = 0.34°), the transition point from linear to nonlinear response (θ = 0.53°), the end of the increment in which

column spalling occurred (θ = 1.13°), ultimate moment (θ = 2.43°), and the instant just before rupture of the bottom-left anchor bolt (θ = 2.78°). The displacement profiles are generally asymmetric, with larger displacements on the left side of the column (measurements from string potentiometer D05) than on the right side (measurements from string potentiometer D06). This is indicative of the column rotating counterclockwise, which contributed to the gap between the bottom corner of the left beam and the grout interface becoming larger and eventually leading to fracture of the bottom-left anchor bolt.

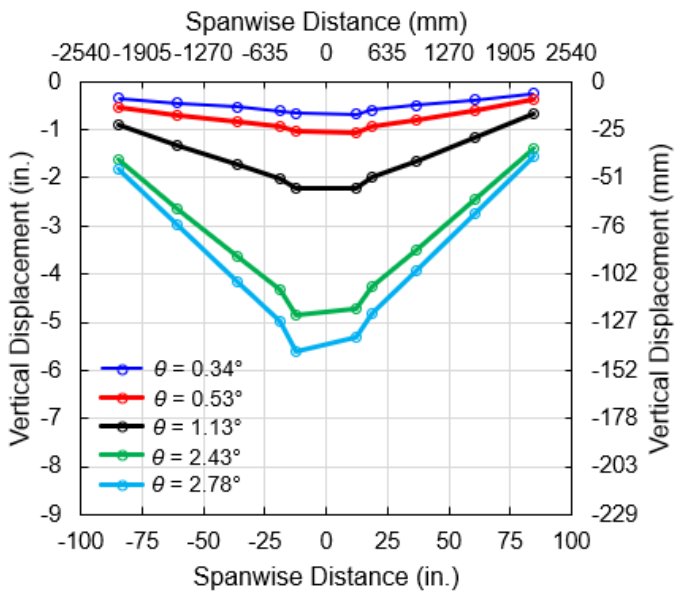

Fig. 4-10. Vertical displacement profiles of the bolted connection assembly.

Fig. 4-11 shows the in-plane rotation of the precast concrete components. The curves indicating rotation measurements from inclinometers on the left beam (R01 and R02) and right beam (R04 and R05) are nearly the same as the curves for the beam chord rotation. This finding indicates that the beams were undergoing rigid body rotations and that deformations were localized at the beam-to-column connections. The rotation measurement from the inclinometer on the column (R03) shows that the column began to rotate counterclockwise at approximately 3.00 in (76 mm) of vertical column displacement. This counterclockwise rotation led to a concentration of axial deformation at the bottom-left anchor bolt, which eventually led to its rupture.

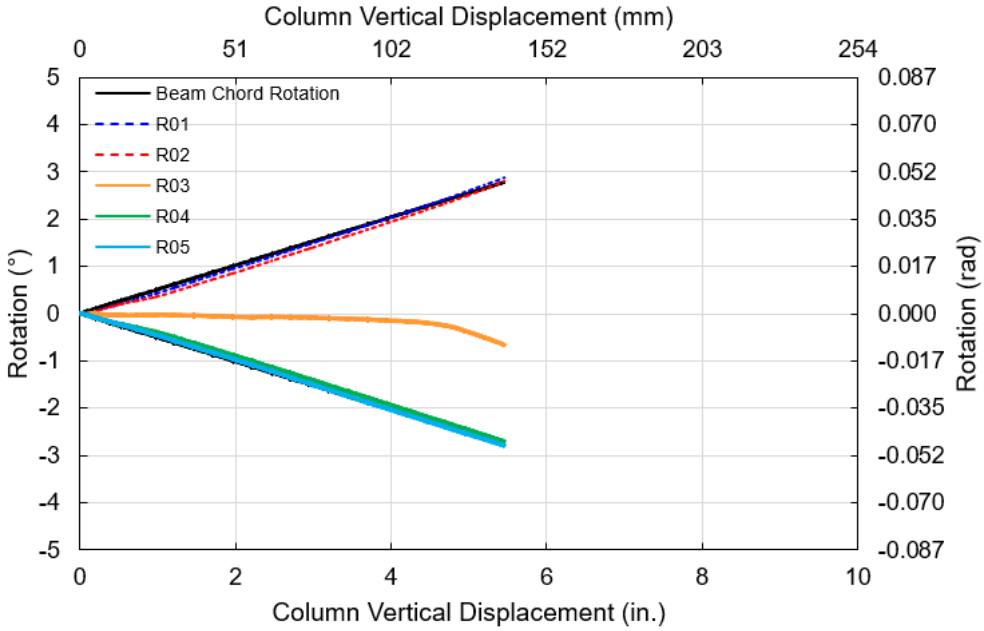

Fig. 4-11. Measured in-plane rotations of the precast concrete beams and columns for the bolted connection assembly.

4.3.4. Strain measurements

Strain gauges on the stirrups of the bolted connection assembly beams measured strains well below what would indicate yield. Strain gauges in the bolted connection assembly beams indicated that flexural yielding of the beams did not occur.

4.4. Bar Coupler

4.4.1. Moment-Rotation Behavior

Fig. 4-12 shows the applied connection moment versus the beam chord rotation up to connection failure for the bar coupler connection assembly. The initial response was linear with a slope of 1007 kip-ft (1365 kN-m) per degree of chord rotation. The moment-rotation response remained linear up to a moment of approximately 393 kip-ft (533 kN-m) and a beam chord rotation of 0.39 degrees. Flexural cracks in the beams initiated during the vertical column displacement increment from 0.50 in to 0.75 in (13 mm to 19 mm). The factored moment demand for which the connections were designed was 234 kip-ft (317 kN-m), and the moment-rotation response did not become nonlinear until this demand was well exceeded.

After the response transitioned to nonlinear at approximately 0.39 degrees of chord rotation and a moment of 393 kip-ft (533 kN-m), the assembly's strength continued to increase until an ultimate moment capacity of 627 kip-ft (850 kN-m) was achieved at 2.65 degrees of chord rotation. During this strength increase up to the ultimate moment capacity, column spalling occurred, followed by a sustained period of vertical displacement increments where no visible

damage was observed. The bar coupler connection assembly achieved the target rotational capacity before reaching its ultimate moment strength.

After the ultimate moment capacity was achieved, the assembly's moment resistance began to decrease. Spalling occurred at the top of the column above the blockout and a large diagonal crack opened on the front face of the column on its left side as the moment continued to decrease. The top right end of the left beam diagonally spalled due to large compressive forces near where the beam bore against the column. At a moment of 531 kip-ft (720 kN-m) and beam chord rotation of 3.71 degrees, the continuity bar connected to the top coupler in the bottom column blockout ruptured, resulting in a substantial decrease in load and subsequent termination of the test. The measured vertical column displacement and corresponding beam chord rotations are presented in Table 4-3.

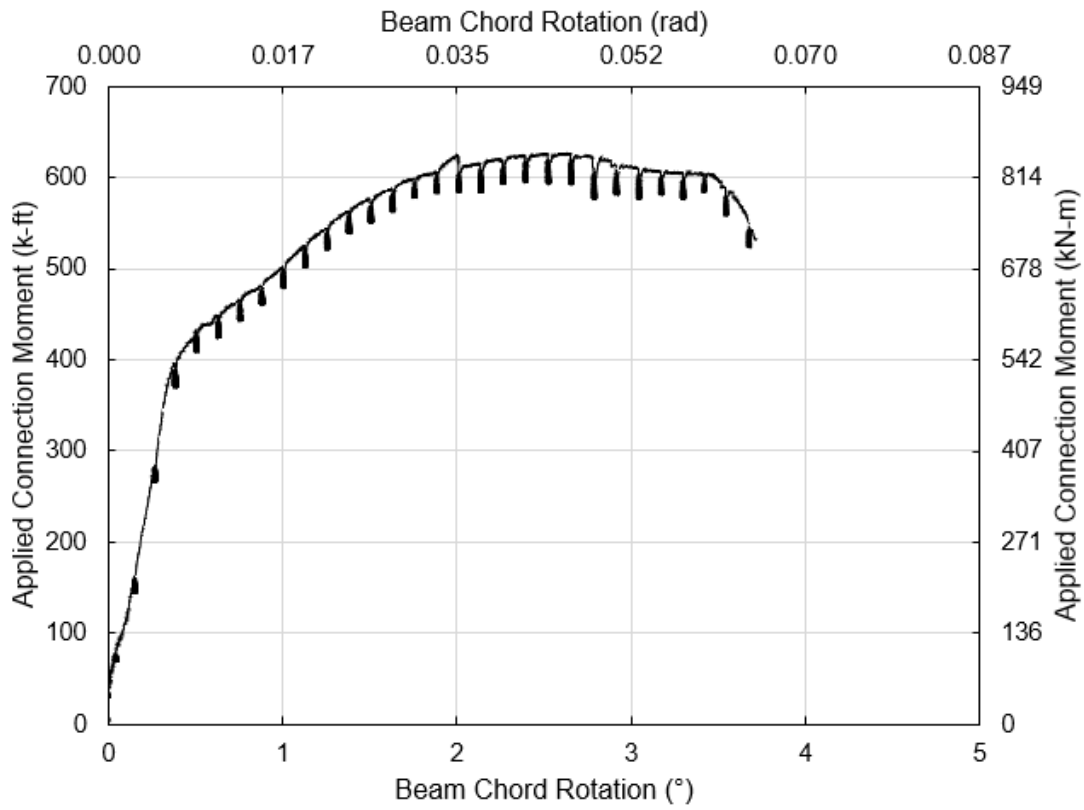

Fig. 4-12. Applied connection moment versus beam chord rotation for the bar coupler connection assembly.

Table 4-3. Measured vertical column displacement at the end of each loading increment (bar coupler).

Increment of Vertical Column Displacement, in (mm)	Measured Vertical Column Displacement, in (mm)	Corresponding Beam Chord Rotation, °	Increment of Vertical Column Displacement, in (mm)	Measured Vertical Column Displacement, in (mm)	Corresponding Beam Chord Rotation, °
0.00 (0)	0.00 (0)	0.00	4.75 (121)	4.15 (105)	2.11
0.25 (6.4)	0.01 (0)	0.01	5.00 (127)	4.40 (112)	2.24
0.50 (13)	0.07 (2)	0.04	5.25 (133)	4.65 (118)	2.37
0.75 (19)	0.29 (7)	0.15	5.50 (140)	4.90 (124)	2.50
1.00 (25)	0.51 (13)	0.26	5.75 (146)	5.16 (131)	2.63
1.25 (32)	0.73 (19)	0.37	6.00 (152)	5.42 (138)	2.76
1.5 (38)	0.97 (25)	0.49	6.25 (159)	5.67 (144)	2.89
1.75 (44)	1.21 (31)	0.62	6.50 (165)	5.92 (150)	3.01
2.00 (51)	1.45 (37)	0.74	6.75 (171)	6.17 (157)	3.14
2.25 (57)	1.70 (43)	0.86	7.00 (178)	6.42 (163)	3.27
2.50 (64)	1.94 (49)	0.99	7.25 (184)	6.66 (169)	3.39
2.75 (70)	2.18 (55)	1.11	7.50 (191)	6.91 (175)	3.51
3.00 (76)	2.42 (62)	1.23	7.75 (197)	7.17 (182)	3.65
3.25 (83)	2.67 (68)	1.36			
3.50 (89)	2.92 (74)	1.48			
3.75 (95)	3.16 (80)	1.61			
4.00 (102)	3.41 (87)	1.74			
4.25 (108)	3.65 (93)	1.86			
4.50 (114)	3.90 (99)	1.99			

4.4.2. Damage Progression and Failure Mode

Shrinkage cracks in the top and bottom grouted pockets were visible before force was applied to the connection assembly by the actuator. No additional cracking was observed during the vertical column displacement increment to 0.25 in (6.4 mm). In the subsequent increment to 0.50 in (12.7 mm) of vertical column displacement, new cracks formed in the grouted pockets and shrinkage cracks that existed before the application of force were extended. During the vertical column displacement increment from 0.50 in to 0.75 in (13 mm to 19 mm), several (approximately four to five per beam face) flexural cracks occurred on the front side of the left and right beam and on the back side of the left beam. The flexural cracks initiated at the bottoms of the beams where the flexural stresses were the largest, and they extended vertically toward the mid-depth of the beams.

During the vertical displacement increment from 1.25 in to 1.50 in (32 mm to 38 mm), the moment-rotation response transitioned to nonlinear, which was supported by the observation

that no additional cracks occurred and existing cracks neither extended nor opened in the beams during this increment. The subsequent vertical displacement increment from 1.50 in to 1.75 in. (38 mm to 44 mm) was accompanied by audible sounds of cracking and spalling at the bottom of the column underneath the beam pockets and on the left and right sides of the column. With continued loading, the column damage became more severe, and the gaps between the column and the bottom of the beams near the connection continued to widen, with the gap between the bottom of the right beam and column growing at a greater pace than the gap between the bottom of the left beam and column. At the end of the vertical displacement increment to 5.75 in (146 mm), the gap between the column and the bottom of the right beam was 1.53 in (39 mm), and the gap between the column and the bottom of the left beam was 0.41 in (10 mm). Deformations were clearly concentrating at the right beam-to-column interface as the continuity bars at the bottom of the right beam continued to elongate, and the top of the right beam bore firmly against the column.

During subsequent displacement increments, the grout in the blockout near the top of the column began to crush and spall under large compressive stresses. During the increment to 7.50 in (191 mm) of vertical column displacement, diagonal spalling occurred at the top right end of the left beam. The connection failed during the increment to 8.00 in (203 mm) of vertical column displacement via tensile rupture of the continuity bar in the right beam, which was connected to the bar coupler at the top of the bottom column blockout. Figure 4-13 shows the ruptured continuity bar after the test was terminated and after grout was chiseled away from the bottom blockout and beam-to-column interface. The rupture occurred outside of the 7.0 in (178 mm) length of bar covered by the debonding sleeve. This finding indicates that the debonding sleeve likely did not perform as intended.

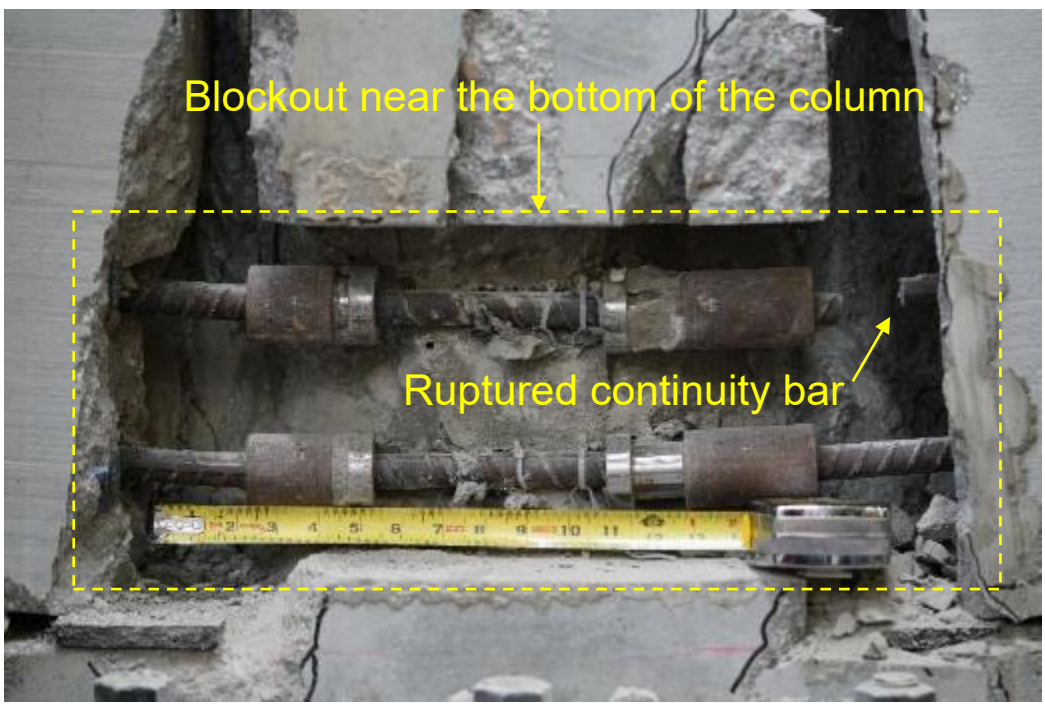

Fig. 4-13. Failure mode of the bar coupler connection assembly.

4.4.3. Displacement Profile and Rotation

Fig. 4-14 shows vertical displacement profiles for the bar coupler connection assembly. Beginning at the first displacement profile and moving sequentially to the last profile from smallest to largest vertical displacements, the profiles correspond to approximately midway through the linear region of assembly response (θ = 0.18°), the transition point from linear to nonlinear response (θ=0.39°), the ultimate moment (θ = 2.65°), and the instant just before rupture of the continuity bar near the bottom of the right beam (θ = 3.71°). As shown in Fig. 4-14, the vertical displacement of the right side of the column (measurements from string potentiometer D06) was larger than that of the left side (measurements from string potentiometer D05) and became more pronounced as loading of the assembly progressed. The difference in displacement of the left and right sides of the column indicates that the column was rotating clockwise, which led to a concentration of tensile force in the lower connections between the right beam and column that eventually led to rupture of the upper continuity bar in the bottom of the right beam.

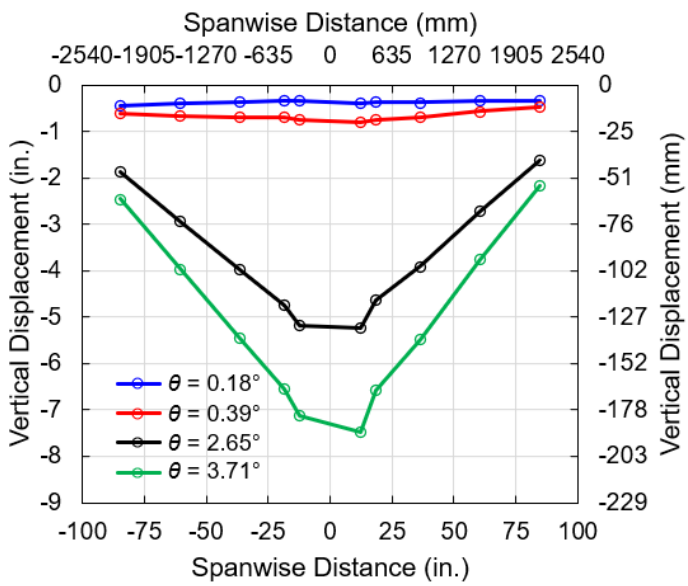

Fig. 4-14. Vertical displacement profiles of the bar coupler connection assembly.

Fig. 4-15 shows the in-plane rotation of the precast concrete beams and column from inclinometer measurements plotted as a function of vertical column displacement. The curve indicating rotation measurements from the column (R03) confirms string potentiometer measurements, which indicated that the column was rotating clockwise with increasing column vertical displacement. The curves indicating rotation measurements from the inclinometers on the left beam (R01 and R02) and right beam (R04 and R05) are nearly the same as the curves for the beam chord rotation. This finding indicates that the beams were undergoing rigid-body rotations and that deformations were localized at the beam-to-column connections.

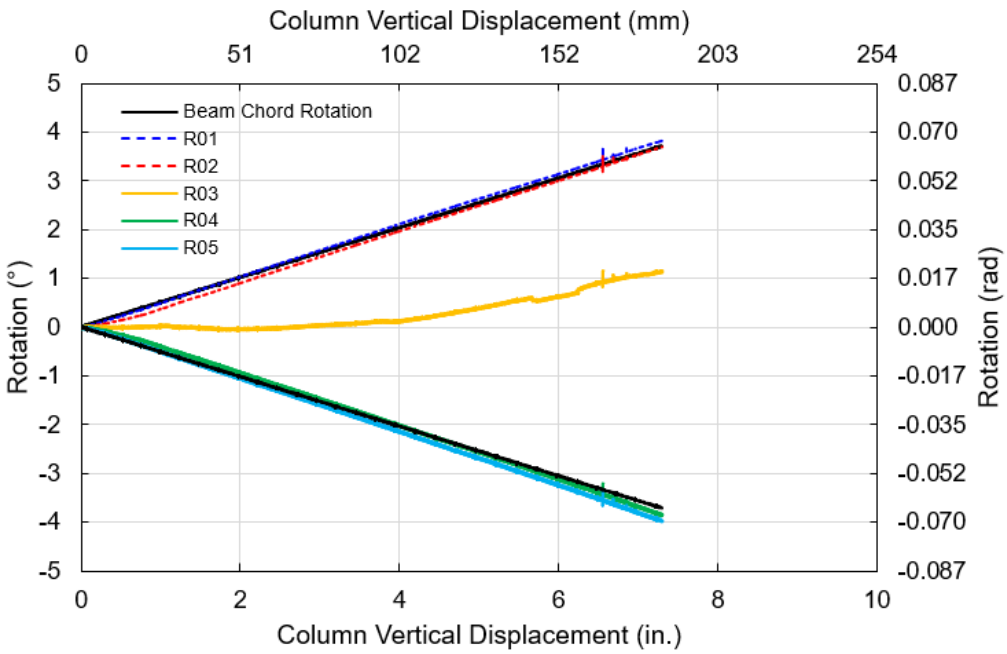

Fig. 4-15. Measured in-plane rotations of the precast concrete beams and columns for the bar coupler connection assembly.

4.4.4. Strain Measurements

Fig. 4-16 shows the reinforcing bar couplers used for the bar coupler connection before the column blockouts in which they were housed were grouted. The couplers are labeled one through four, with the couplers housed in the top column blockout labeled “1” and “2”, and the couplers housed in the bottom column blockout labeled “3” and “4”. Two strain gauges were affixed near the midlength of each bar coupler, one on the top side of the bar and one on the bottom side of the bar at the same cross-section location. Figure 4-17 was obtained by plotting the measured axial strains in each bar coupler as a function of the vertical displacement of the column. Positive values on the vertical axis indicate tensile strain, and negative values indicate compressive strain. The strains were plotted until the strain gauges either malfunctioned or the test terminated. As expected, the largest strains were measured in couplers 3 and 4, which were placed under tension as the column displaced downward. The measured strains exceeded 1.5% for couplers 3 and 4, which is substantially above the yield strain of the bars. The tensile strains measured at the top and bottom of coupler 3 were nearly equal through the duration of the test, indicating that the coupler underwent nearly pure axial loading. Coupler 1 initially experienced compressive strains before transitioning to bending, as was indicated by the compressive strains on the top side of the bar and the tensile strains on the bottom side of the bar. Only tensile strains were measured in coupler 2, but both strain gauges affixed to the coupler malfunctioned before the test terminated, so it is unclear whether tensile strains remained for the duration of the test.

The grout that filled the column blockouts was chiseled away after the test was terminated, revealing that the bar couplers remained intact and their reinforcing bars did not rupture.

Rupture ultimately occurred outside of the debonded region of the No. 7 continuity bar in the right beam that was connected to coupler 3.

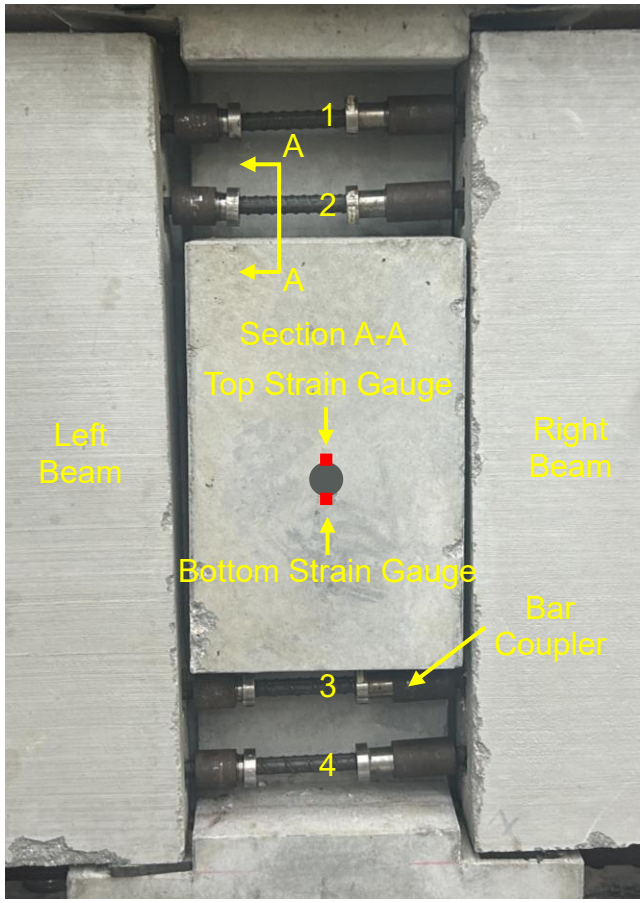

Fig. 4-16. Labeling scheme for bar couplers.

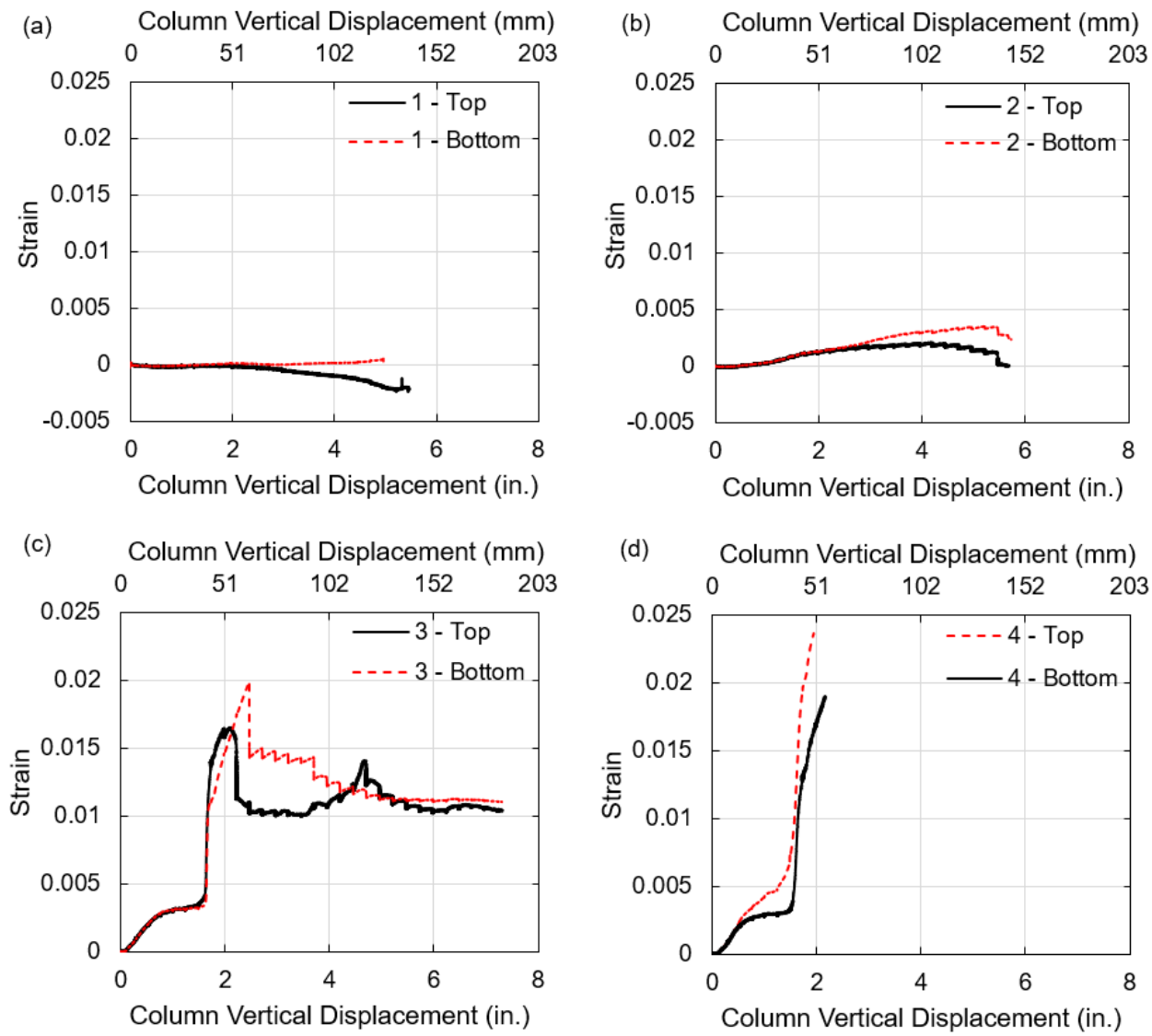

Fig. 4-17. Strains in the bar couplers.

The measured strains in the shear reinforcement of both beams were very small and remained well below the yield strain of the bars for the duration of the test. The measured strains in the flexural reinforcement of the beams indicated that flexural yielding of the beams did not occur. A strain of 0.0026 was indicative of yield in any reinforcing bar, assuming the A706 Grade 60 steel that was used for the flexural and shear reinforcement had a yield strength of 74 ksi (510 MPa) and an elastic modulus of 29,000 ksi (200 GPa).

4.5. Grouted Bar

4.5.1. Moment-Rotation Behavior

Fig. 4-18 shows the applied connection moment versus beam chord rotation up to connection failure for the grouted bar connection assembly. The initial response was linear with a slope of 1036 kip-ft (1404 kN-m) per degree of chord rotation and remained linear up to approximately 0.35 degrees of chord rotation and a moment of 366 kip-ft (496 kN-m). The stiffness of the grouted bar connection assembly was nearly equal to that of the bar coupler connection assembly. This finding was expected considering that the link and continuity bars used for the bar coupler connection assembly and the continuity bars used for the grouted bar connection assembly were both made from No. 7 ASTM A706 Gr. 80 steel and featured similar total lengths of debonding sleeve applied to the flexural reinforcing bars. The expectation of similar stiffnesses also arose because the connections are similar in concept, since they both have four layers of deformed bar reinforcement along the height of the connection. This four-layer configuration contrasts with the other three connection assemblies, which each had two layers of steel components that provided moment continuity.

After the transition to nonlinear response, the connection assembly achieved an ultimate moment of 509 kip-ft (690 kN-m) at a beam chord rotation of 1.04 degrees. Immediately after the ultimate moment was achieved, the moment-rotation response descended sharply until 1.18 degrees of beam chord rotation before transitioning to a descent at a more gradual slope until connection failure. This bilinear post-peak response suggests that a loss in mechanical interlock between the ribs of the continuity bar and surrounding concrete occurred, which led to the initial steep reduction in moment. The frictional resistance that remained between the continuity bar and surrounding concrete was adequate to prevent bar pullout and allow the continuity bar to continue to plastically deform until tensile rupture. High-fidelity finite element modeling of this connection assembly will ultimately be used to better understand the failure progression. Ultimately, connection failure occurred at 272 kip-ft (369 kN-m) of moment and 2.44 degrees of beam chord rotation. The measured vertical column displacement and corresponding beam chord rotations are presented in Table 4-4.

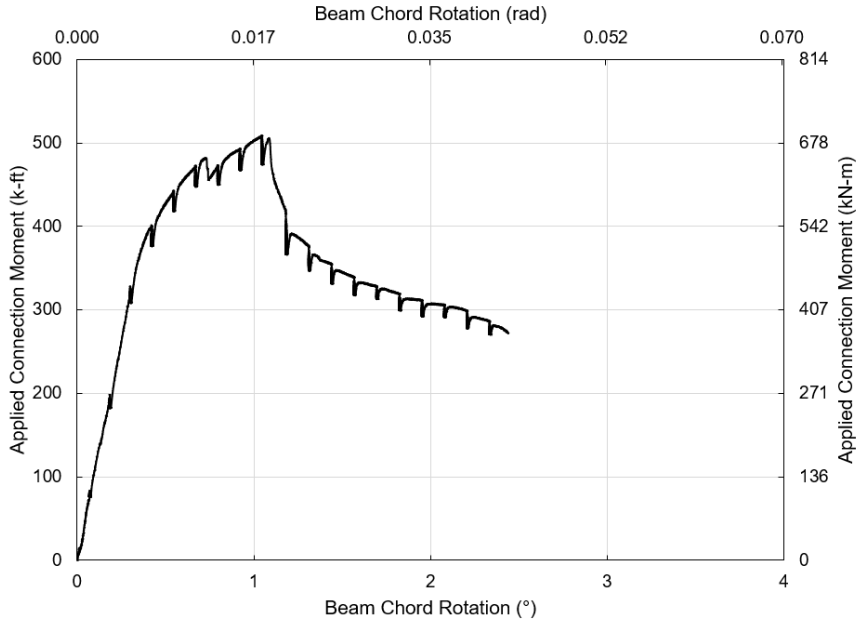

Fig. 4-18. Applied connection moment versus beam chord rotation for the grouted bar connection assembly.

Table 4-4. Measured vertical column displacement at the end of each loading increment (grouted bar).

Increment of Vertical Column Displacement, in (mm)	Measured Vertical Column Displacement, in (mm)	Corresponding Beam Chord Rotation, °	Increment of Vertical Column Displacement, in (mm)	Measured Vertical Column Displacement, in (mm)	Corresponding Beam Chord Rotation, °
0.00 (0)	0.00 (0)	0.00	2.75 (70)	2.57 (65)	1.31
0.25 (6.4)	0.14 (4)	0.07	3.00 (76)	2.83 (72)	1.44
0.50 (13)	0.36 (9)	0.18	3.25 (83)	3.08 (78)	1.57
0.75 (19)	0.59 (15)	0.30	3.50 (89)	3.33 (85)	1.69
1.00 (25)	0.83 (21)	0.42	3.75 (95)	3.58 (91)	1.82
1.25 (32)	1.07 (27)	0.54	4.00 (102)	3.82 (97)	1.94
1.5 (38)	1.32 (34)	0.67	4.25 (108)	4.07 (103)	2.07
1.75 (44)	1.56 (40)	0.80	4.50 (114)	4.33 (110)	2.21
2.00 (51)	1.81 (46)	0.92	4.75 (121)	4.58 (116)	2.33
2.25 (57)	2.05 (52)	1.04			
2.50 (64)	2.32 (59)	1.18			

4.5.2. Damage Progression and Failure Mode

Cracks in the beam-to-column grout interface, small concrete spalls near the bottom of the front faces of the beams, and cracks in the grouted hand holes existed before force was applied to the assembly. During the increment to 0.25 in (6.4 mm) of vertical column displacement, a crack that existed in the grout at the left beam-to-column interface near the bottom of the

column pocket before the application of force, propagated upward by approximately 2.00 in (50 mm). Approximately three flexural cracks each, occurred on the front and back faces of both the left and right beams during the subsequent vertical column displacement increment to 0.50 in (13 mm). The flexural cracks initiated at the bottom of the beam faces and extended upward past the mid-depth of the beams. During the same increment to 0.50 in (13 mm) of vertical column displacement, surface spalling occurred on the right side of the column behind the column pocket, and cracks propagated through the grouted hand holes located on the front faces of the beams. A substantial number of additional flexural cracks occurred on the front and back faces of the beams during the increment to 0.75 in (19 mm) of vertical column displacement, and existing flexural cracks continued to propagate upward.

During the vertical column displacement increment from 0.75 in to 1.00 in (19 mm to 25 mm), the moment-rotation response transitioned to nonlinear and a 0.20 in (5 mm) gap between the column and bottom of the right beam opened at the grouted interface. During subsequent increments of vertical column displacement, existing flexural cracks propagated, and the spalling on the right side of the column behind the column pocket worsened. After the increment from 2.25 in to 2.5 in (57 mm to 64 mm) of vertical column displacement, no new flexural cracks in the beams occurred nor did existing cracks further propagate, and gaps at the bottom of the beams between the beam ends and grouted interface began to consistently widen with increasing vertical column displacement. By this point, cracks had developed near the top of the column owing to the top ends of the beams bearing against the column and creating large compressive stresses. Ultimately, the connection failed via rupture of the continuity bar directly above the bottom continuity bar. The rupture occurred near the left beam-to-column interface within the length of bar that was debonded from the concrete (see Fig. 4-19).

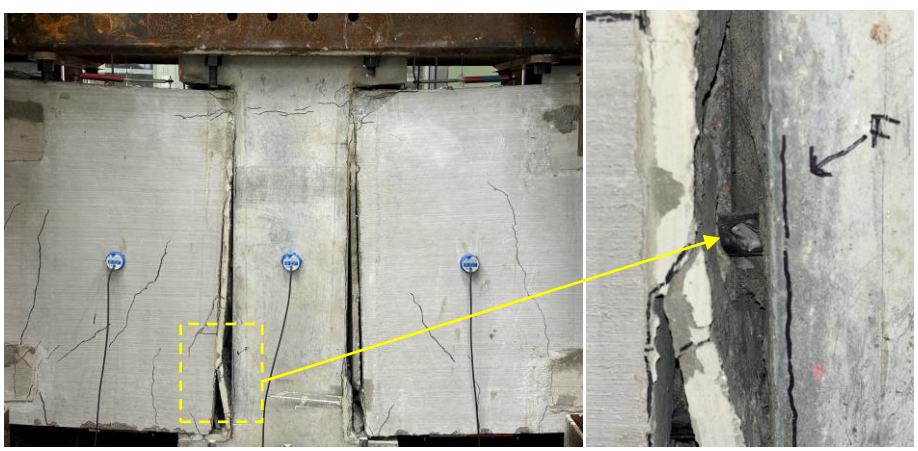

Fig. 4-19. Failure mode of the grouted bar connection assembly.

4.5.3. Displacement Profile and Rotation

Fig. 4-20 shows vertical displacement profiles for the grouted bar connection assembly. Beginning at the first displacement profile and moving sequentially to the last profile from smallest to largest vertical displacements, the profiles correspond to approximately midway

through the linear region of assembly response (θ = 0.19°), the transition point from linear to nonlinear response (θ = 0.35°), the ultimate moment (θ = 1.04°), and the instant just before rupture of the continuity bar located directly above the bottom continuity bar (θ = 2.44°). All the displacement profiles are fairly symmetric, with the exception of noticeable asymmetry resulting from different displacement measurements of the left side of the column compared to those on the right side. Displacements were larger on the right side of the column for most of the test, with the last displacement profile showing a slightly larger displacement of the left side of the column. This finding indicates that the column was initially rotating clockwise before transitioning to a slightly counterclockwise rotation.

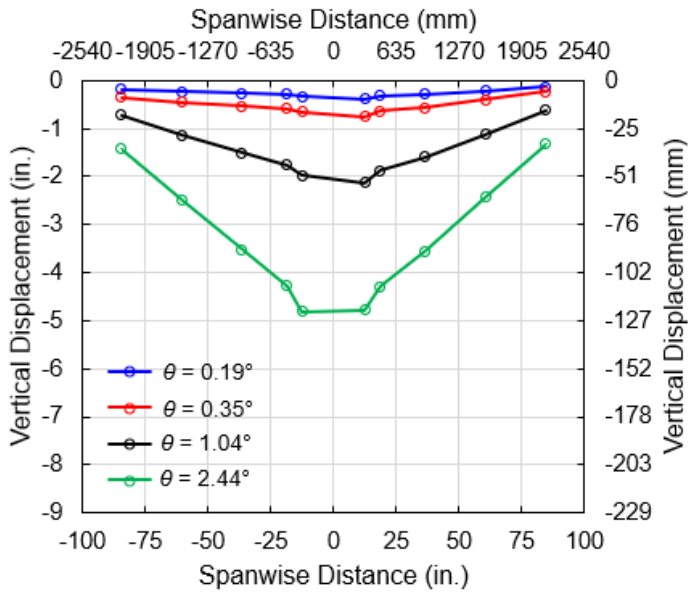

Fig. 4-20. Vertical displacement profiles of the grouted bar connection assembly.

Fig. 4-21 shows the in-plane rotation of the precast concrete beams and column from inclinometer measurements plotted as a function of vertical column displacement. In a manner similar to the previously discussed connection assembly beams, the beams in the grouted bar connection assembly rotated as rigid bodies, as indicated by the close agreement between the inclinometer measurements and beam chord rotation curves. As shown in Fig. 4-21, the column (R03) rotated clockwise until 1.40 in (36 mm) of vertical column displacement (0.72 degrees of beam chord rotation) and then gradually began to rotate counterclockwise for the remainder of the test. This counterclockwise rotation of the column led to a concentration of deformation at the left beam-to-column interface, which led to rupture of the continuity bar at this location.

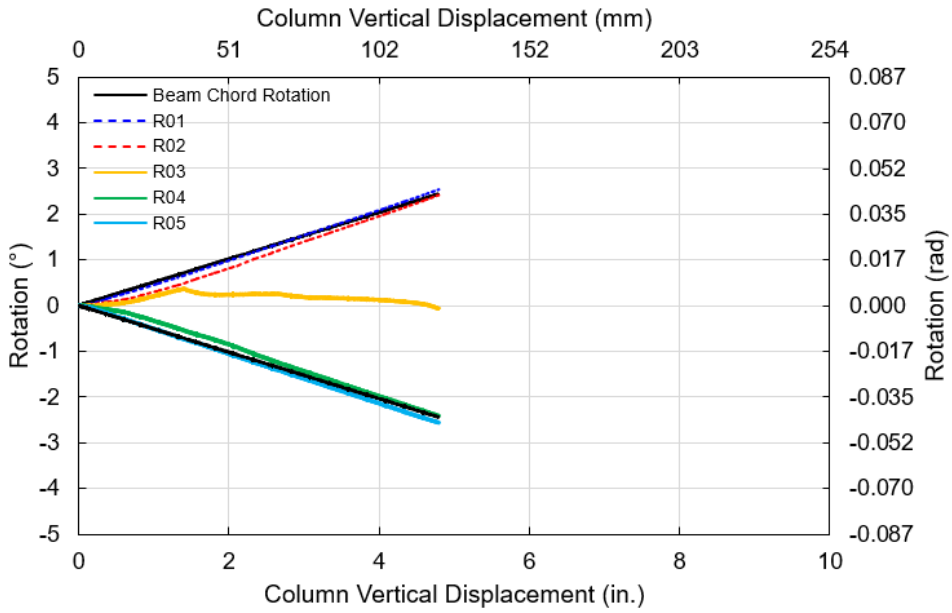

Fig. 4-21. Measured in-plane rotations of the precast concrete beams and columns for the grouted bar connection assembly.

4.5.4. Strain Measurements

Fig. 4-22 shows measured strains of the flexural reinforcing steel in the bottom of the left beam as a function of column vertical displacement (see Appendix B for gauge locations). The steel yielded at a column vertical displacement of 0.85 in (22 mm) and a beam chord rotation of 0.43 degrees. A strain of 0.0026 was considered as indicative of yield in any reinforcing bar, assuming that the ASTM A706 Grade 60 (414 MPa) steel had a yield strength of 74 ksi (510 MPa) and an elastic modulus of 29,000 ksi (200 GPa). The initiation of yielding of the flexural reinforcing occurred near where the moment versus rotation response transitioned from linear to nonlinear at 0.35 degrees of beam chord rotation. After yielding, both steel reinforcing bars achieved maximum strains of 0.0029 at approximately 2.08 in (53 mm) of column vertical displacement, which corresponded to 1.06 degrees of beam chord rotation. The maximum strains occurred near when the connection assembly achieved its ultimate moment at 1.04 degrees of beam chord rotation. After the maximum strains were reached, the strains in the bars began to decrease before eventually plateauing. The plateauing of the strains in the reinforcing steel coincided with a concentration of strain in the grouted continuity bar that eventually ruptured.

The flexural reinforcing steel in the right beam did not yield. The largest strain gauge measurements in the right beam were from gauges 51 and 52, which had maximum strains of 0.0017 and 0.0020, respectively.

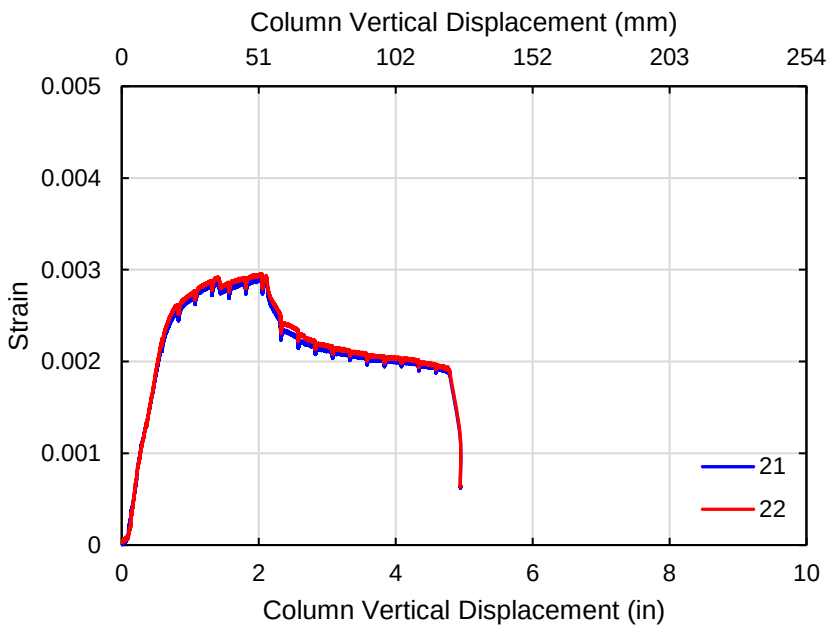

Fig. 4-22. Strain in flexural reinforcing bars at the bottom of the left beam (grouted bar connection assembly).

4.6. Modified Link Plate

4.6.1. Moment-Rotation Behavior

Fig. 4-23 shows the applied connection moment versus beam chord rotation up to connection failure for the modified link plate connection assembly. The initial response was linear with a slope of 2595 kip-ft (3518 kN-m) per degree of chord rotation. The response quickly transitioned to nonlinear at a moment of approximately 121 kip-ft (164 kN-m), which corresponded to a beam chord rotation of 0.05 degrees. This transition to nonlinear response was accompanied by the occurrence of flexural cracks on the front and back faces of the beams, which extended from the bottom of the beams and upward past their mid-depth in some cases. The factored moment demand for which the connections were designed was 234 kip-ft (317 kN-m), and the moment-rotation response was nonlinear when this demand was achieved at a beam chord rotation of 0.12 degrees.

After the transition to nonlinear response, an ultimate moment of 472 kip-ft (640 kN-m) was achieved at a beam chord rotation of 0.72 degrees. Shortly after the ultimate moment was achieved, rupture occurred through the reduced-width section of the bottom-left link plate at a moment of 469 kip-ft (636 kN-m) and a beam chord rotation of 0.76 degrees. The failure was brittle in nature, with only a very small reduction in moment before net tensile rupture of the link plate occurred. The measured vertical column displacement and corresponding beam chord rotations are presented in Table 4-5.

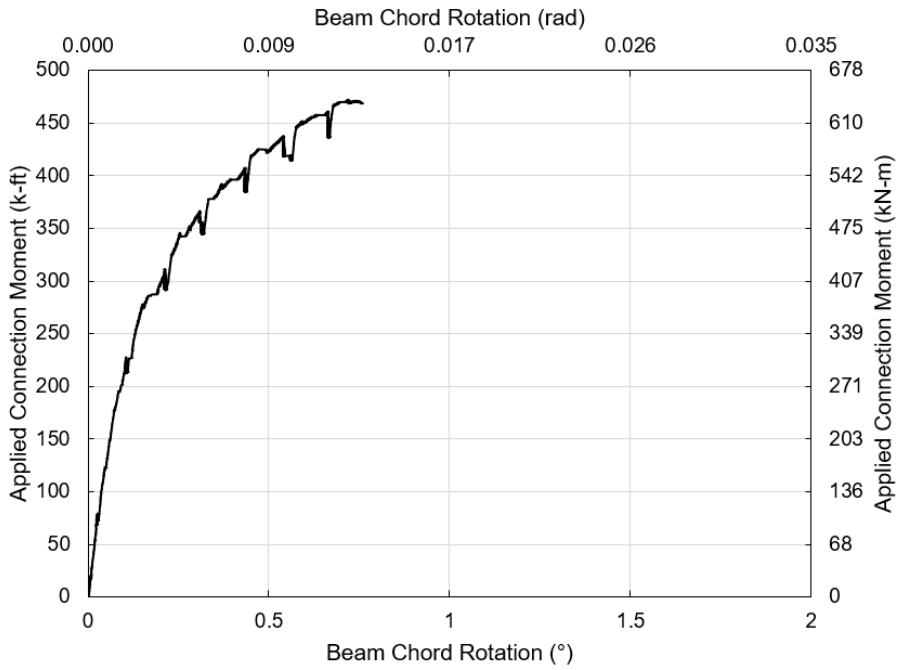

Fig. 4-23. Applied connection moment versus beam chord rotation for the modified link plate connection assembly.

Table 4-5. Measured vertical column displacement at the end of each loading increment (modified link plate).

Increment of Vertical Column Displacement, in (mm)	Measured Vertical Column Displacement, in (mm)	Corresponding Beam Chord Rotation, °
0.00 (0)	0.00 (0)	0.00
0.25 (6.4)	0.05 (1)	0.03
0.50 (13)	0.21 (5)	0.11
0.75 (19)	0.42 (11)	0.21
1.00 (25)	0.61 (15)	0.31
1.25 (32)	0.85 (22)	0.43
1.5 (38)	1.06 (27)	0.54
1.75 (44)	1.31 (33)	0.66

4.6.2. Damage Progression and Failure Mode

During the first increment to 0.25 in (6.4 mm) of vertical column displacement, small horizontal cracks formed on the front faces of the beams near where the upper link plates protruded from the ends of the beams. During the increment from 0.25 in to 0.50 in (6.4 mm to 13 mm) of

vertical column displacement, flexural cracking initiated on the front and back faces of both the left and right beams. A few of the flexural cracks extended upward past the mid-depth of the beams. Subsequent increments caused an increase in the number of flexural cracks as well as the propagation of existing cracks. During the increment from 1.25 in to 1.50 in (32 mm to 38 mm) of vertical column displacement, small diagonal cracks propagated from the left and right pins on the back faces of the beams. During the following increment from 1.50 in to 1.75 in (38 mm to 44 mm) of vertical column displacement, no new cracks formed and only minor extensions of the flexural cracks on the front and back faces of the beams were observed. Rupture of the bottom-left link plate occurred during the increment from 1.75 in to 2.00 in (44 mm to 51 mm) of vertical column displacement (Fig. 4-24).

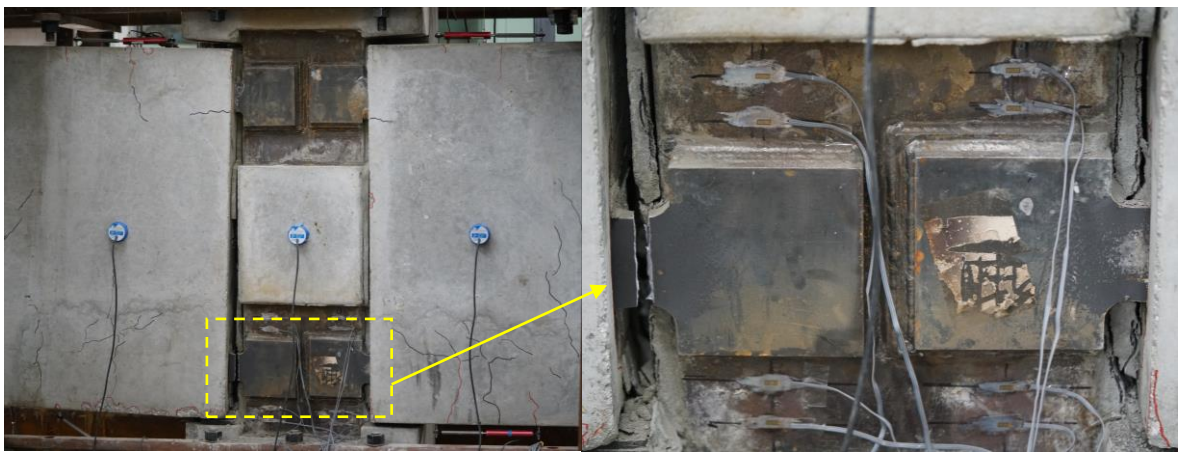

Fig. 4-24. Failure mode of the modified link plate connection assembly.

4.6.3. Displacement Profile and Rotation

Fig. 4-25 shows vertical displacement profiles for the modified link plate connection assembly. Beginning at the first displacement profile and moving sequentially to the last profile from smallest to largest vertical displacements, the profiles correspond to approximately midway through the linear region of assembly response (θ = 0.02°), the transition point from linear to nonlinear response (θ = 0.05°), the ultimate moment (θ = 0.72°), and the instant just before rupture of the bottom-left link plate (θ = 0.76°). The displacement profiles have an appearance of marked asymmetry due to the small vertical displacements that the assembly underwent compared to the displacements of the other connection assemblies. The largest discrepancy in symmetric displacement measurements occurred in the measurements of the left and right sides of the column, with their difference being as large as 0.44 in (11 mm) near the end of the test. The displacement profiles indicate that the column was rotating counterclockwise, which contributed to the concentration of deformation in the bottom-left link plate that eventually led to its rupture.

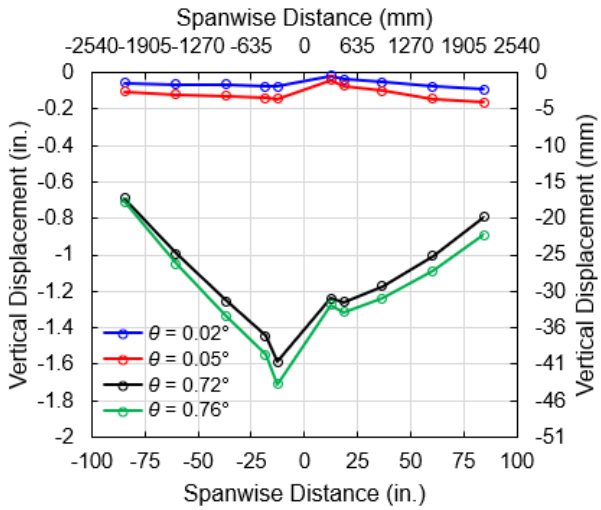

Fig. 4-25. Vertical displacement profiles of the modified link plate connection assembly.

Fig. 4-26 shows the in-plane rotation of the precast concrete beams and column from inclinometer measurements plotted as a function of vertical column displacement. The curves indicating rotation measurements from inclinometers on the left beam (R01 and R02) and right beam (R04 and R05) are nearly the same as the curves for the beam chord rotation. This finding indicates that the beams were undergoing rigid body rotations and that deformations were localized at the beam-to-column connections. The curve indicating rotation measurements of the column (R03) shows that the column was rotating increasingly counterclockwise for the duration of the test, which was also confirmed by the string potentiometer measurements.

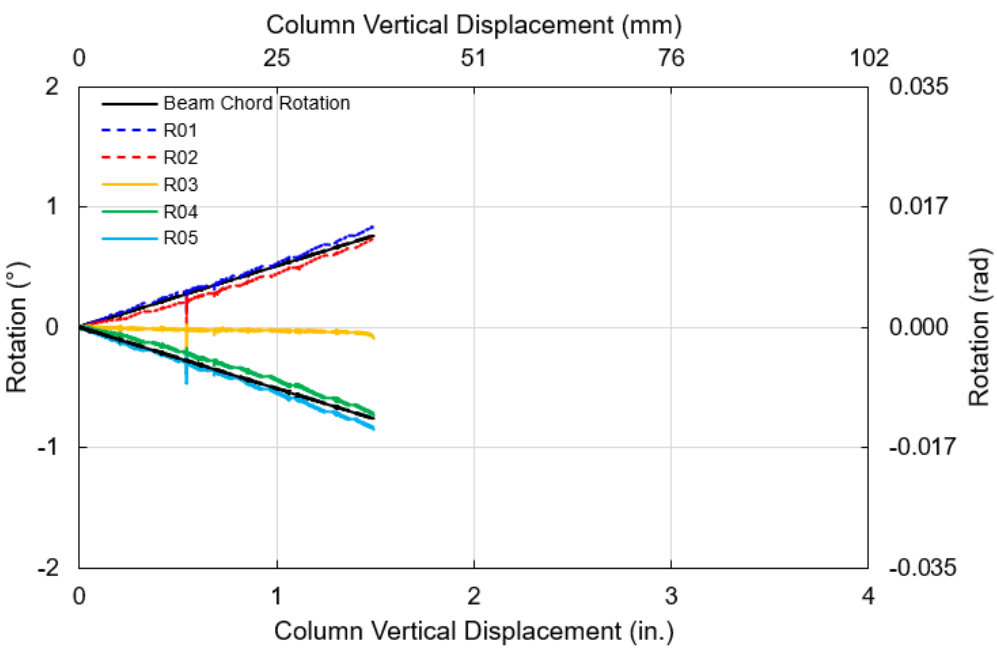

Fig. 4-26. Measured in-plane rotations of the precast concrete beams and columns for the modified link plate connection assembly.

4.6.4. Strain Measurements

After the moment connections for the modified link plate connection assembly were made, eight strain gauges were affixed to the front surface of the steel channel embedded at the bottom of the column. The strain gauges were oriented parallel to the length of the beams to measure the surface strains induced in the steel channel by the transfer of tensile force from the link plates. The steel channels embedded in the column were made from a dual-certified hot-rolled carbon steel, which met the requirements of both ASTM A36 (ASTM 2019) and ASTM A572 Grade 50 (ASTM 2021c) specifications. The strains remained under 0.0005 for the duration of the test, which is substantially less than the nominal yield strain of the steel (0.0017). The nominal yield strain of the steel channel was obtained by dividing the nominal yield stress of the steel of 50 ksi (345 MPa) by its elastic modulus of 29,000 ksi (200 GPa).

Fig. 4-27 shows measured axial strains in all four link plates. Strain gauges were affixed to the front surface of the reduced-width section of the link plates (see Appendix B for gauge locations). The gauges indicated tensile strains (positive values) in the bottom link plates and compressive strains (negative values) in the top link plates, which was expected based on the location of the link plates. The largest tensile strains were in the bottom-left link plate, which was the link plate that eventually ruptured through its reduced-width section. The top-left and top-right link plates experienced compressive strains, but at a magnitude that was smaller than that of the tensile strains in the bottom link plates.

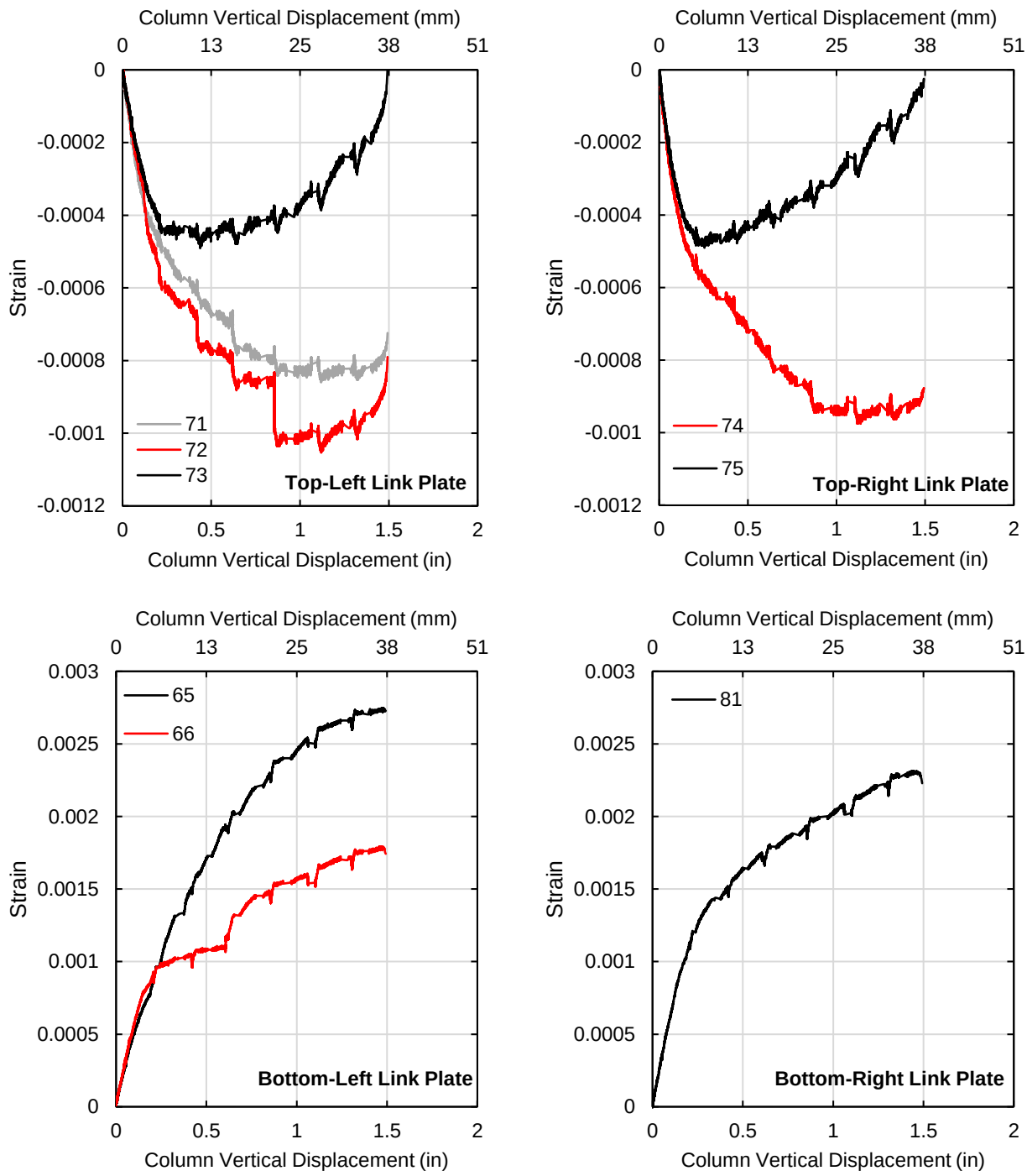

Fig. 4-27. Strains in the link plates.

Strain gauges were installed on the anchorage bars in pairs on opposite sides of the bars at the same cross-section location. Figure 4-28 shows measured strains in the anchorage bars according to the locations of strain gauges shown in Appendix B. The strain gauges on the anchorage bars near the tops of the beams recorded compressive strains (negative values),

whereas the strain gauges on the anchorage bars near the bottoms of the beams recorded tensile strains (positive values). The anchorage bars near the bottom of the left beam experienced slightly larger tensile strains than the anchorage bars near the bottom of the right beam, which was expected, since connection failure occurred in the bottom-left link plate.

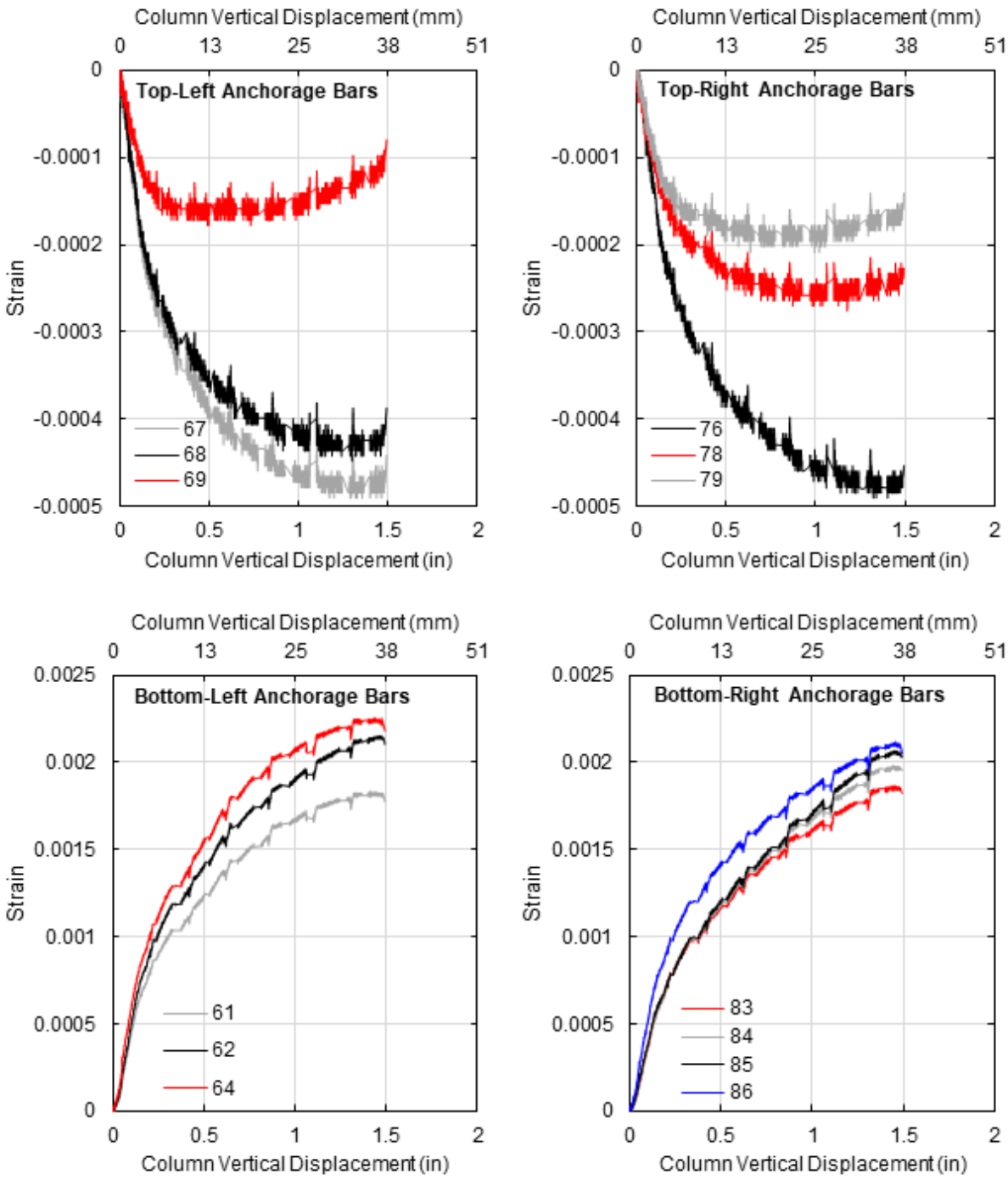

Fig. 4-28. Strains in the anchorage bars.

4.7. Summary and Discussion

Figure 4-29 shows a comparison plot of the vertical force versus column vertical displacement for all five connection assemblies. Table 4-6 summarizes important parameters that characterize the behavior of all five connection assemblies. The link plate connection assembly was the stiffest of the assemblies, being more than 5 times stiffer than the threaded rod connection assembly, and approximately 2.5 times stiffer than the bar coupler and grouted bar connection assemblies, which had similar stiffnesses. The high stiffness of the link plate connection assembly was attributed to the continuity developed through welding of the link plates to the channels embedded in the columns. In contrast, the other connection assemblies used discrete connection components (threaded couplers and grouted reinforcing bars) that allowed for larger initial vertical displacement to occur once loading began.

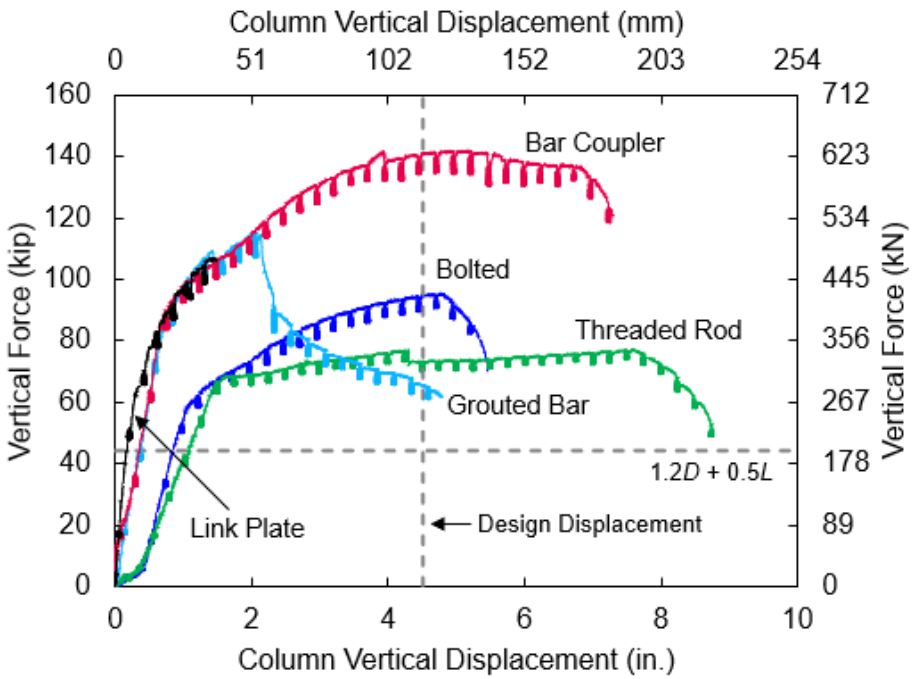

Fig. 4-29. Force versus displacement responses for all five connection assemblies.

Table 4-6. Summary of experimental results.

Performance Metric	Threaded Rod	Bolted	Bar Coupler	Grouted Bar	Modified Link Plate
Stiffness, kip-ft/° (kN-m/°)	474 (643)	713 (967)	1007 (1365)	1036 (1405)	2595 (3518)
Ultimate moment, kip-ft (kN-m)	340 (461)	419 (568)	627 (850)	509 (690)	472 (640)
Rotation at ultimate moment, °	3.87	2.43	2.65	1.04	0.72
Moment at failure, kip-ft (kN-m)	222 (301)	308 (418)	531 (720)	272 (369)	469 (636)
Rotation at failure, °	4.44	2.78	3.71	2.44	0.76
Ratio of moment demand to ultimate moment	0.69	0.56	0.37	0.46	0.50

The connection assembly beams in this test program were designed to resist a combination of bending and shear loads. Concrete will crack under load when its internal stresses exceed its strength. Because the formation of cracks in concrete precedes other failure modes, cracking is an important damage mechanism that can be used to compare the performance of the connection assemblies. Since the assemblies were designed to develop concentrated rotations at the beam-to-column connections, the beams were not expected to undergo substantial cracking/damage, in contrast to if the assemblies had relied on distributed curvature (flexural yielding) in the beams to resist load. The threaded rod and bolted connection assemblies had flexural cracking initiate in their beams at a later loading increment than in the other connection assemblies. These two connection assemblies were also the least stiff. The bar coupler connection assembly suffered the most severe and extensive cracking and damage, with much of the damage concentrated at the top of the column near the grouted blockout and at the top of the left beam near where it bore against the column.

The bar coupler connection assembly had the greatest moment capacity of the connection assemblies, achieving an ultimate moment of 627 kip-ft (850 kN-m) at 2.65 degrees of chord rotation. The grouted bar connection assembly had the second greatest moment capacity [509 kip-ft (690 kN-m)], followed by the modified link plate connection assembly [472 kip-ft (640 kN-m)], bolted connection assembly [419 kip-ft (568 kN-m)] and then the threaded rod connection assembly [340 kip-ft (461 kN-m)]. The required moment demand stipulated by design was 234 kip-ft (317 kN-m), and all five connection assemblies successfully sustained this demand before failure. Table 4-6 shows the ratio of the moment demand to ultimate moment for each connection assembly, which will be referred to as the demand-capacity ratio (DCR). The bar coupler connection assembly had the lowest DCR of 0.37, whereas the threaded rod connection assembly had the highest DCR of 0.69. The other three connection assemblies had DCRs between those of the bar coupler connection assembly and threaded rod connection assembly. These DCRs indicate that the connection assemblies had adequate strength, but DCRs alone are not adequate to assess the ability of the connection assemblies to withstand the applicable design gravity loading under sudden column loss. However, a robustness index can be used to determine whether collapse from gravity loading would be arrested under sudden column loss. Further information on the robustness index and a comparison of the robustness indexes between the connection assemblies is provided in Sec. 5.

Rotational capacity is another key response characteristic of structural connections that can indicate enhanced collapse resistance of a structure. In the context of this report, rotational capacity is used to quantify the ductility of the tested connection assemblies. Ductility is a measure of the ability of a structural component or system to sustain plastic deformation without failure. The rotational capacity of the connection assemblies is defined as the beam chord rotation corresponding to their ultimate moment capacity. Using this definition of rotational capacity, the threaded rod connection assembly had a rotational capacity of 3.87 degrees, which is the largest among the connection assemblies and nearly 70 % larger than the 2.29-degree target rotational capacity that the connection assemblies were designed to achieve. The bar coupler and bolted connection assemblies had rotational capacities of 2.65 degrees and 2.43 degrees, respectively, which both exceeded the target design rotational capacity. The high strength and stiffness of the grouted bar connection assembly came at a

sacrifice of ductility, as it had a rotational capacity of 1.04 degrees. If the full connection response is considered, the grouted bar connection assembly was able to sustain the required gravity loading and exceed the target design rotational capacity, as connection failure occurred at 2.44 degrees of chord rotation. The modified link plate connection assembly severely underperformed regarding ductility, as it had a rotational capacity of 0.72 degrees. The lack of ductility of the modified link plate connection assembly is attributed to a fabrication error which resulted in welding along the edges of the reduced-width section of the link plates. These welds provided excess axial restraint which encouraged axial deformations to concentrate along only a small length of the reduced-width section of the link plates, ultimately leading to premature connection failure.

The purpose of this study was to generate experimental data that characterizes the behavior of novel precast concrete beam-to-column moment connections. Comparisons of the results from each test were made in this section to help ascertain which connection concept(s) would be most effective at arresting disproportionate collapse under a simulated column removal scenario. Although efforts were made to limit variability between each connection assembly test (i.e., ensuring the only variable was the connection concept that was implemented), there was inevitably variation between tests. Because no replicate connection assemblies were fabricated or tested to understand the potential for specimen-to-specimen variations in rotational capacity, stiffness, strength, or damage progression, there are plans to conduct high-fidelity computational modeling to help quantify how potential specimen-to-specimen variations might affect the behavior of the connection assemblies.

5. Structural Robustness

5.1. Background

Robustness can be defined as the ability of a structural system to operate without failure under a broad range of loadings (Zaghi et al., 2016). For example, a robust structure would be expected to resist substantial damage when subjected to extreme loads, such as those produced by hurricanes, earthquakes, and explosions. In the context of disproportionate collapse, a building is considered robust if it can sustain an initial local failure without an ensuing collapse of all or part of the building. Numerous frameworks or methodologies have been proposed by various researchers to quantify structural robustness, and a succinct review and discussion of many of these approaches can be found in Bao et al. (2017).

An energy-based framework that has been widely accepted in the research community was developed by Izzuddin et al. (2008). Within that framework, estimates of the capacity of a structural system under a dynamic loading scenario, such as sudden column loss, can be ascertained from a static pushdown test of the structural system with an unsupported column. The framework operates under the premise that at the instant when the maximum vertical displacement above the removed column is reached, the kinetic energy of the system is zero and the external work done by the gravity loading is equal to the internal energy (i.e., the energy absorbed by the structure). Bao et al. (2017) used this framework in conjunction with aspects of other research to develop a robustness index *R*. In the same article, Bao et al. (2017) presented a case study in which robustness indexes were calculated for two 10-story reinforced concrete buildings: one using intermediate moment frames and one using special moment frames. The buildings were modeled in LS-DYNA (Hallquist, 2007) using a reduced-order finite element (FE) approach and were subjected to seven different column removal scenarios in which a single column was removed at the first-story level in each scenario. Static pushdown analyses were conducted to determine if the buildings could sustain the applicable gravity loading on the floor system after removal of a single column. The robustness index of the special moment frame building was greater than that of the intermediate moment frame building, indicating that the stringent seismic design and detailing practices of the special moment frame building resulted in superior robustness against column loss.

The robustness index quantifies the ability of a structure to withstand gravity loading under sudden column loss, with a value above unity indicating that the collapse will be arrested. The robustness index, *R* for the connection assemblies can be calculated using the following equation:

$$\boldsymbol{R} = \frac{\mathbf{1}}{\boldsymbol{P_G \Delta_u}} \int_{\mathbf{0}}^{\Delta_u} \boldsymbol{P}(\Delta)\, \boldsymbol{d}\Delta \qquad (\mathbf{5.1})$$

where

P_G = factored service-level gravity load acting on the unsupported column according to the extraordinary events load case ($1.2D + 0.5L + A_k$) specified in ASCE 7-22 (ASCE 2022)
Δ_u = vertical displacement of the unsupported column corresponding to the ultimate static load

Δ = vertical displacement of the unsupported column
$P(\Delta)$ = force-displacement relationship obtained from static pushdown, taken in this report as the vertical force versus displacement response measured during the precast concrete connection assembly test

When calculating R, the load or load effect resulting from the extraordinary event A_k equals 0 and plays no role in the determination of the factored service-level gravity load acting on the unsupported column according to the extraordinary events load case, P_G because the load effect resulting from the extraordinary event (column loss) was physically considered in the testing by pushing down the unsupported column. Taking A_k as equal to 0 is also fully consistent with performing Alternative Load Path Analysis under the guidance in the ASCE/SEI 76-23 *Standard for Mitigation of Disproportionate Collapse Potential in Buildings and Other Structures* (ASCE 2023).

5.2. Results, Comparisons, and Limitations

Figure 5-1 shows the force versus displacement curves up to connection failure of all five connection assemblies for both static loading and sudden column loss. The sudden column loss curves were derived by numerically integrating the static loading curves over the interval from zero to maximum column vertical displacement, normalizing by the column vertical displacement at each subinterval to obtain units of force, and then plotting the normalized values as a function of the static column vertical displacement. The resistances to sudden column loss are less than the resistances to static column loss because the resistances to sudden column loss account for the detrimental dynamic effects induced by sudden column loss. The ultimate capacities under sudden column loss are indicated by the point where the vertical dashed line intersects the sudden column-loss curves. The vertical dashed lines intersect the static loading curves at the points at which their ultimate capacities are achieved.

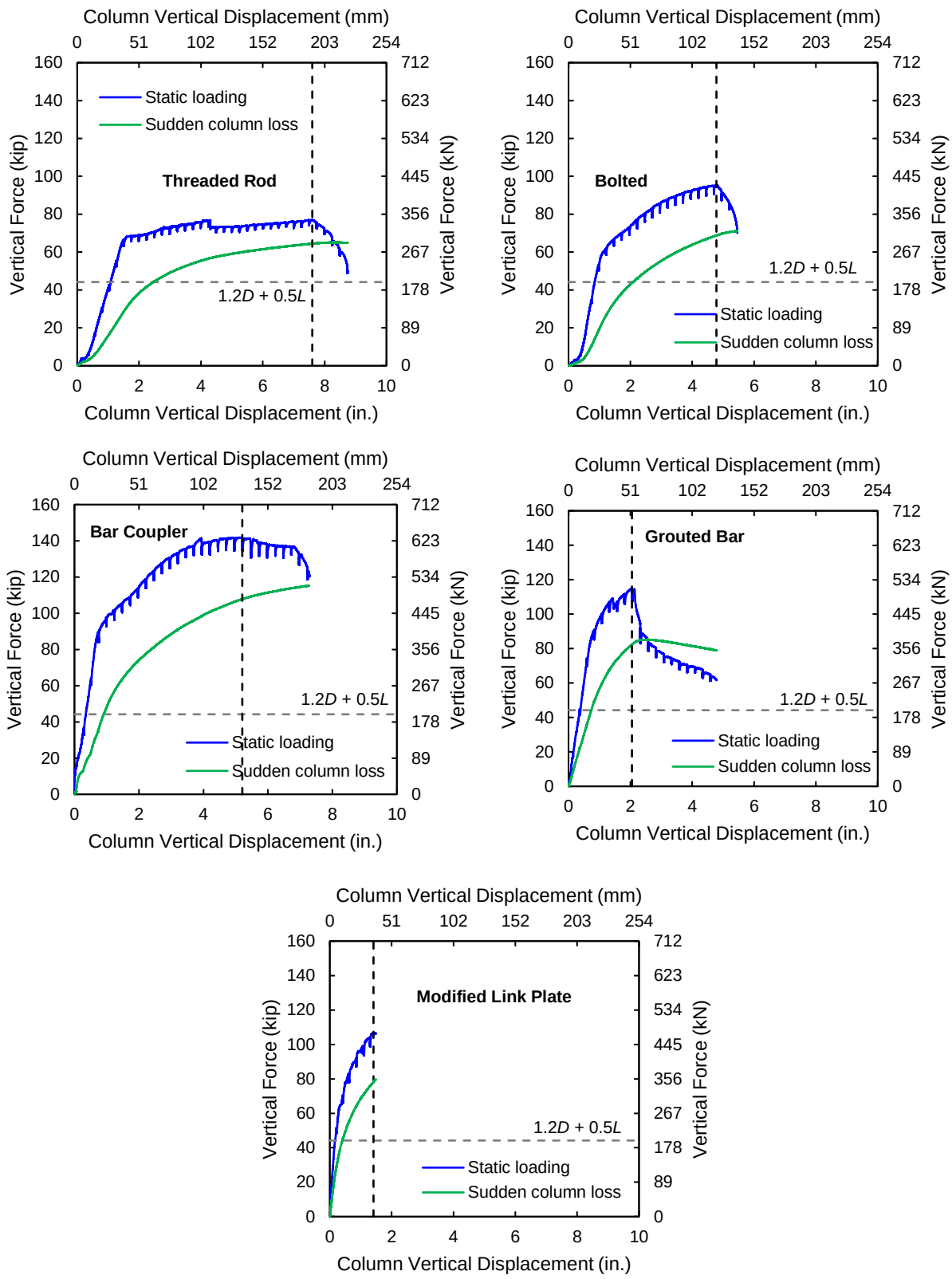

Fig. 5-1 Force versus displacement responses considering static loading and sudden column loss.

Table 5-1 shows the robustness index of each connection assembly rounded to the nearest tenth. The robustness index was obtained by normalizing the sudden column loss capacities by the factored service-level gravity loading of 44.2 kip (197 kN), which is indicated in Fig. 5-1 by the horizontal dashed lines labeled "1.2*D* + 0.5*L*." Each connection assembly had a robustness index greater than unity, indicating reserve capacity against collapse during sudden column loss under the applicable service-level gravity loads. As an example, the robustness indexes for the bolted and threaded rod connection assemblies indicate they could sustain loads 60 % and 50 % greater, respectively, than the 44.2 kip (197 kN) that they would need to sustain under sudden column loss to prevent collapse.

Table 5-1. Robustness indexes of the tested assemblies

Connection	Robustness Index
Threaded Rod	1.5
Bolted	1.6
Bar Coupler	2.4
Grouted Bar	1.9
Modified Link Plate	1.8

Among the five precast moment connection assemblies, the bar coupler connection assembly had the largest robustness index (2.5) and the greatest strength, while the threaded rod connection assembly had the smallest robustness index (1.5) and the least strength. There is a direct correlation between the robustness index and the strength of the connection assemblies. Stated differently, the robustness index increases with ultimate force/moment strength of the connection assemblies. This finding indicates that strength is more influential on the robustness index compared to ductility. In fact, ductility only indirectly influences the robustness index, specifically in cases where strength (i.e., resistance to vertical load) increases with increased ductility due to geometric nonlinearity.

6. Summary and Conclusions

This report presented an experimental study of five precast concrete moment-frame assemblies tested under a column-removal scenario. Each assembly used a different, novel connection concept intended to address potential vulnerabilities that were observed by NIST researchers during full-scale testing of precast concrete moment-resisting spandrel beam-to-column connection assemblies that used conventional welded link plates. One of the five connection assemblies required field welding, whereas the other four connection assemblies used grouted steel bars or mechanical couplers to make moment connections. The assemblies were derived at a five-eighth scale from a 10-story prototype building and consisted of two spandrel beams connected to a central stub column. The central column was subjected to monotonically increasing vertical displacement until connection failure.

The results of the connection assembly tests were evaluated with respect to strength, stiffness, rotational capacity, and damage progression. The fabrication details of the specimens and procedures to erect and make the connections in a laboratory setting were also discussed in detail, focusing on the advantages and disadvantages of each connection concept.

The following main conclusions were reached based on the test results.

1. In the laboratory, the threaded rod assembly's moment connections were the easiest to assemble of all the connection assemblies. The coarse threads and long lengths of the threadbars provided flexibility to make the connections quickly and easily. The bar coupler and grouted bar connection assemblies' moment connections were more difficult to make compared to the threaded rod and bolted connection assemblies' moment connections because of the grouting operation that was required. The bar coupler and grouted bar connection assemblies required a flowable grout, and thus, a grout pump and formwork were necessary. Besides the connections for the modified link plate connection assembly, the connections in the other assemblies could be made by hand, thus eliminating the need for costly field welding and specialized labor.

2. Strength and ductility are two characteristics that can play a critical role in enhancing collapse resistance. The bar coupler connection assembly performed exceptionally well with respect to both; it achieved an ultimate moment strength of 627 kip-ft (850 kN-m), which was 23 % greater than the strength achieved by the grouted bar connection assembly, which was the second strongest of the five tested assemblies. The bar coupler connection assembly was also remarkably ductile with a rotation at ultimate moment of 2.65 degrees, which is nearly 16 % greater than the design target rotational capacity of 2.29 degrees and second to the threaded rod connection assembly, which had a rotation at ultimate moment of 3.87 degrees.

3. All the connection assemblies had a robustness index greater than unity, indicating that they could have sustained loads greater than the 44.2 kip (197 kN) that they would need to sustain to prevent collapse under sudden column loss.

4. All the connection assemblies failed as was intended by their design. Each connection assembly had components that were designed as ductile fuses, and it was within these fuses that deformations localized and failure ultimately occurred. For the modified link plate connection assembly, failure occurred by rupture of the bottom-left link plate. For the threaded

rod and bolted connection assemblies, failure occurred via tensile rupture of one of the threaded rods or anchor bolts. For the grouted bar and bar coupler connection assemblies, failure occurred via tensile rupture of one of the deformed reinforcement bars. The ability to control the failure modes of the connection assemblies through capacity design principles indicates the appropriateness of the design procedures that were used. The designs resulted in predictable behavior of the connection assemblies, which suggests the suitability of these connections for use in precast concrete construction.

6.1. Recommendations

To ensure proper fit-up during erection, care should be taken during the production of the precast concrete beams and columns. For the threaded rod and bolted connection assemblies, the couplers should be level with no out-of-plane skewness and should be secured to ensure that they do not move during casting. For the bolted connection, it is recommended that the anchor bolt threads be rolled instead of cut because rolled threads will likely be easier to thread into the coupling nuts embedded in the column. The process by which rolled threads are created results in threads that are typically free of surface imperfections and more resistant to damage, making them the preferred choice to ensure ease of construction in the field.

It is recommended that the bar coupler connection assembly use couplers that maximize erection tolerances to ensure that the connections can be easily made. The couplers used for the bar coupler connection assembly were from Headed Reinforcement Corp. (HRC). The HRC's XL series couplers were used because they provided extra erection tolerances compared to their 500/510 series couplers. Specifically, the XL series couplers feature lengthened collars to accommodate distances between the upset ends of the connection components of up to 1.00 in (25 mm).

The force versus displacement responses of the grouted bar and bar coupler connection assemblies closely matched until approximately 2.00 in (51 mm) of column vertical displacement was reached, at which point the strength of the grouted bar connection assembly began to decrease. It is postulated that the continuity bars in the grouted bar connection assembly were not fully debonded from the grout over the entire 21 in (533 mm) length, as was stipulated in the design. Had these bars been fully debonded over the entire 21 in (533 mm), the strains in the bars would have been distributed over a greater length (i.e., the strains would have been more uniform along the debonded length), resulting in a more ductile and stable response. Instead, strain appeared to quickly concentrate in one cross-section of the continuity bar, leading to its eventual rupture. It is recommended that a rigid material such as PVC piping be used to ensure that no bond develops between the continuity bars and surrounding grout.

For the modified link plate connection assembly, it is recommended that the link plates be secured so that they do not move during casting. Care also should be taken to ensure that the plates are not skewed so that welding can occur without the need for filler plates. Since a fabrication error led to the link plates having welds along the edges of their reduced width, computational modeling will need to be used to further investigate the behavior of the as-designed modified link plate connection assembly.

Although all the connection assemblies were designed to nominally have the same capacity, the ultimate moment strength of the bar coupler and grouted bar connection assemblies was at least 50 % larger than that of the threaded rod connection assembly, which had the lowest ultimate moment strength of the assemblies. This substantial difference in strength did not prevent the capacity design approach used for these connection assemblies from working as intended. However, designers should be aware of this difference in strength in case a different design approach is used. The greater strengths of the bar coupler and grouted bar connection assemblies compared to the strengths of the other connection assemblies is attributed to their greater continuity, which was provided by four layers of deformed bar reinforcement. In contrast to the four-layer configuration, the other three connection assemblies had two layers of steel components that provided continuity.

References

ACI (2005) *ACI 318-05 Building Code Requirements for Structural Concrete* (American Concrete Institute, Farmington Hills, MI).

AISC (2005) *ANSI/AISC 360-05 Specification for Structural Steel Buildings* (American Institute of Steel Construction, Chicago, IL).

ASCE (2005) *SEI/ASCE 7-05 Minimum Design Loads for Buildings and Other Structures* (American Society of Civil Engineers, Reston, VA).

ASCE (2022) *SEI/ASCE 7-22 Minimum Design Loads and Associated Criteria for Buildings and Other Structures* (American Society of Civil Engineers, Reston, VA).

ASCE (2023) *SEI/ASCE 76-23 Standard for Mitigation of Disproportionate Collapse Potential in Buildings and Other Structures* (American Society of Civil Engineers, Reston, VA).

ASTM International (2016) *ASTM A706/A706M-16 – Standard Specification for Deformed and Plain Low-Alloy Steel Bars for Concrete Reinforcement* (ASTM International, West Conshohocken, PA).

ASTM International (2017) *ASTM C496/C496M-17 – Standard Test Method for Splitting Tensile Strength of Cylindrical Concrete Specimens* (ASTM International, West Conshohocken, PA).

ASTM International (2018) *ASTM A722/A722M-18 – Standard Specification for High-Strength Steel Bars for Prestressed Concrete* (ASTM International, West Conshohocken, PA).

ASTM International (2019) *ASTM A36/A36M-19 – Standard Specification for Carbon Structural Steel* (ASTM International, West Conshohocken, PA).

ASTM International (2020a) *ASTM C1107/C1107M-20 – Standard Specification for Packaged Dry, Hydraulic-Cement Grout (Nonshrink)* (ASTM International, West Conshohocken, PA).

ASTM International (2020b) *ASTM F1554-20 – Standard Specification Anchor Bolts, Steel, 36, 55, and 105-ksi Yield Strength* (ASTM International, West Conshohocken, PA).

ASTM International (2021a) *ASTM C109/C109M-21 – Standard Test Method for Compressive Strength of hydraulic Cement Mortars (Using 2-in. or [50 mm] Cube Specimens)* (ASTM International, West Conshohocken, PA).

ASTM International (2021b) *ASTM C39/C39M-21 – Standard Test Method for Compressive Strength of Cylindrical Concrete Specimens* (ASTM International, West Conshohocken, PA).

ASTM International (2021c) *ASTM A572/A572M-21 – Standard Specification for Carbon Structural Steel* (ASTM International, West Conshohocken, PA).

ASTM International (2022) *ASTM C469/C469M-22 – Standard Test Method for Static Modulus of Elasticity and Poisson's Ratio of Concrete in Compression* (ASTM International, West Conshohocken, PA).

AWS (2020) *Structural Welding Code – Steel* (American Welding Society, Miami, FL).

Bao Y, Main JA, Noh SY (2017) Evaluation of Structural Robustness against Column Loss: Methodology and Application to RC Frame Buildings. *Journal of Structural Engineering* 143(8):04017066. https://doi.org/10.1061/(ASCE)ST.1943-541X.0001795

French CW, Amu O, Tarzikhan C (1989a) Connections between Precast Elements—Failure Outside Connection Region. *ASCE Journal of Structural Engineering* 115(2): 316–340. https://doi.org/10.1061/(ASCE)0733-9445(1989)115:2(316)

French CW, Hafner M, Jayashankar V (1989b) Connection between Precast Elements—Failure within Connection Region. *ASCE Journal of Structural Engineering* 115(12): 3171–3192. https://doi.org/10.1061/(ASCE)0733-9445(1989)115:12(3171)

Hallquist J (2007) LS-DYNA Keyword User's Manual. (Livermore Software Technology Corp., Livermore, CA).

ICC (2006) *2006 International Building Code* (International Code Council, Club Hills, IL).

Izzuddin BA, Vlassis AG, Elghazouli AY, Nethercot DA (2008) Progressive Collapse of Multi-Storey Buildings Due to Sudden Column Loss – Part I: Simplified Assessment Framework. *Engineering Structures* 30(5):1308-1318. https://doi.org/10.1016/j.engstruct.2007.07.011

Kim J, Dasgupta P, Ghosh SK (2009) Assessment of the Ability of Seismic Structural Systems to Withstand Progressive Collapse: Design of Precast Concrete Frame Building (Seismic Design Category D). Report submitted to the National Institute of Standards and Technology, Gaithersburg, MD.

Lew HS, Bao Y, Sadek F, Main JA, Pujol S, Sozen MA (2011) An Experimental and Computational Study of Reinforced Concrete Assemblies Under a Column Removal Scenario. *NIST TN 1720*, National Institute of Standards and Technology, Gaithersburg, MD. https://doi.org/10.6028/NIST.TN.1720

Main JA, Bao Y, Lew HS, Sadek F, Chiarito VP, Robert SD, Torres JO (2015) An Experimental and Computational Study of Precast Concrete Moment Frames Under a Column Removal Scenario. *NIST TN 1886*, National Institute of Standards and Technology, Gaithersburg, MD. https://doi.org/10.6028/NIST.TN.1886

Palmieri L, Saqan E, French C, Kreger M (1996) Ductile Connections for Precast Concrete Frame Systems. *Mete A. Sozen Symposium - A Tribute from His Students*. ACI SP 162-13: 313–355.

PCI (2017) *PCI Design Handbook*, 8th Edition (Precast/Prestressed Concrete Institute Chicago, IL).

Quiel S, Naito C, and Fallon C (2017) Experimental Evaluation of a New Moment Connection for Progressive Collapse Resistant Precast Concrete Frames. *ATLSS Report 16-08*, Lehigh University, Bethlehem, PA. 10.13140/RG.2.2.28215.62884

Sadek F, Main JA, Lew HS, Robert SD, Chiarito VP, El-Tawil S (2010) An Experimental and Computational Study of Steel Moment Connections Under a Column Removal Scenario. *NIST TN 1669*, National Institute of Standards and Technology, Gaithersburg, MD.

Taylor BN, Kuyatt CE (1994) Guidelines for Evaluating and Expressing the Uncertainty of NIST Measurement Results. NIST TN 1297, National Institute of Standards and Technology, Gaithersburg, MD.

Thonstad T, Weigand J, Ammons M, Main J, Phan L (2025) Comprehensive Design of New Connections for Enhancing the Robustness of Precast Concrete Frame Structures. *NIST TN 2348A*, National Institute of Standards and Technology, Gaithersburg, MD. https://doi.org/10.6028/NIST.TN.2348A

Zaghi AE, Padgett JE, Bruneau M, Barbato M, Li Y, Mitrani-Reiser J, McBride A (2016) Establishing Common Nomenclature, Characterizing the Problem, and Identifying Future Opportunities in Multihazard Design. *Journal of Structural Engineering* 142(12):H2516001. https://doi.org/10.1061/(ASCE)ST.1943-541X.0001586

Appendix A. Design Drawings

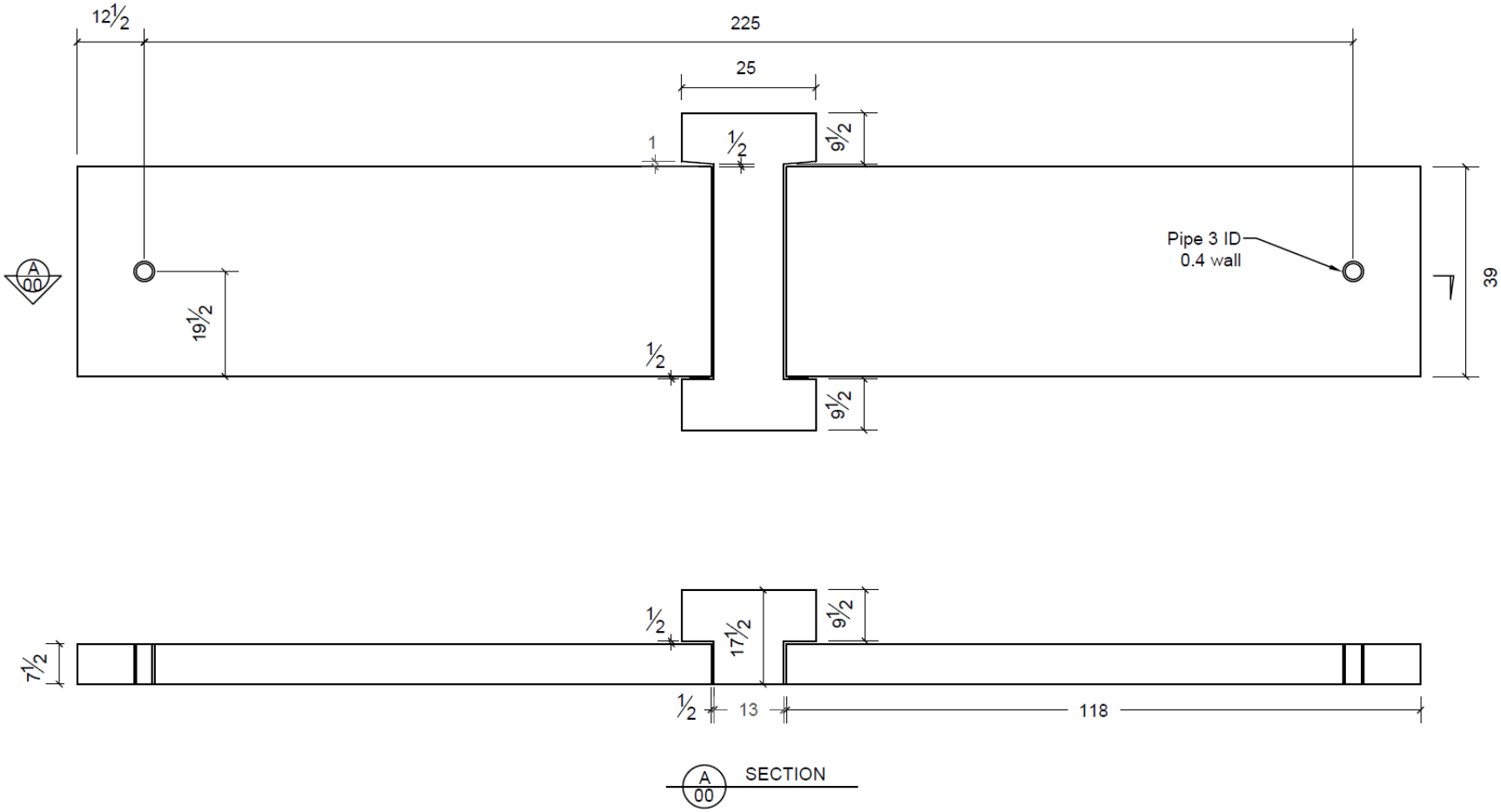

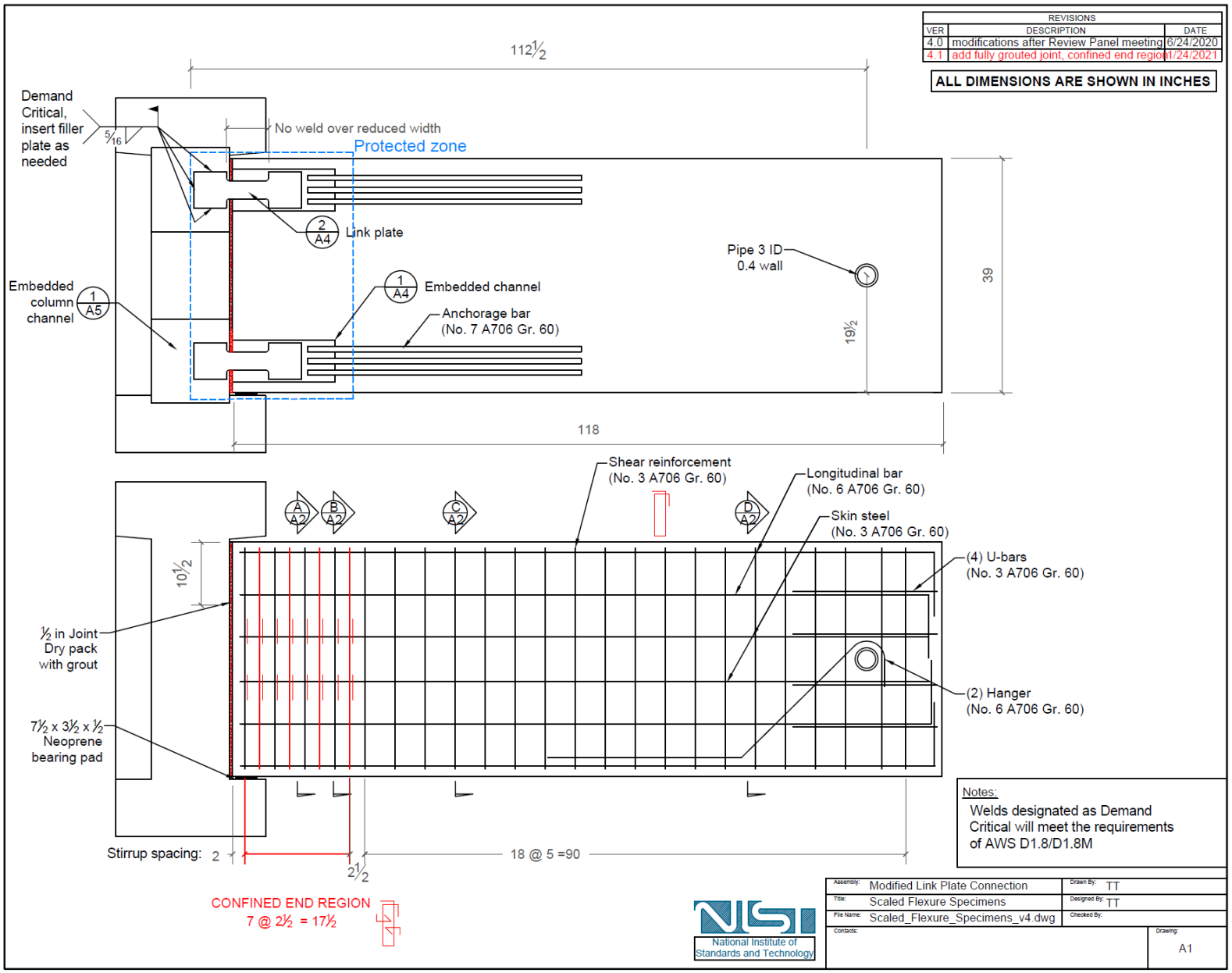
REVISIONS
VER DESCRIPTION DATE
4.0 modifications after Review Panel meeting 6/24/2020
4.1 add fully grouted joint, confined end region 1/24/2021
ALL DIMENSIONS ARE SHOWN IN INCHES
112½
Demand Critical, insert filler plate as needed
5/16
No weld over reduced width
Protected zone
2 A4 Link plate
Pipe 3 ID 0.4 wall
39
Embedded column channel
1 A5
1 A4 Embedded channel
Anchorage bar (No. 7 A706 Gr. 60)
19½
118
Shear reinforcement (No. 3 A706 Gr. 60)
Longitudinal bar (No. 6 A706 Gr. 60)
A A2
B A2
C A2
D A2
Skin steel (No. 3 A706 Gr. 60)
10½
(4) U-bars (No. 3 A706 Gr. 60)
½ in Joint Dry pack with grout
(2) Hanger (No. 6 A706 Gr. 60)
7½ x 3½ x ½ Neoprene bearing pad
Stirrup spacing: 2
2½
18 @ 5 =90
CONFINED END REGION
7 @ 2½ = 17½
Notes:
Welds designated as Demand Critical will meet the requirements of AWS D1.8/D1.8M
National Institute of Standards and Technology
Assembly: Modified Link Plate Connection
Drawn By: TT
Title: Scaled Flexure Specimens
Designed By: TT
File Name: Scaled_Flexure_Specimens_v4.dwg
Checked By:
Contacts:
Drawing: A1

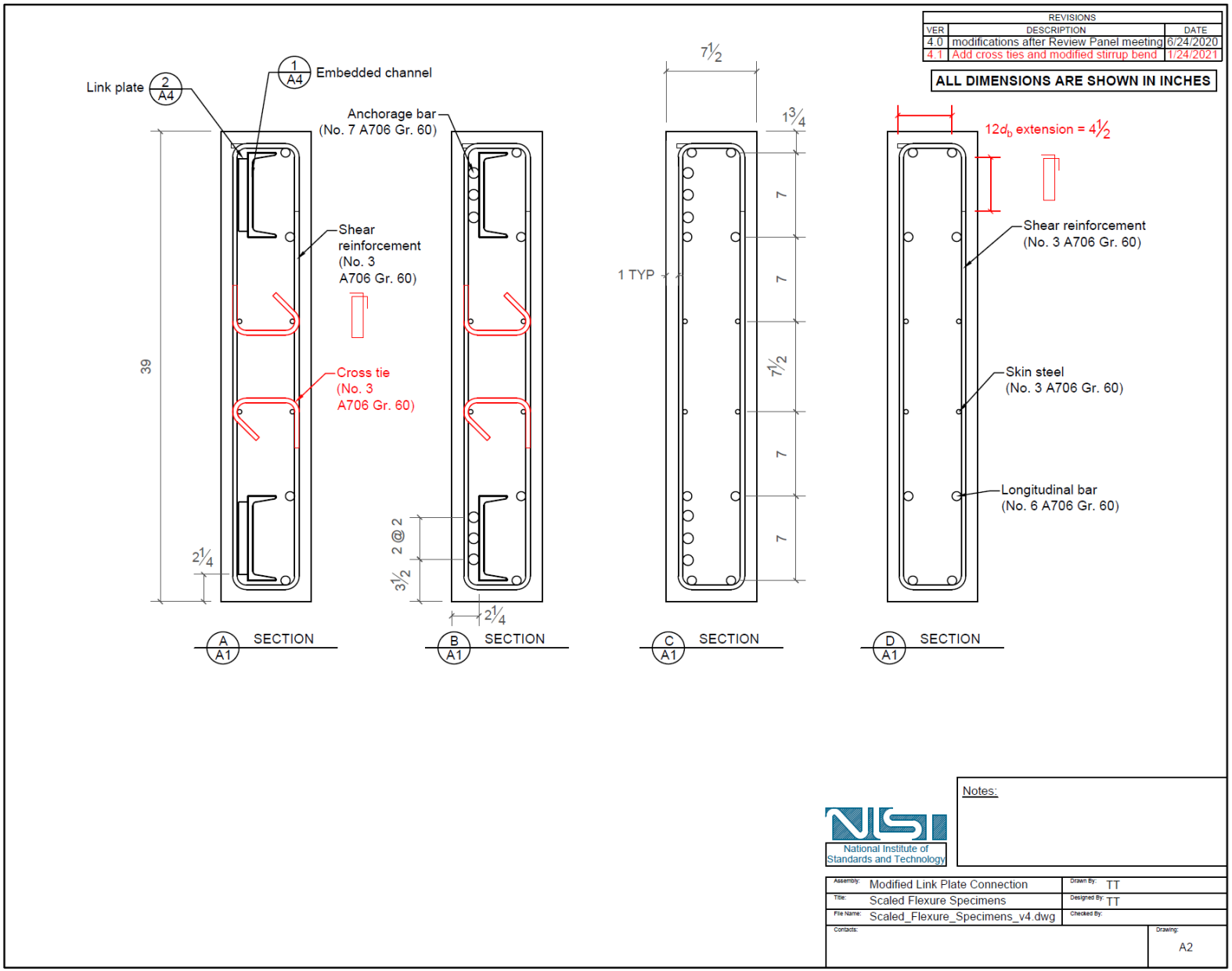
REVISIONS
VER | DESCRIPTION | DATE
4.0 | modifications after Review Panel meeting | 6/24/2020
4.1 | Add cross ties and modified stirrup bend | 1/24/2021
ALL DIMENSIONS ARE SHOWN IN INCHES
Link plate 2 A4
1 A4 Embedded channel
Anchorage bar (No. 7 A706 Gr. 60)
Shear reinforcement (No. 3 A706 Gr. 60)
Cross tie (No. 3 A706 Gr. 60)
39
2¼
2 @ 2
3½
2¼
7½
1¾
7
7
7½
7
7
1 TYP
12d_b extension = 4½
Shear reinforcement (No. 3 A706 Gr. 60)
Skin steel (No. 3 A706 Gr. 60)
Longitudinal bar (No. 6 A706 Gr. 60)
A A1 SECTION
B A1 SECTION
C A1 SECTION
D A1 SECTION
Notes:
National Institute of Standards and Technology
Assembly: Modified Link Plate Connection
Drawn By: TT
Title: Scaled Flexure Specimens
Designed By: TT
File Name: Scaled_Flexure_Specimens_v4.dwg
Checked By:
Contacts:
Drawing: A2

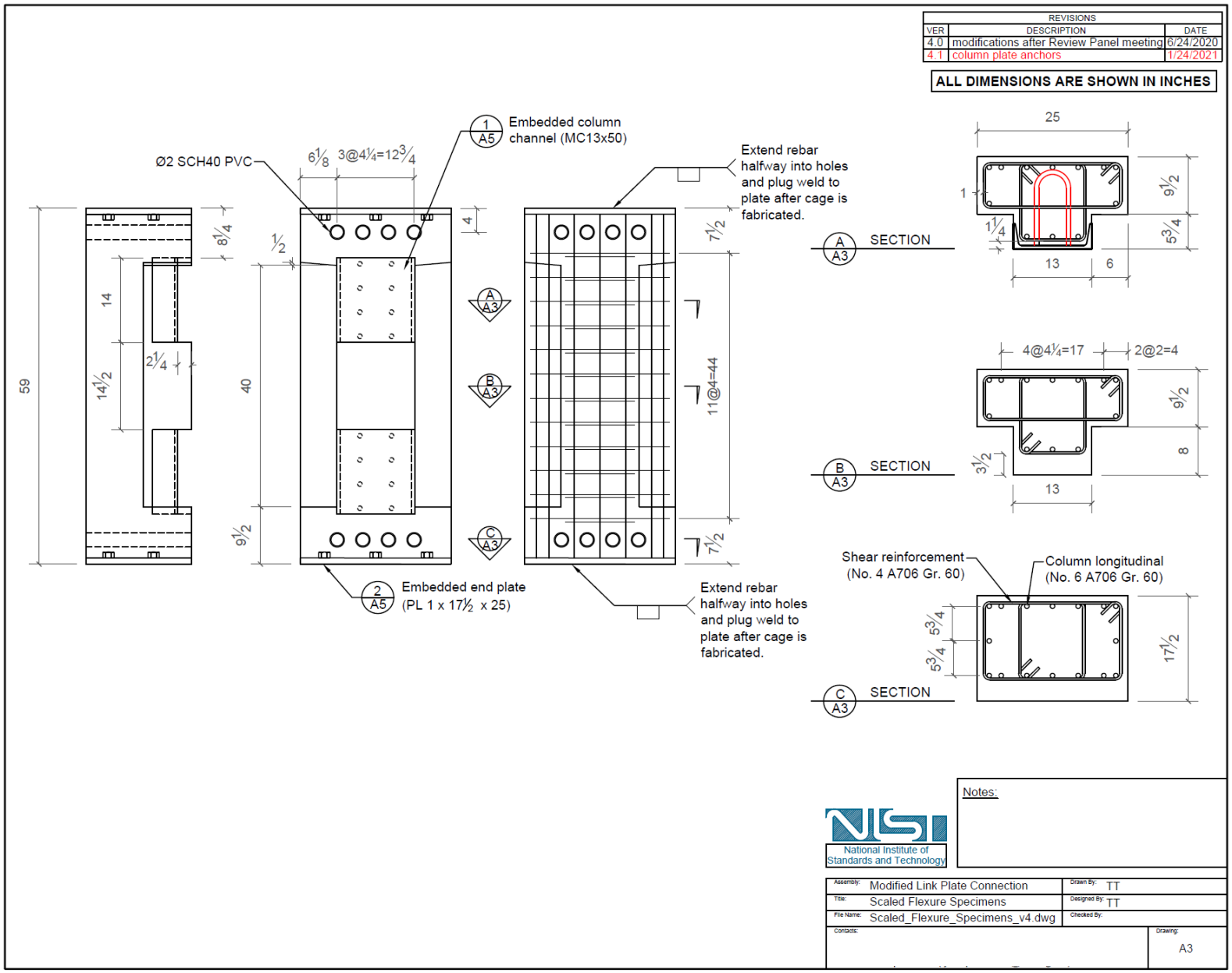
REVISIONS
VER DESCRIPTION DATE
4.0 modifications after Review Panel meeting 6/24/2020
4.1 column plate anchors 1/24/2021
ALL DIMENSIONS ARE SHOWN IN INCHES
Ø2 SCH40 PVC
6⅛ 3@4¼=12¾
1 A5 Embedded column channel (MC13x50)
Extend rebar halfway into holes and plug weld to plate after cage is fabricated.
2 A5 Embedded end plate (PL 1 x 17½ x 25)
Extend rebar halfway into holes and plug weld to plate after cage is fabricated.
59
8¼
14
14½
2¼
½
40
9½
4
7½
11@4=44
7½
A A3
B A3
C A3
A A3 SECTION
25
1
1¼
9½
5¾
13
6
B A3 SECTION
4@4¼=17
2@2=4
9½
8
3½
13
C A3 SECTION
Shear reinforcement (No. 4 A706 Gr. 60)
Column longitudinal (No. 6 A706 Gr. 60)
5¾
5¾
17½
National Institute of Standards and Technology
Notes:
Assembly: Modified Link Plate Connection
Title: Scaled Flexure Specimens
File Name: Scaled_Flexure_Specimens_v4.dwg
Drawn By: TT
Designed By: TT
Checked By:
Contacts:
Drawing: A3

REVISIONS		
VER	DESCRIPTION	DATE
4.0	modifications after Review Panel meeting	6/24/2020
4.1	air holes	1/24/2021

ALL DIMENSIONS ARE SHOWN IN INCHES

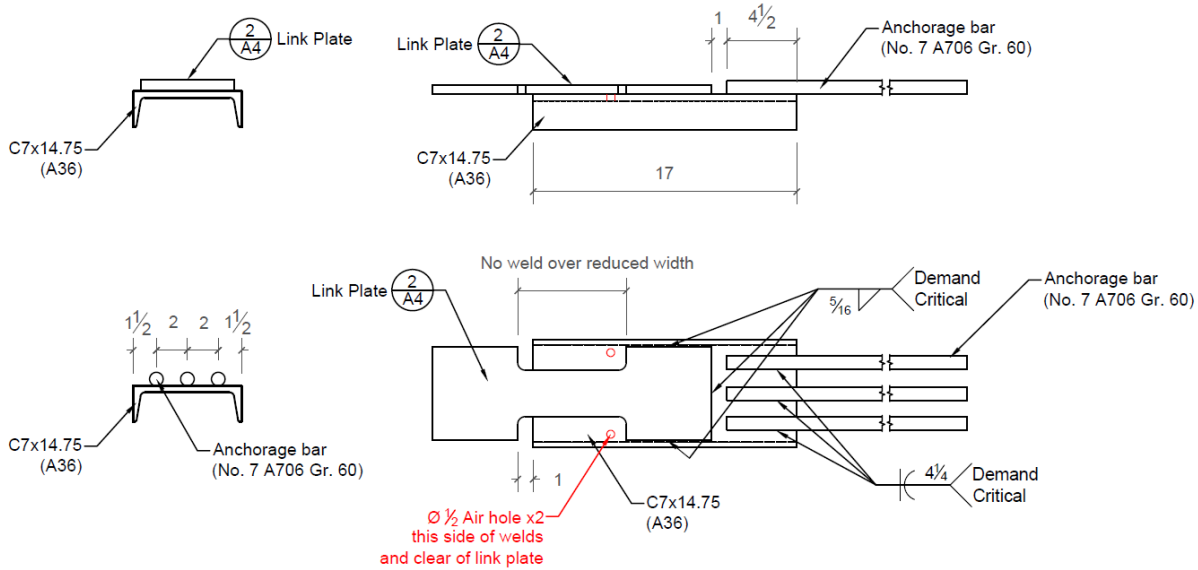

1 A1 EMBEDDED CHANNEL DETAIL

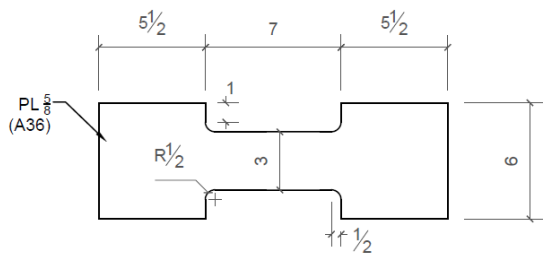

2 A1 LINK PLATE DETAIL

Notes:
Welds designated as Demand Critical will meet the requirements of AWS D1.8/D1.8M

National Institute of Standards and Technology

Assembly:	Modified Link Plate Connection	Drawn By:	TT
Title:	Scaled Flexure Specimens	Designed By:	TT
File Name:	Scaled_Flexure_Specimens_v4.dwg	Checked By:	
Contacts:		Drawing:	A4

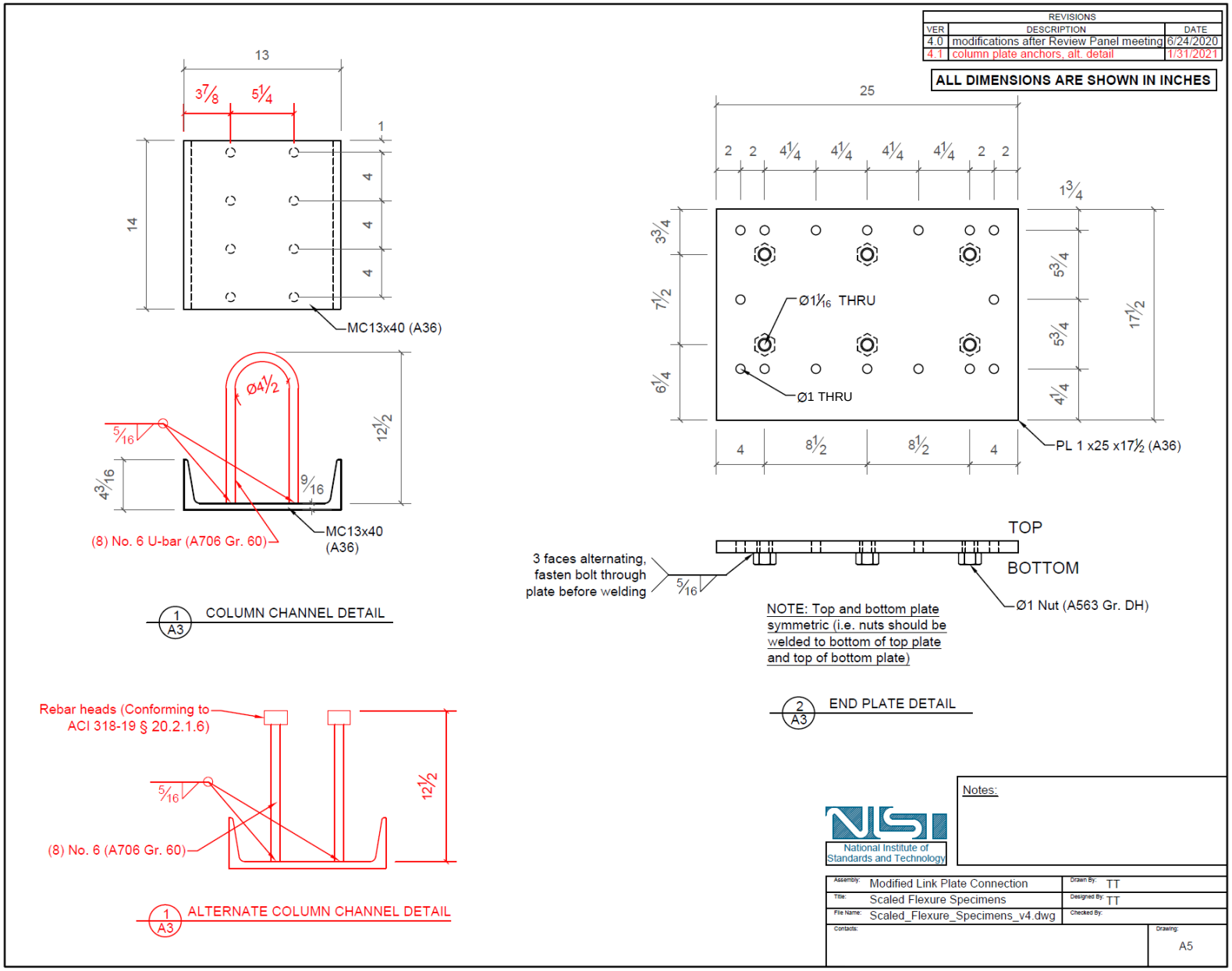
REVISIONS
VER DESCRIPTION DATE
4.0 modifications after Review Panel meeting 6/24/2020
4.1 column plate anchors, alt. detail 1/31/2021
ALL DIMENSIONS ARE SHOWN IN INCHES
13
3 7/8
5 1/4
1
14
4
4
4
MC13x40 (A36)
Ø4 1/2
5/16
4 3/16
9/16
12 1/2
(8) No. 6 U-bar (A706 Gr. 60)
MC13x40 (A36)
1 A3 COLUMN CHANNEL DETAIL
25
2 2 4 1/4 4 1/4 4 1/4 4 1/4 2 2
1 3/4
3 3/4
7 1/2
6 1/4
Ø1 1/16 THRU
Ø1 THRU
5 3/4
5 3/4
4 1/4
17 1/2
4 8 1/2 8 1/2 4
PL 1 x25 x17 1/2 (A36)
TOP
BOTTOM
3 faces alternating, fasten bolt through plate before welding
5/16
Ø1 Nut (A563 Gr. DH)
NOTE: Top and bottom plate symmetric (i.e. nuts should be welded to bottom of top plate and top of bottom plate)
2 A3 END PLATE DETAIL
Rebar heads (Conforming to ACI 318-19 § 20.2.1.6)
5/16
12 1/2
(8) No. 6 (A706 Gr. 60)
1 A3 ALTERNATE COLUMN CHANNEL DETAIL
Notes:
National Institute of Standards and Technology
Assembly: Modified Link Plate Connection
Title: Scaled Flexure Specimens
File Name: Scaled_Flexure_Specimens_v4.dwg
Contacts:
Drawn By: TT
Designed By: TT
Checked By:
Drawing: A5

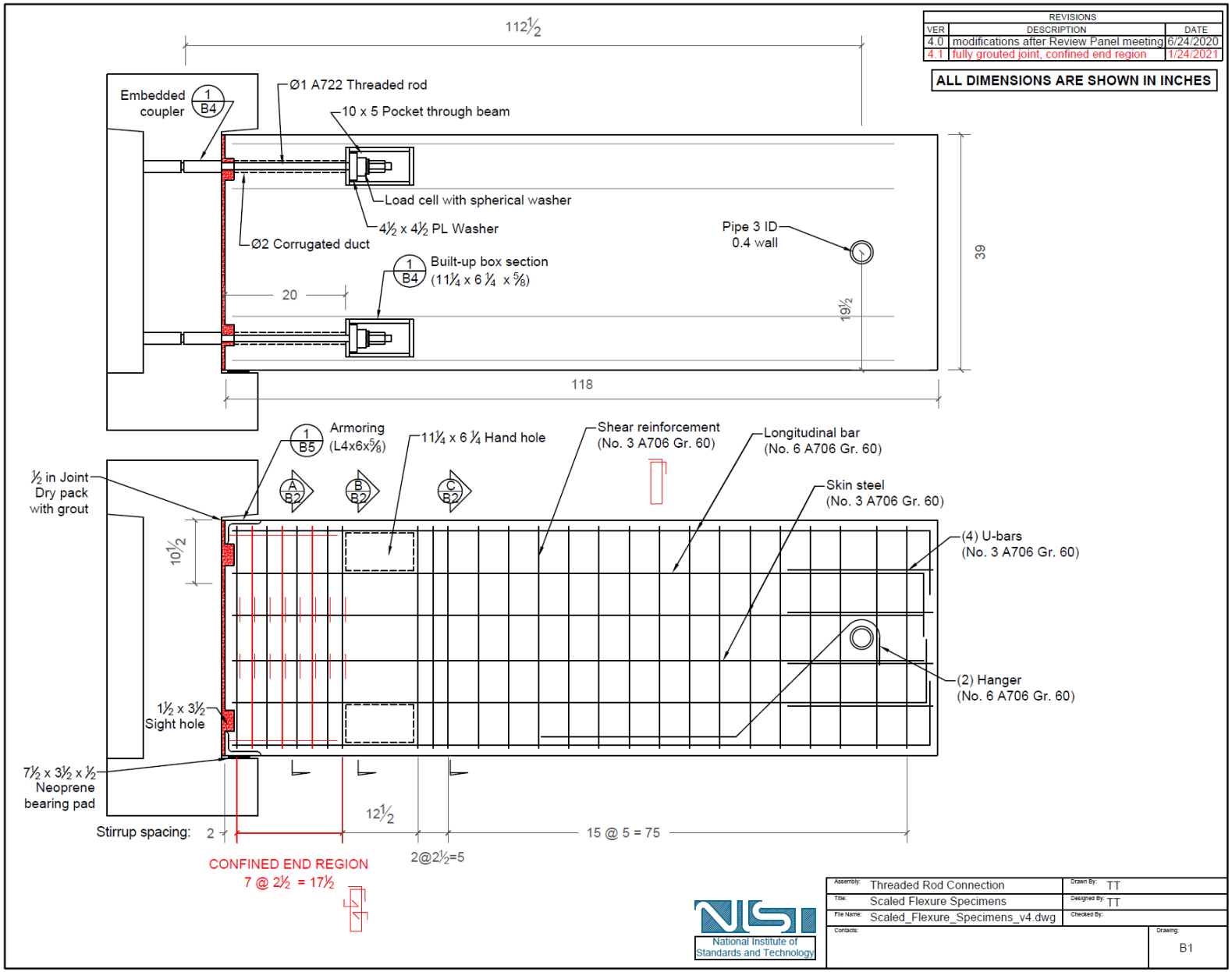
REVISIONS
VER | DESCRIPTION | DATE
4.0 | modifications after Review Panel meeting | 6/24/2020
4.1 | fully grouted joint, confined end region | 1/24/2021
ALL DIMENSIONS ARE SHOWN IN INCHES
112½
Embedded coupler
1 B4
Ø1 A722 Threaded rod
10 x 5 Pocket through beam
Load cell with spherical washer
4½ x 4½ PL Washer
Ø2 Corrugated duct
Pipe 3 ID
0.4 wall
1 B4
Built-up box section
(11¼ x 6¼ x ⅝)
20
19½
39
118
1 B5
Armoring
(L4x6x⅝)
11¼ x 6¼ Hand hole
Shear reinforcement
(No. 3 A706 Gr. 60)
Longitudinal bar
(No. 6 A706 Gr. 60)
½ in Joint
Dry pack
with grout
A B2
B B2
C B2
Skin steel
(No. 3 A706 Gr. 60)
10½
(4) U-bars
(No. 3 A706 Gr. 60)
(2) Hanger
(No. 6 A706 Gr. 60)
1½ x 3½
Sight hole
7½ x 3½ x ½
Neoprene
bearing pad
Stirrup spacing:
2
12½
15 @ 5 = 75
2@2½=5
CONFINED END REGION
7 @ 2½ = 17½
National Institute of Standards and Technology
Assembly: Threaded Rod Connection
Title: Scaled Flexure Specimens
File Name: Scaled_Flexure_Specimens_v4.dwg
Contacts:
Drawn By: TT
Designed By: TT
Checked By:
Drawing: B1

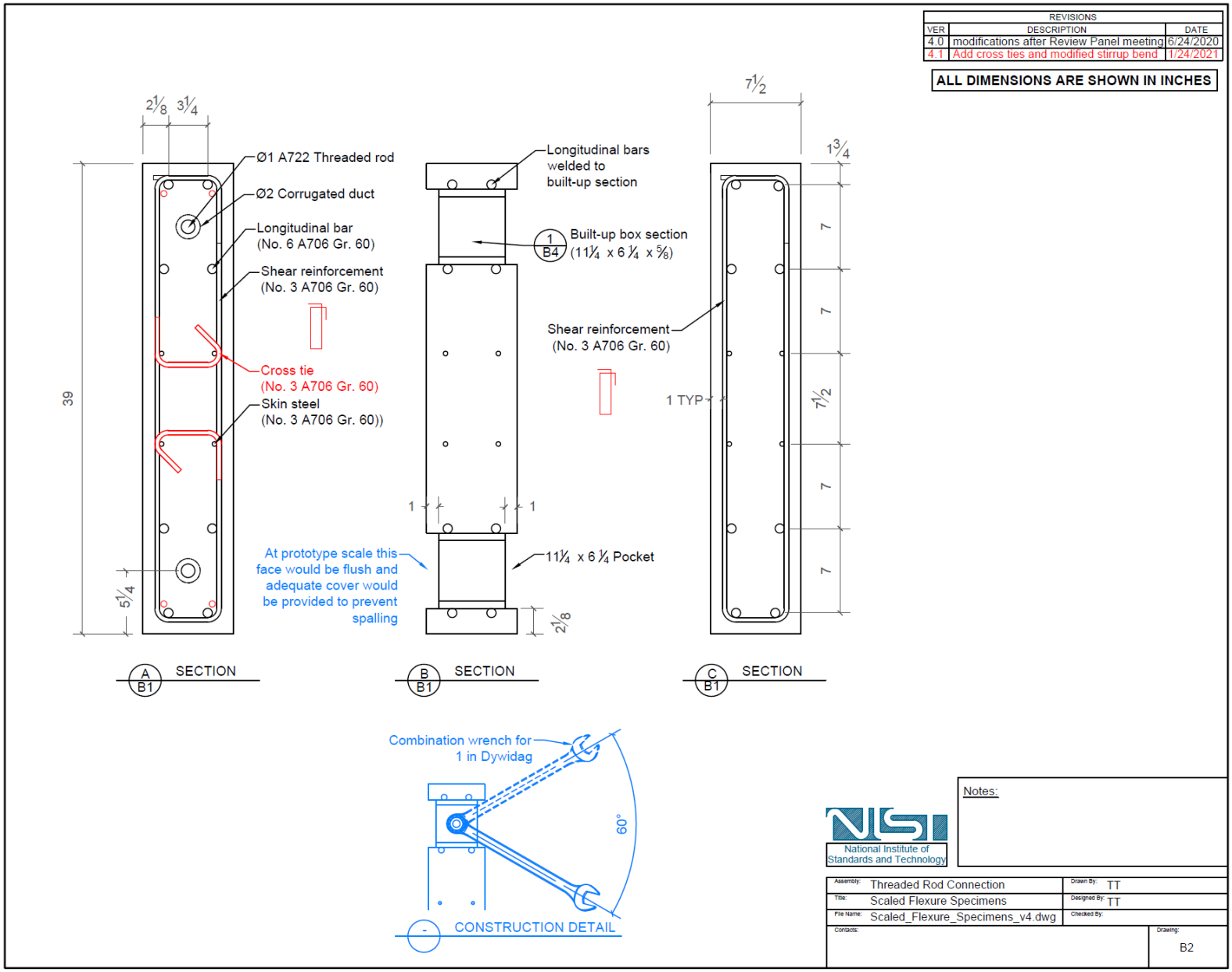
REVISIONS
VER | DESCRIPTION | DATE
4.0 | modifications after Review Panel meeting | 6/24/2020
4.1 | Add cross ties and modified stirrup bend | 1/24/2021
ALL DIMENSIONS ARE SHOWN IN INCHES
2⅛ 3¼
Ø1 A722 Threaded rod
Ø2 Corrugated duct
Longitudinal bar (No. 6 A706 Gr. 60)
Shear reinforcement (No. 3 A706 Gr. 60)
Cross tie (No. 3 A706 Gr. 60)
Skin steel (No. 3 A706 Gr. 60))
39
5¼
A B1 SECTION
Longitudinal bars welded to built-up section
1 B4 Built-up box section (11¼ x 6¼ x ⅝)
Shear reinforcement (No. 3 A706 Gr. 60)
1
1
At prototype scale this face would be flush and adequate cover would be provided to prevent spalling
11¼ x 6¼ Pocket
2⅛
B B1 SECTION
7½
1¾
7
7
1 TYP
7½
7
7
C B1 SECTION
Combination wrench for 1 in Dywidag
60°
- CONSTRUCTION DETAIL
National Institute of Standards and Technology
Notes:
Assembly: Threaded Rod Connection
Drawn By: TT
Title: Scaled Flexure Specimens
Designed By: TT
File Name: Scaled_Flexure_Specimens_v4.dwg
Checked By:
Contacts:
Drawing: B2

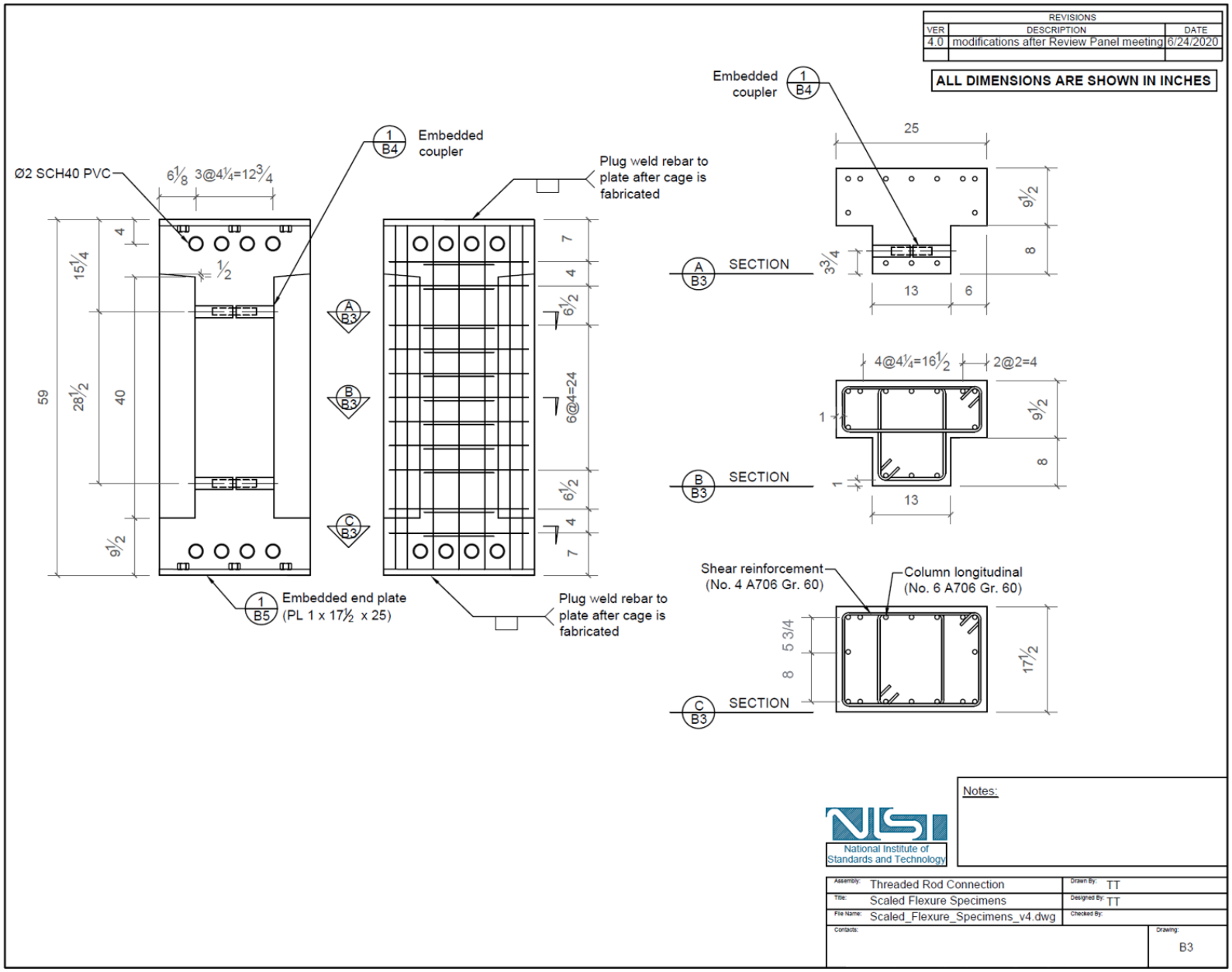
REVISIONS
VER DESCRIPTION DATE
4.0 modifications after Review Panel meeting 6/24/2020
ALL DIMENSIONS ARE SHOWN IN INCHES
Embedded coupler 1 B4
Ø2 SCH40 PVC
6⅛ 3@4¼=12¾
Plug weld rebar to plate after cage is fabricated
A B3
B B3
C B3
SECTION
4@4¼=16½
2@2=4
Shear reinforcement (No. 4 A706 Gr. 60)
Column longitudinal (No. 6 A706 Gr. 60)
Embedded end plate (PL 1 x 17½ x 25) 1 B5
Notes:
National Institute of Standards and Technology
Assembly: Threaded Rod Connection
Title: Scaled Flexure Specimens
File Name: Scaled_Flexure_Specimens_v4.dwg
Drawn By: TT
Designed By: TT
Checked By:
Contacts:
Drawing: B3

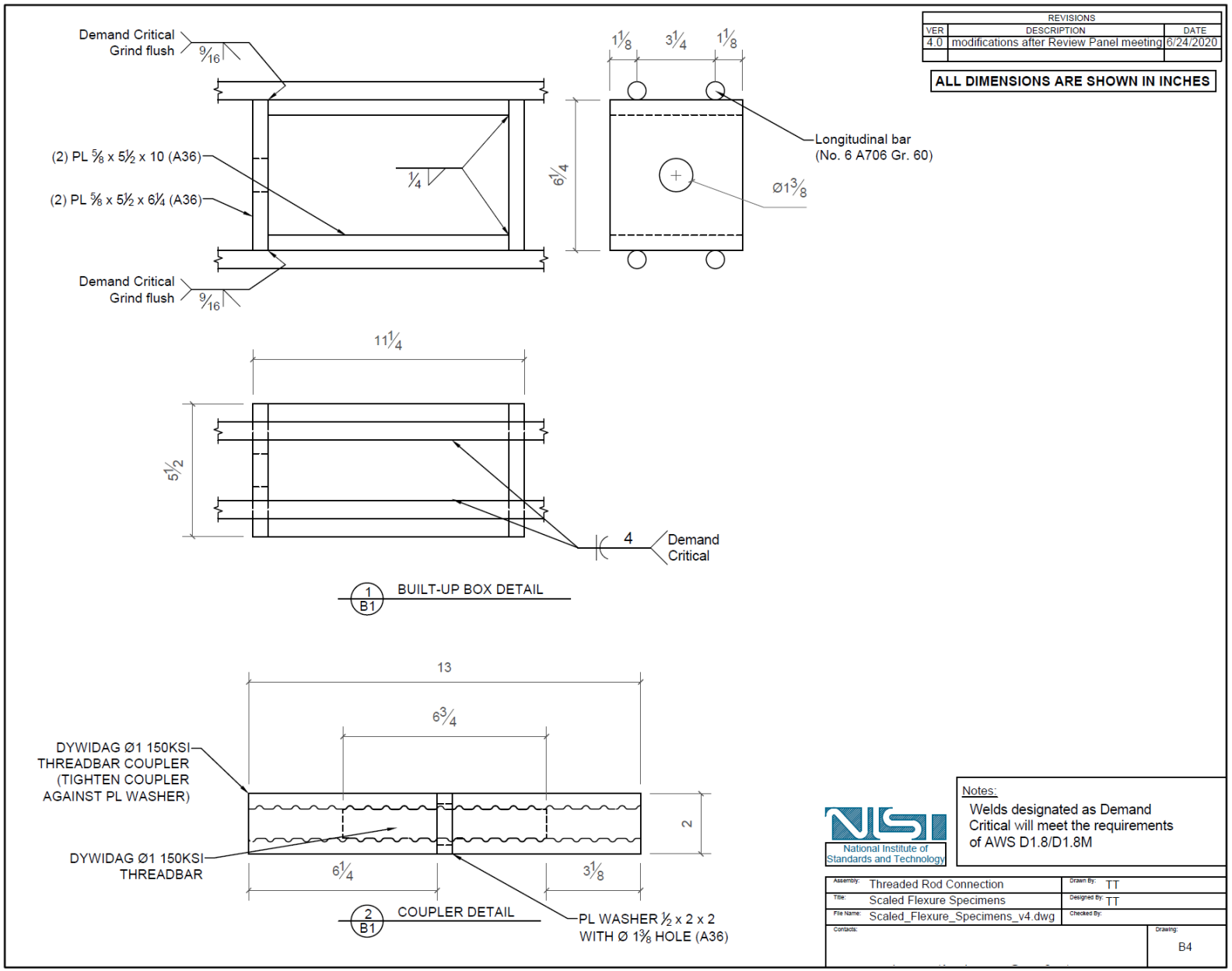
REVISIONS
VER DESCRIPTION DATE
4.0 modifications after Review Panel meeting 6/24/2020
ALL DIMENSIONS ARE SHOWN IN INCHES
Demand Critical
Grind flush
9/16
(2) PL 5/8 x 5 1/2 x 10 (A36)
(2) PL 5/8 x 5 1/2 x 6 1/4 (A36)
1/4
1 1/8
3 1/4
1 1/8
6 1/4
Longitudinal bar
(No. 6 A706 Gr. 60)
Ø1 3/8
11 1/4
5 1/2
4
Demand
Critical
1
B1
BUILT-UP BOX DETAIL
13
6 3/4
DYWIDAG Ø1 150KSI
THREADBAR COUPLER
(TIGHTEN COUPLER
AGAINST PL WASHER)
DYWIDAG Ø1 150KSI
THREADBAR
2
6 1/4
3 1/8
2
2
B1
COUPLER DETAIL
PL WASHER 1/2 x 2 x 2
WITH Ø 1 3/8 HOLE (A36)
National Institute of
Standards and Technology
Notes:
Welds designated as Demand
Critical will meet the requirements
of AWS D1.8/D1.8M
Assembly: Threaded Rod Connection
Drawn By: TT
Title: Scaled Flexure Specimens
Designed By: TT
File Name: Scaled_Flexure_Specimens_v4.dwg
Checked By:
Contacts:
Drawing:
B4

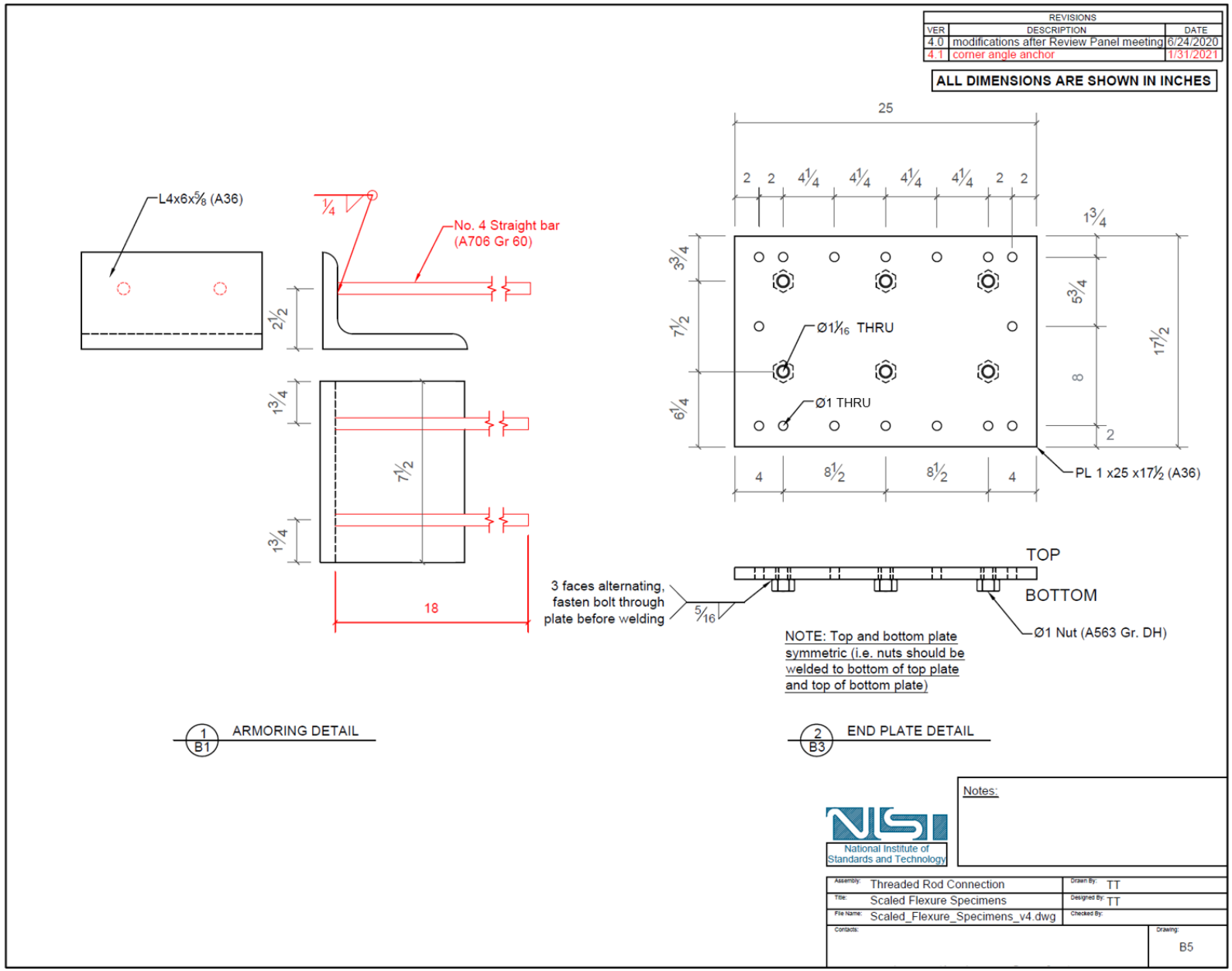
REVISIONS
VER | DESCRIPTION | DATE
4.0 | modifications after Review Panel meeting | 6/24/2020
4.1 | corner angle anchor | 1/31/2021
ALL DIMENSIONS ARE SHOWN IN INCHES
L4x6x5/8 (A36)
1/4
No. 4 Straight bar (A706 Gr 60)
2 1/2
1 3/4
7 1/2
1 3/4
18
1 B1 ARMORING DETAIL
25
2 2 4 1/4 4 1/4 4 1/4 4 1/4 2 2
1 3/4
3 3/4
7 1/2
6 1/4
5 3/4
8
2
17 1/2
Ø1 1/16 THRU
Ø1 THRU
4 8 1/2 8 1/2 4
PL 1 x25 x17 1/2 (A36)
TOP
BOTTOM
3 faces alternating, fasten bolt through plate before welding
5/16
Ø1 Nut (A563 Gr. DH)
NOTE: Top and bottom plate symmetric (i.e. nuts should be welded to bottom of top plate and top of bottom plate)
2 B3 END PLATE DETAIL
Notes:
National Institute of Standards and Technology
Assembly: Threaded Rod Connection
Drawn By: TT
Title: Scaled Flexure Specimens
Designed By: TT
File Name: Scaled_Flexure_Specimens_v4.dwg
Checked By:
Contacts:
Drawing: B5

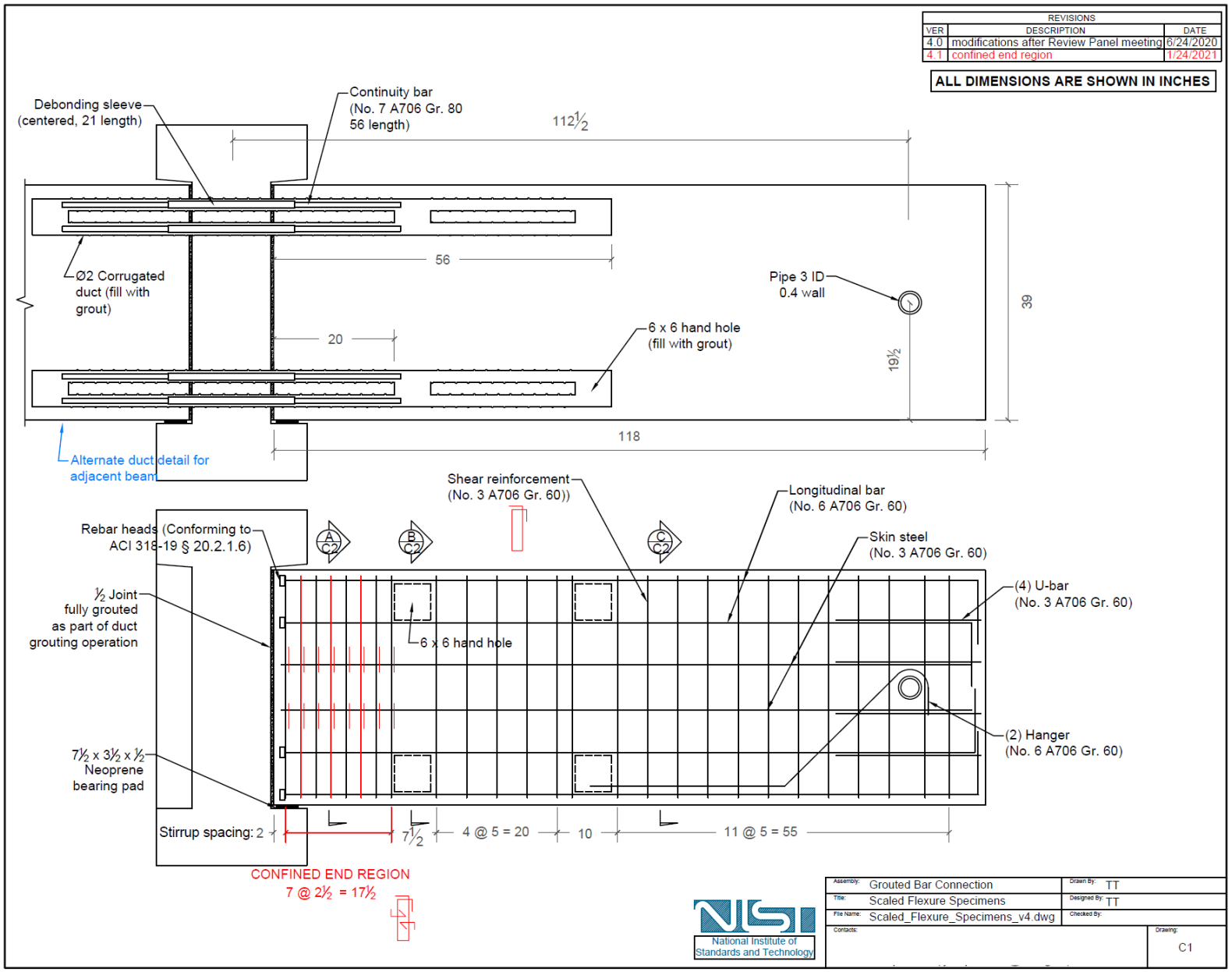
REVISIONS
VER DESCRIPTION DATE
4.0 modifications after Review Panel meeting 6/24/2020
4.1 confined end region 1/24/2021
ALL DIMENSIONS ARE SHOWN IN INCHES
Debonding sleeve (centered, 21 length)
Continuity bar (No. 7 A706 Gr. 80 56 length)
112½
56
Ø2 Corrugated duct (fill with grout)
Pipe 3 ID 0.4 wall
39
20
6 x 6 hand hole (fill with grout)
19½
118
Alternate duct detail for adjacent beam
Shear reinforcement (No. 3 A706 Gr. 60))
Longitudinal bar (No. 6 A706 Gr. 60)
Rebar heads (Conforming to ACI 318-19 § 20.2.1.6)
A C2
B C2
C C2
Skin steel (No. 3 A706 Gr. 60)
½ Joint fully grouted as part of duct grouting operation
(4) U-bar (No. 3 A706 Gr. 60)
6 x 6 hand hole
(2) Hanger (No. 6 A706 Gr. 60)
7½ x 3½ x ½ Neoprene bearing pad
Stirrup spacing: 2
7½
4 @ 5 = 20
10
11 @ 5 = 55
CONFINED END REGION
7 @ 2½ = 17½
National Institute of Standards and Technology
Assembly: Grouted Bar Connection
Drawn By: TT
Title: Scaled Flexure Specimens
Designed By: TT
File Name: Scaled_Flexure_Specimens_v4.dwg
Checked By:
Contacts:
Drawing: C1

REVISIONS		
VER	DESCRIPTION	DATE
4.0	modifications after Review Panel meeting	6/24/2020
4.1	Add cross ties and modified stirrup bend	1/24/2021

ALL DIMENSIONS ARE SHOWN IN INCHES

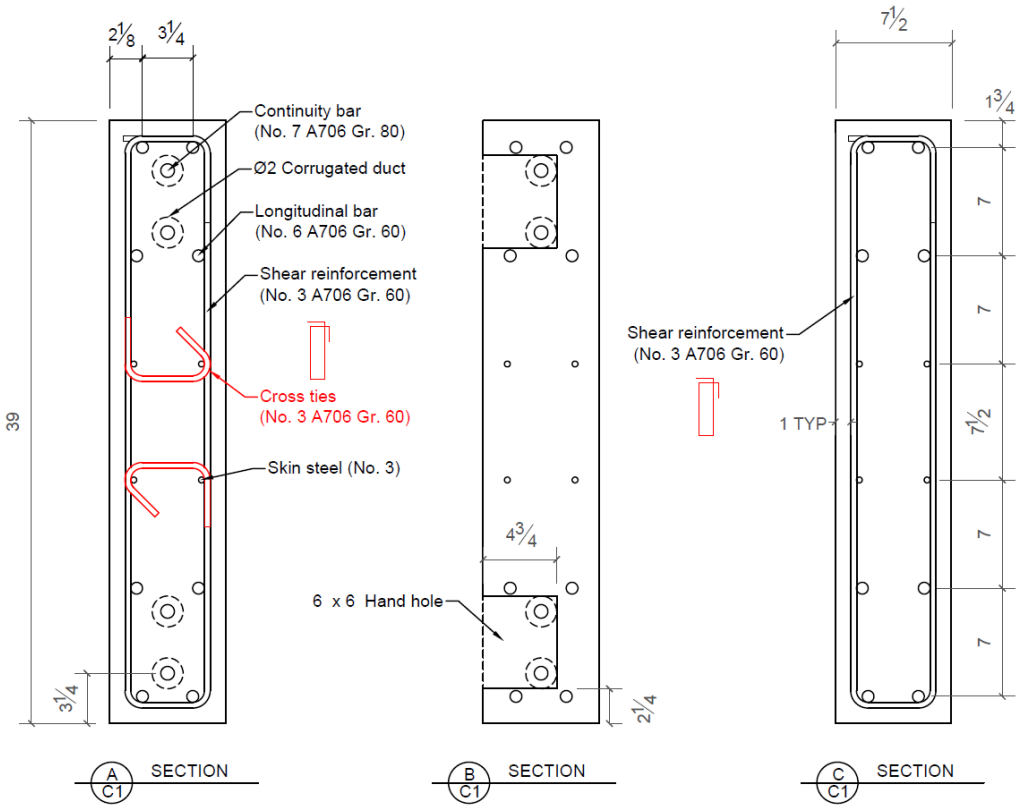

Notes:

National Institute of Standards and Technology

Assembly:	Grouted Bar Connection	Drawn By:	TT
Title:	Scaled Flexure Specimens	Designed By:	TT
File Name:	Scaled_Flexure_Specimens_v4.dwg	Checked By:	
Contacts:		Drawing:	C2

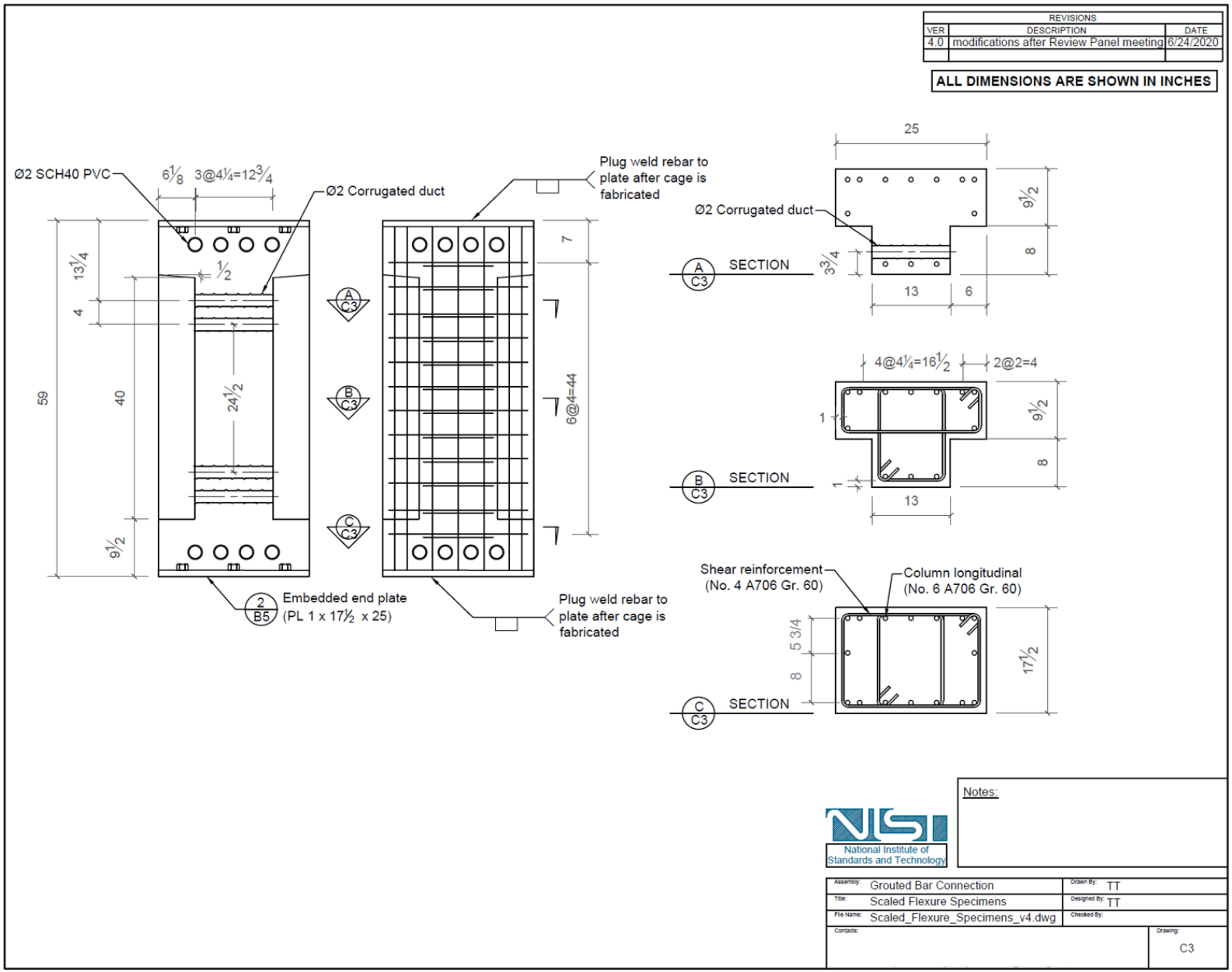
REVISIONS
VER DESCRIPTION DATE
4.0 modifications after Review Panel meeting 6/24/2020
ALL DIMENSIONS ARE SHOWN IN INCHES
Ø2 SCH40 PVC
6⅛ 3@4¼=12¾
Ø2 Corrugated duct
Plug weld rebar to plate after cage is fabricated
13¼
½
4
59
40
24½
9½
7
6@4=44
A C3
B C3
C C3
2 B5
Embedded end plate (PL 1 x 17½ x 25)
Plug weld rebar to plate after cage is fabricated
25
Ø2 Corrugated duct
9½
8
3¾
13
6
SECTION
4@4¼=16½
2@2=4
1
9½
8
1
13
SECTION
Shear reinforcement (No. 4 A706 Gr. 60)
Column longitudinal (No. 6 A706 Gr. 60)
5 3/4
8
17½
SECTION
Notes:
National Institute of Standards and Technology
Assembly: Grouted Bar Connection
Drawn By: TT
Title: Scaled Flexure Specimens
Designed By: TT
File Name: Scaled_Flexure_Specimens_v4.dwg
Checked By:
Contacts:
Drawing: C3

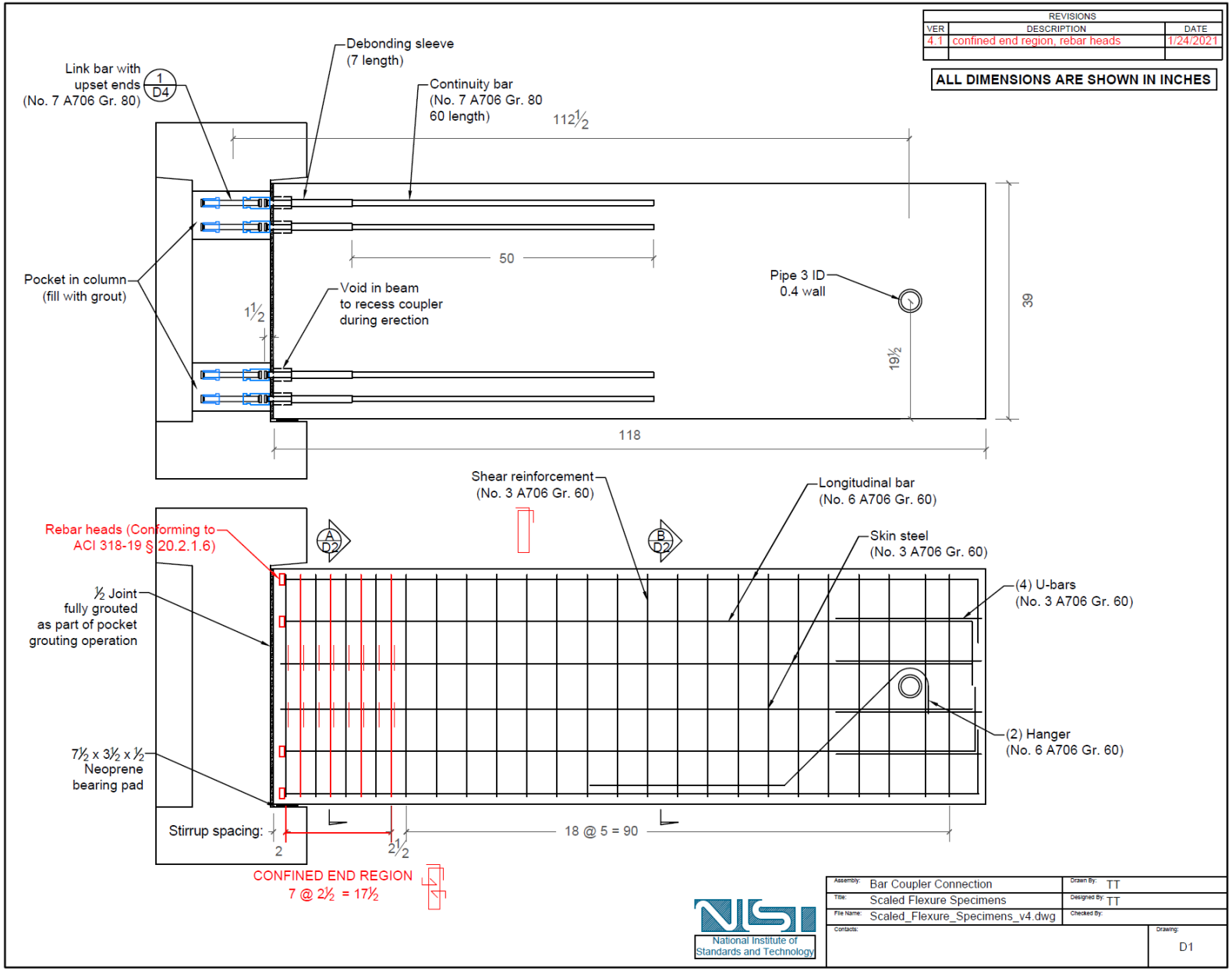
REVISIONS
VER DESCRIPTION DATE
4.1 confined end region, rebar heads 1/24/2021
ALL DIMENSIONS ARE SHOWN IN INCHES
Link bar with upset ends (No. 7 A706 Gr. 80)
1 D4
Debonding sleeve (7 length)
Continuity bar (No. 7 A706 Gr. 80 60 length)
112½
50
Pocket in column (fill with grout)
Void in beam to recess coupler during erection
1½
Pipe 3 ID 0.4 wall
19½
39
118
Shear reinforcement (No. 3 A706 Gr. 60)
Longitudinal bar (No. 6 A706 Gr. 60)
Rebar heads (Conforming to ACI 318-19 § 20.2.1.6)
A D2
B D2
Skin steel (No. 3 A706 Gr. 60)
½ Joint fully grouted as part of pocket grouting operation
(4) U-bars (No. 3 A706 Gr. 60)
(2) Hanger (No. 6 A706 Gr. 60)
7½ x 3½ x ½ Neoprene bearing pad
Stirrup spacing:
2
2½
18 @ 5 = 90
CONFINED END REGION
7 @ 2½ = 17½
National Institute of Standards and Technology
Assembly: Bar Coupler Connection
Drawn By: TT
Title: Scaled Flexure Specimens
Designed By: TT
File Name: Scaled_Flexure_Specimens_v4.dwg
Checked By:
Contacts:
Drawing: D1

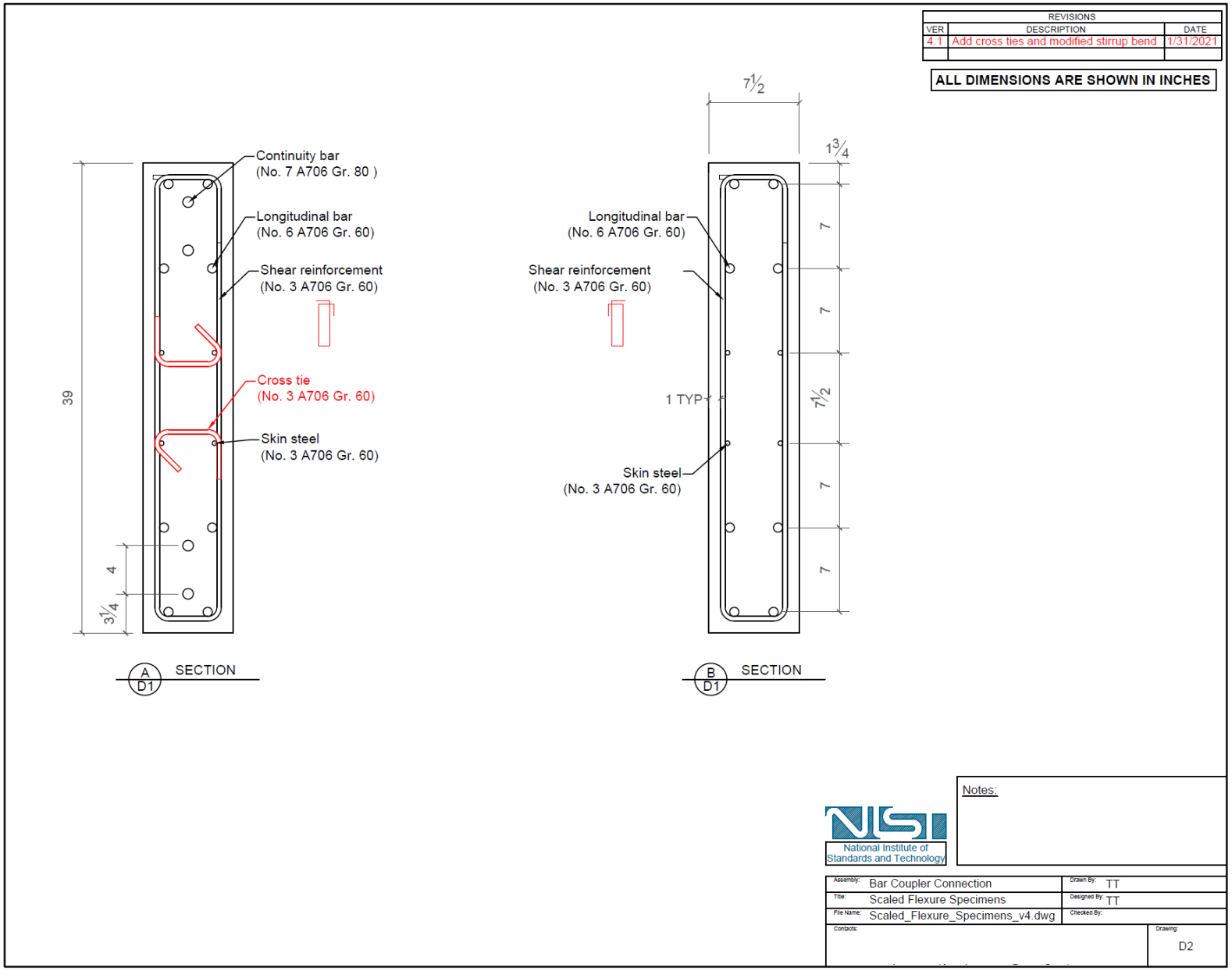
REVISIONS
VER
DESCRIPTION
DATE
4.1
Add cross ties and modified stirrup bend
1/31/2021
ALL DIMENSIONS ARE SHOWN IN INCHES
Continuity bar
(No. 7 A706 Gr. 80)
Longitudinal bar
(No. 6 A706 Gr. 60)
Shear reinforcement
(No. 3 A706 Gr. 60)
Cross tie
(No. 3 A706 Gr. 60)
Skin steel
(No. 3 A706 Gr. 60)
39
4
3¼
A
D1
SECTION
7½
1¾
7
7
7½
7
7
1 TYP
Longitudinal bar
(No. 6 A706 Gr. 60)
Shear reinforcement
(No. 3 A706 Gr. 60)
Skin steel
(No. 3 A706 Gr. 60)
B
D1
SECTION
Notes:
National Institute of Standards and Technology
Assembly: Bar Coupler Connection
Drawn By: TT
Title: Scaled Flexure Specimens
Designed By: TT
File Name: Scaled_Flexure_Specimens_v4.dwg
Checked By:
Contacts:
Drawing:
D2

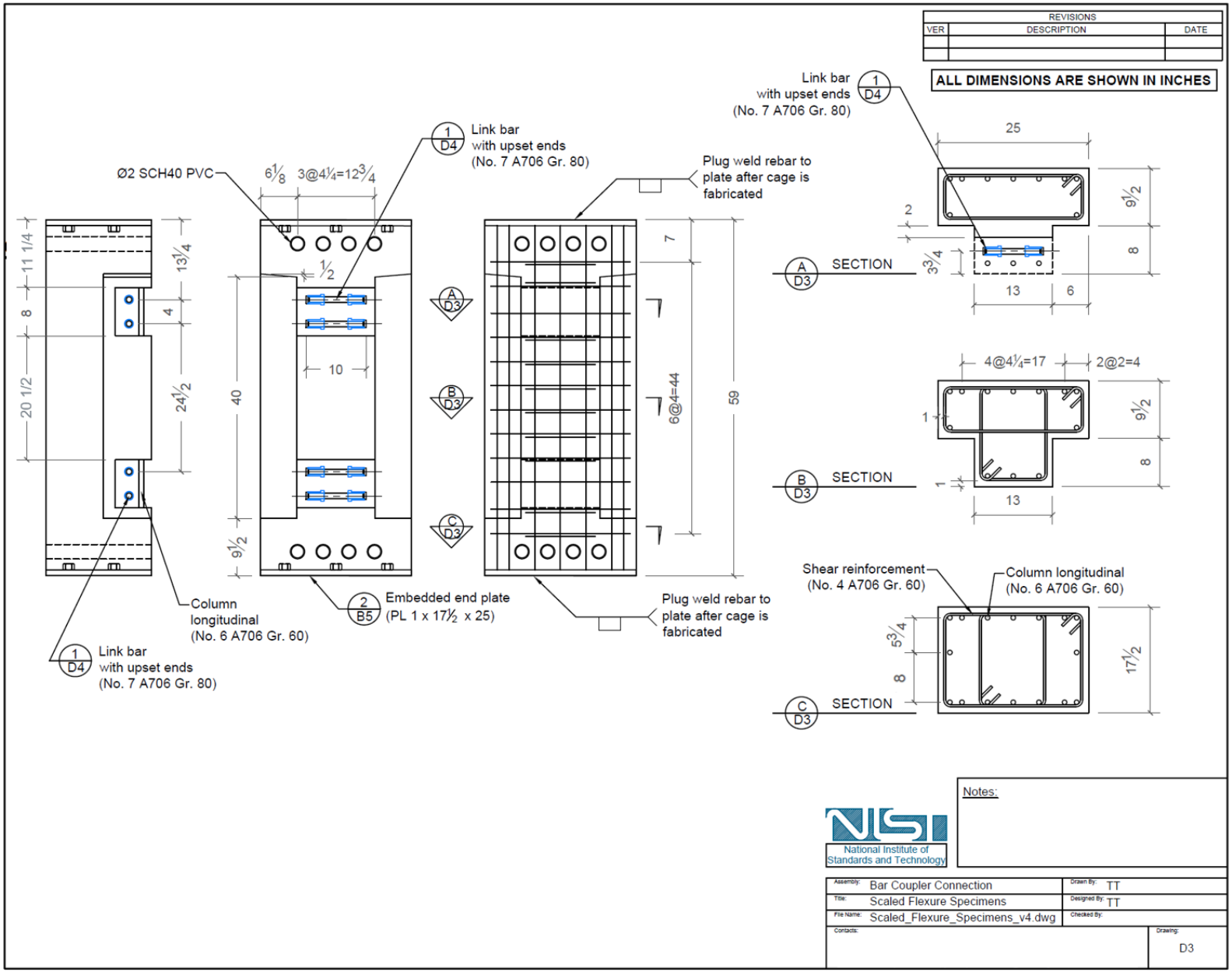
REVISIONS
VER
DESCRIPTION
DATE
ALL DIMENSIONS ARE SHOWN IN INCHES
Link bar with upset ends (No. 7 A706 Gr. 80)
Ø2 SCH40 PVC
6⅛ 3@4¼=12¾
Plug weld rebar to plate after cage is fabricated
Column longitudinal (No. 6 A706 Gr. 60)
Embedded end plate (PL 1 x 17½ x 25)
SECTION
4@4¼=17
2@2=4
Shear reinforcement (No. 4 A706 Gr. 60)
Column longitudinal (No. 6 A706 Gr. 60)
Notes:
National Institute of Standards and Technology
Assembly: Bar Coupler Connection
Title: Scaled Flexure Specimens
File Name: Scaled_Flexure_Specimens_v4.dwg
Drawn By: TT
Designed By: TT
Checked By:
Contacts:
Drawing: D3

REVISIONS		
VER	DESCRIPTION	DATE

ALL DIMENSIONS ARE SHOWN IN INCHES

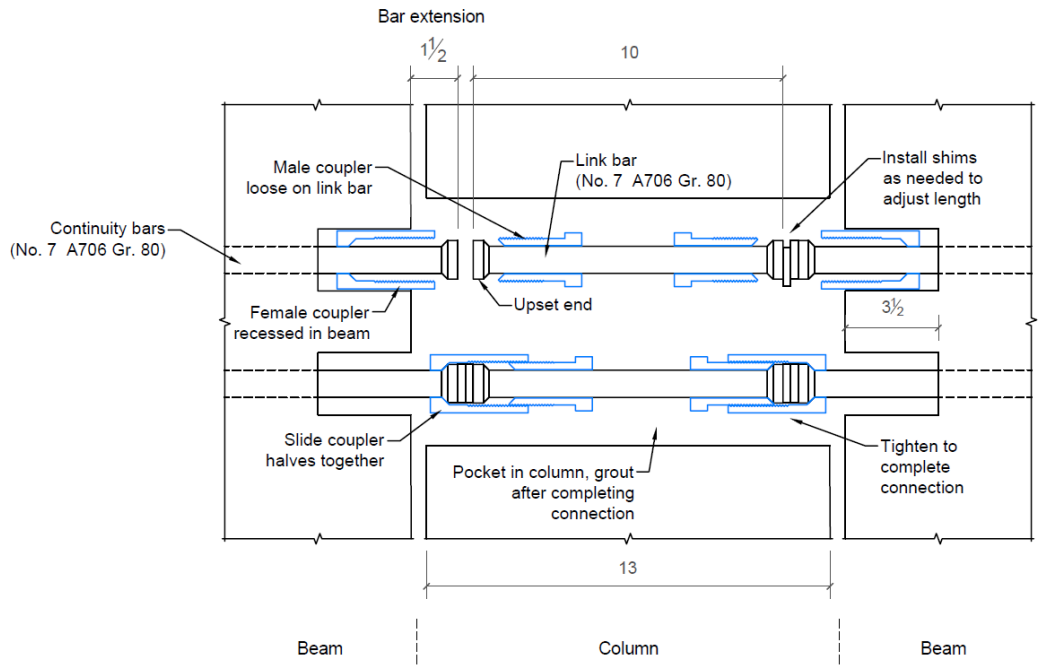

1 D1 SPLICE DETAIL

National Institute of Standards and Technology

Notes:
Bar coupler HRC 500XL / 510 XL
or equivalent, conforming to
ACI 318-19 §25.5.7.1

Assembly:	Bar Coupler Connection	Drawn By:	TT
Title:	Scaled Flexure Specimens	Designed By:	TT
File Name:	Scaled_Flexure_Specimens_v4.dwg	Checked By:	
Contacts:		Drawing:	D4

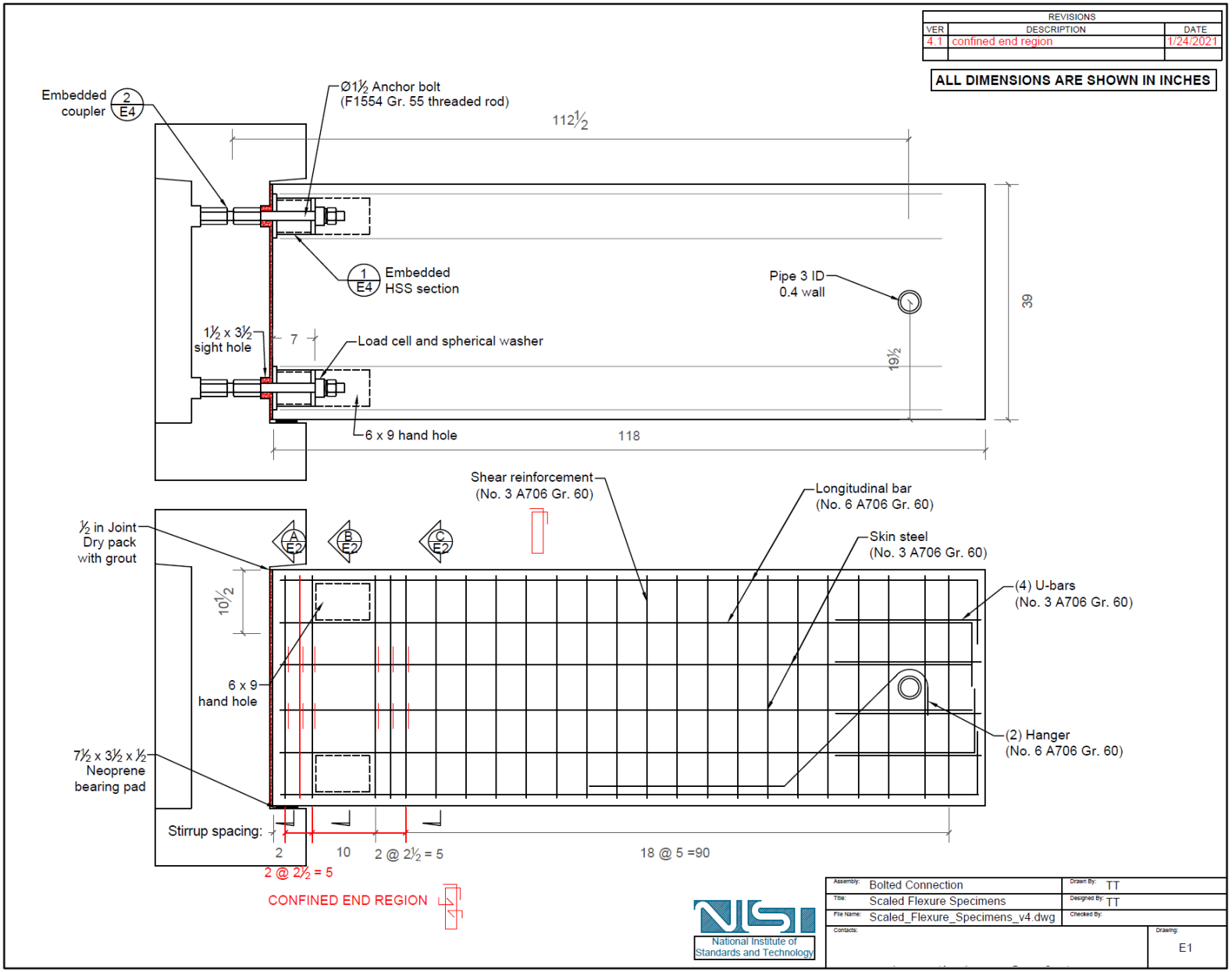
REVISIONS
VER DESCRIPTION DATE
4.1 confined end region 1/24/2021
ALL DIMENSIONS ARE SHOWN IN INCHES
Embedded coupler 2 E4
Ø1½ Anchor bolt (F1554 Gr. 55 threaded rod)
112½
1 E4 Embedded HSS section
Pipe 3 ID 0.4 wall
39
1½ x 3½ sight hole
7
Load cell and spherical washer
19½
6 x 9 hand hole
118
Shear reinforcement (No. 3 A706 Gr. 60)
Longitudinal bar (No. 6 A706 Gr. 60)
½ in Joint Dry pack with grout
A E2
B E2
C E2
Skin steel (No. 3 A706 Gr. 60)
10½
(4) U-bars (No. 3 A706 Gr. 60)
6 x 9 hand hole
(2) Hanger (No. 6 A706 Gr. 60)
7½ x 3½ x ½ Neoprene bearing pad
Stirrup spacing:
2
10
2 @ 2½ = 5
18 @ 5 =90
2 @ 2½ = 5
CONFINED END REGION
National Institute of Standards and Technology
Assembly: Bolted Connection
Drawn By: TT
Title: Scaled Flexure Specimens
Designed By: TT
File Name: Scaled_Flexure_Specimens_v4.dwg
Checked By:
Contacts:
Drawing: E1

REVISIONS		
VER	DESCRIPTION	DATE
4.1	New section, replaced fiber mesh reinf.	1/31/2021

ALL DIMENSIONS ARE SHOWN IN INCHES

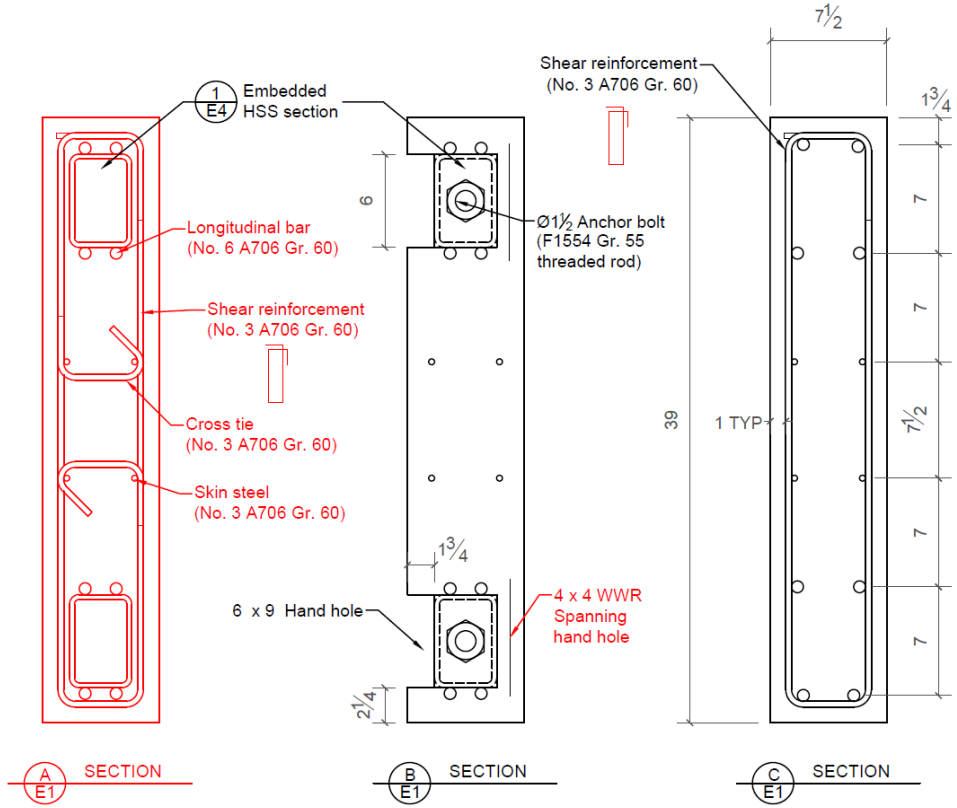

Notes:

National Institute of Standards and Technology

Assembly:	Bolted Connection	Drawn By:	TT
Title:	Scaled Flexure Specimens	Designed By:	TT
File Name:	Scaled_Flexure_Specimens_v4.dwg	Checked By:	
Contacts:		Drawing:	E2

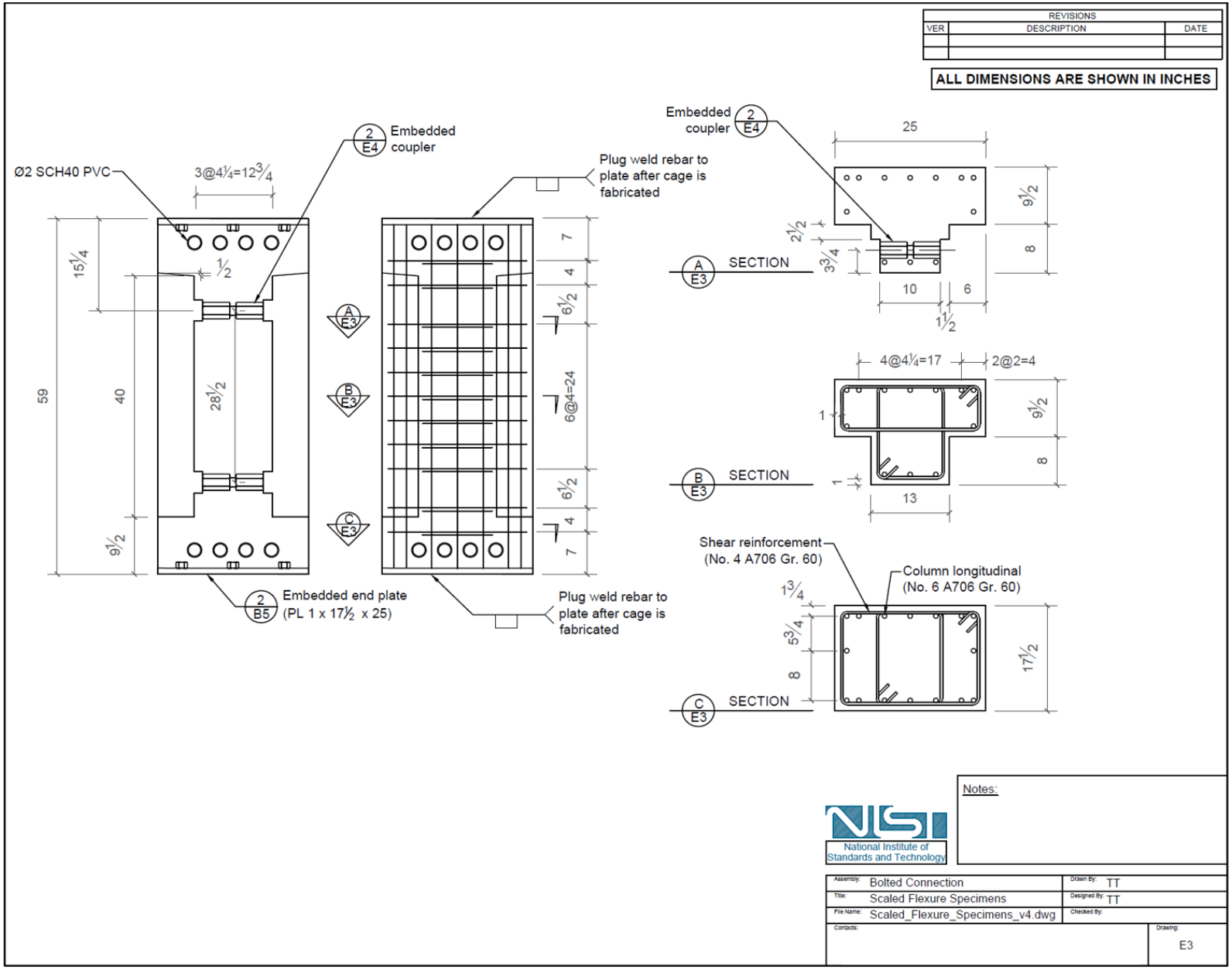
REVISIONS
VER
DESCRIPTION
DATE
ALL DIMENSIONS ARE SHOWN IN INCHES
Ø2 SCH40 PVC
3@4¼=12¾
2 E4 Embedded coupler
Plug weld rebar to plate after cage is fabricated
15¼
½
59
40
28½
9½
A E3
B E3
C E3
7
4
6½
6@4=24
6½
4
7
2 B5 Embedded end plate (PL 1 x 17½ x 25)
Plug weld rebar to plate after cage is fabricated
Embedded coupler 2 E4
25
9½
2½
3¾
8
A E3 SECTION
10
6
1½
4@4¼=17
2@2=4
1
9½
8
B E3 SECTION
1
13
Shear reinforcement (No. 4 A706 Gr. 60)
Column longitudinal (No. 6 A706 Gr. 60)
1¾
5¾
8
17½
C E3 SECTION
Notes:
National Institute of Standards and Technology
Assembly: Bolted Connection
Drawn By: TT
Title: Scaled Flexure Specimens
Designed By: TT
File Name: Scaled_Flexure_Specimens_v4.dwg
Checked By:
Contacts:
Drawing: E3

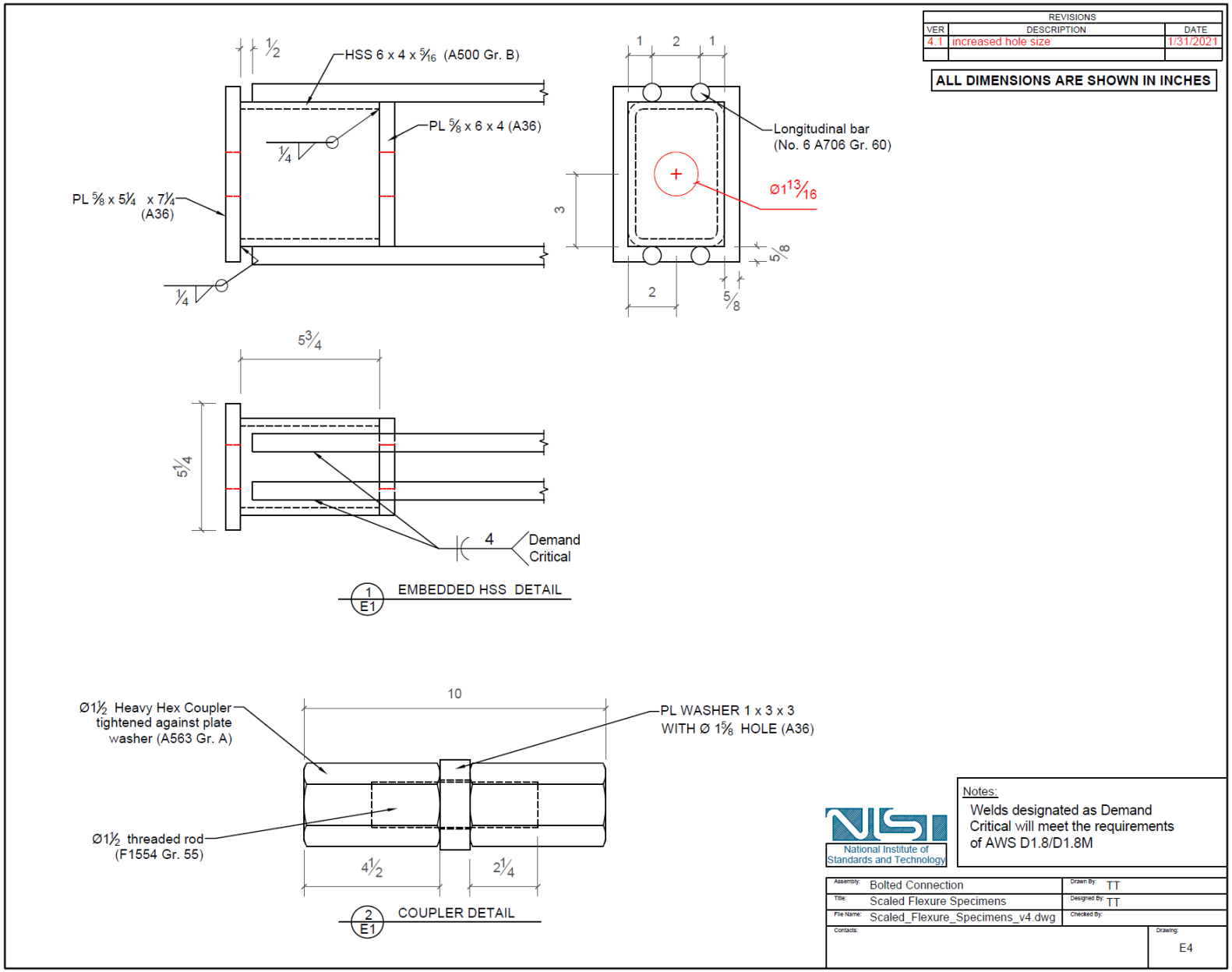
REVISIONS
VER DESCRIPTION DATE
4.1 increased hole size 1/31/2021
ALL DIMENSIONS ARE SHOWN IN INCHES
1/2
HSS 6 x 4 x 5/16 (A500 Gr. B)
PL 5/8 x 6 x 4 (A36)
1/4
PL 5/8 x 5 1/4 x 7 1/4 (A36)
1/4
1 2 1
Longitudinal bar (No. 6 A706 Gr. 60)
Ø1 13/16
3
5/8
2
5/8
5 3/4
5 1/4
4
Demand Critical
1 E1
EMBEDDED HSS DETAIL
10
Ø1 1/2 Heavy Hex Coupler tightened against plate washer (A563 Gr. A)
PL WASHER 1 x 3 x 3 WITH Ø 1 5/8 HOLE (A36)
Ø1 1/2 threaded rod (F1554 Gr. 55)
4 1/2
2 1/4
2 E1
COUPLER DETAIL
National Institute of Standards and Technology
Notes:
Welds designated as Demand Critical will meet the requirements of AWS D1.8/D1.8M
Assembly: Bolted Connection
Drawn By: TT
Title: Scaled Flexure Specimens
Designed By: TT
File Name: Scaled_Flexure_Specimens_v4.dwg
Checked By:
Contacts:
Drawing: E4

Appendix B. Locations of Strain Gauges

This appendix contains schematics showing the locations of electrical resistance strain gauges that were applied to the reinforcing steel in the beams and selected steel components of each connection assembly.

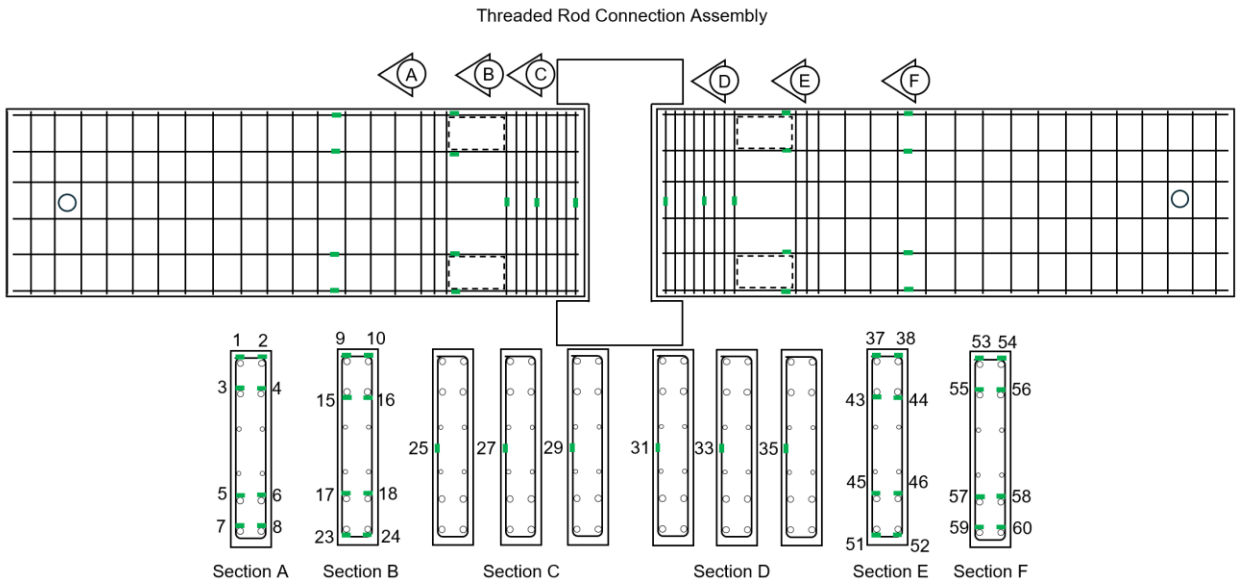

Fig. B-1. Locations of strain gauges on the beam steel reinforcement for the threaded rod connection assembly.

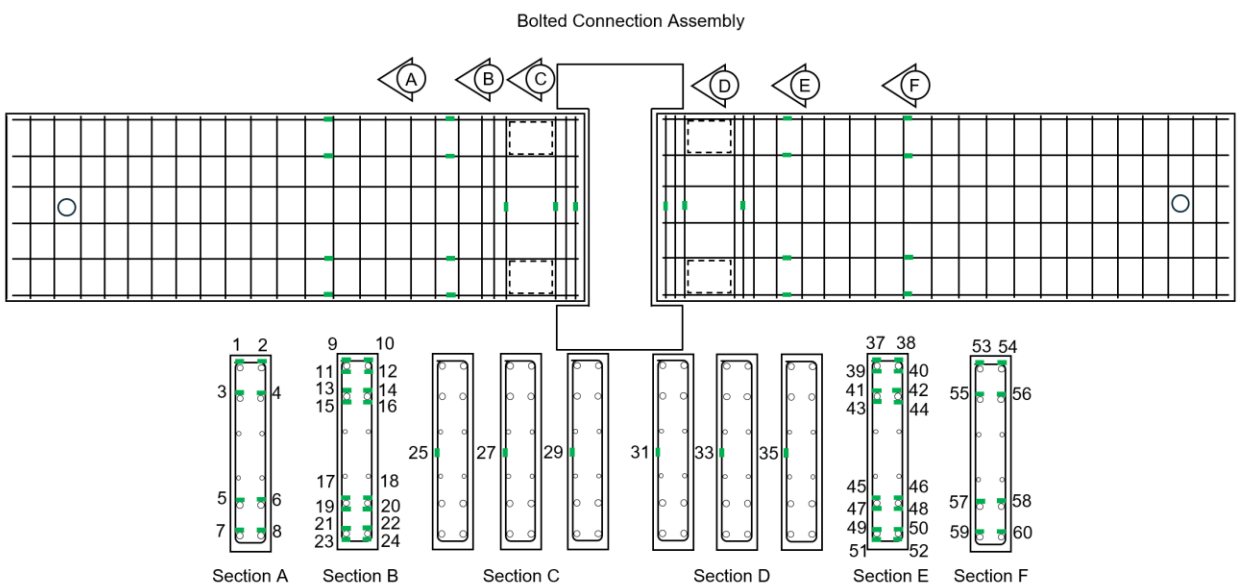

Fig. B-2. Locations of strain gauges on the beam steel reinforcement for the bolted connection assembly.

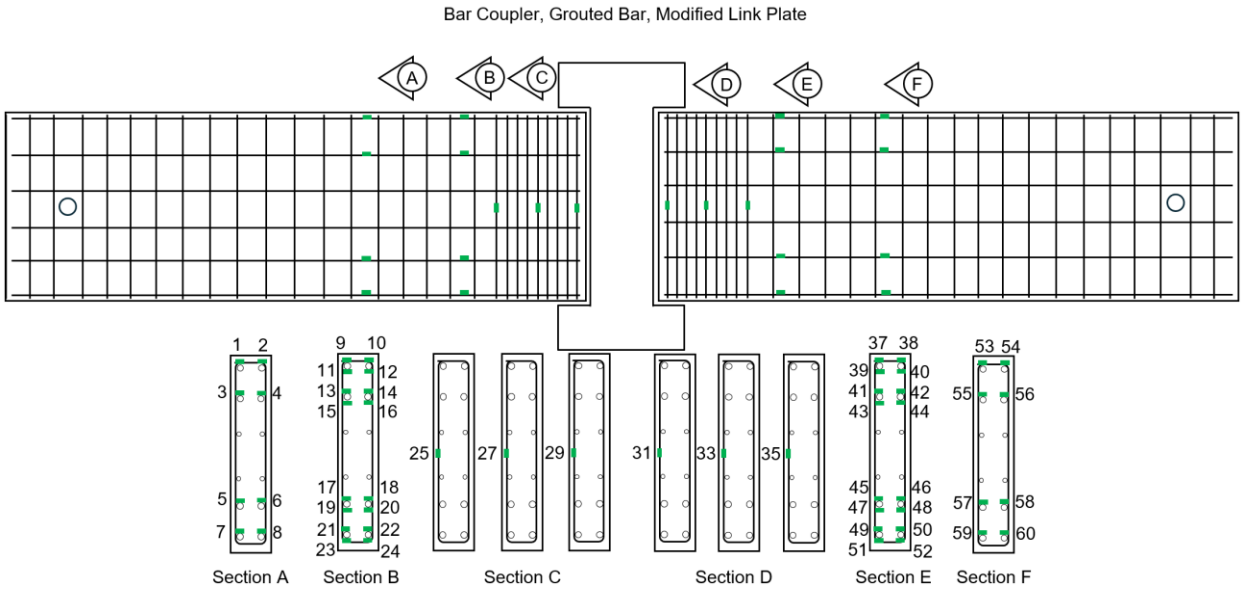

Fig. B-3. Locations of strain gauges on the beam steel reinforcement for the bar coupler, grouted bar, and modified link plate connection assemblies.

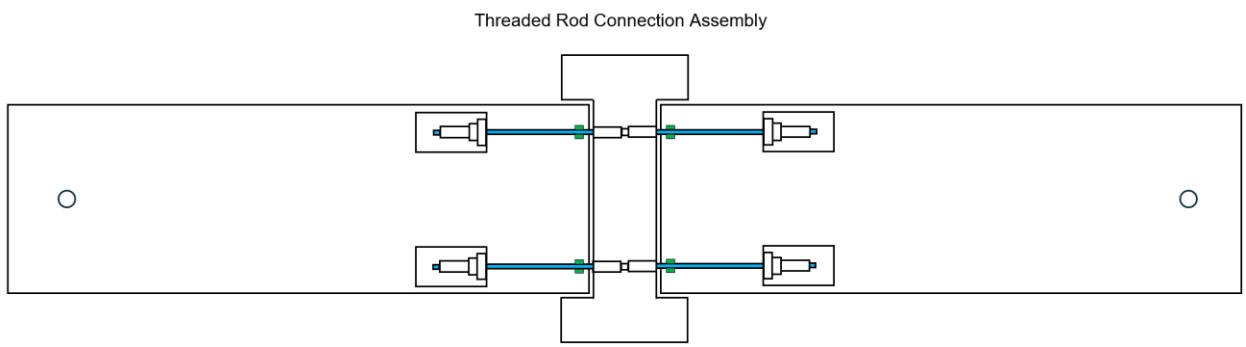

Fig. B-4. Locations of strain gauges on the threadbars for the threaded rod connection assembly.

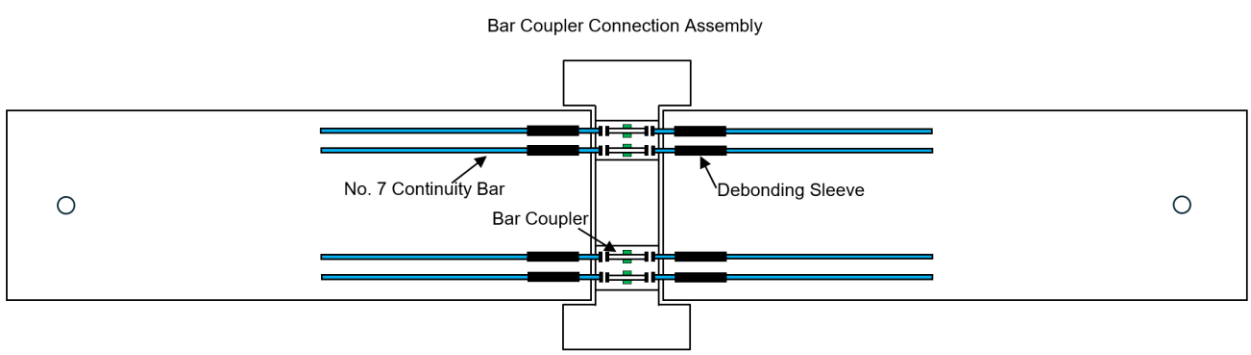

Fig. B-5. Locations of strain gauges on the No. 7 link bars (couplers) for the bar coupler connection assembly.

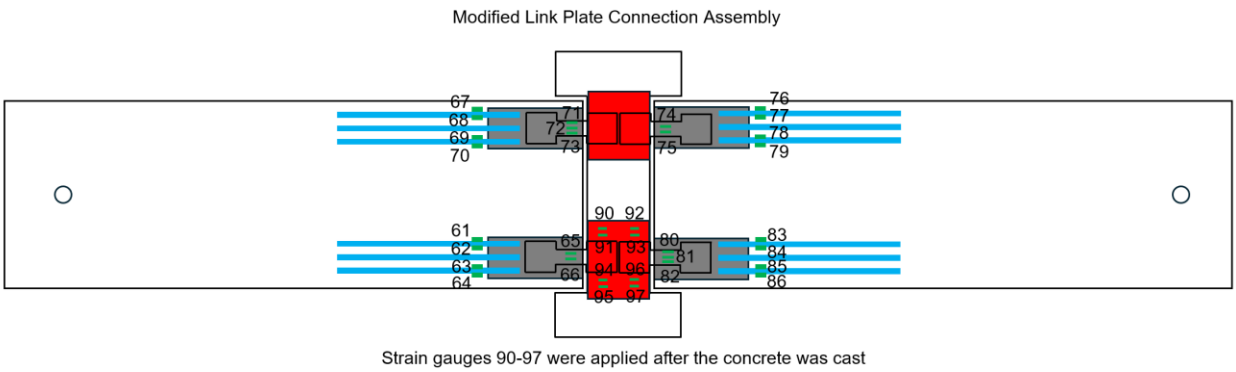

Fig. B-6. Locations of strain gauges on steel components for the modified link plate connection assembly.